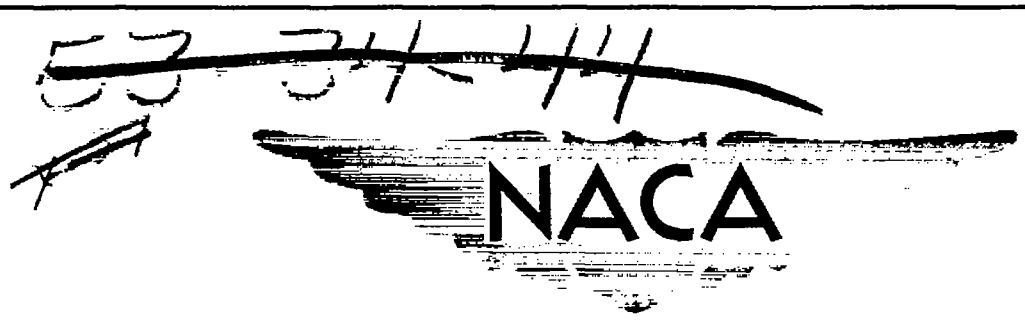

RESEARCH MEMORANDUM

TRANSONIC-WING INVESTIGATION IN THE LANGLEY 8-FOOT HIGH-SPEED TUNNEL AT HIGH SUBSONIC MACH NUMBERS AND AT A MACH NUMBER OF 1.2

ANALYSIS OF PRESSURE DISTRIBUTION OF WING-FUSELAGE CONFIGURATION HAVING A WING OF 45° SWEEPBACK, ASPECT RATIO 4, TAPER RATIO 0.6, AND NACA 65A006 AIRFOIL SECTION

By Donald L. Loving and Bruce B. Estabrooks

Langley Aeronautical Laboratory
Langley Field, Va.

[redacted]

NATIONAL ADVISORY COMMITTEE
FOR AERONAUTICS

WASHINGTON
September 6, 1951

[redacted]

Classification cancelled (or changed to Unclassified)

By authority of NASA Tech Rl Announcement #102

By ... 22 June 56

NK

GRADE OF OFFICER MAKING CHANGE

5 Apr 61

DATE

NATIONAL ADVISORY COMMITTEE FOR AERONAUTICS

RESEARCH MEMORANDUM

TRANSONIC-WING INVESTIGATION IN THE LANGLEY 8-FOOT HIGH-SPEED TUNNEL AT HIGH SUBSONIC MACH NUMBERS AND AT A MACH NUMBER OF 1.2

ANALYSIS OF PRESSURE DISTRIBUTION OF WING-FUSELAGE CONFIGURATION HAVING A WING OF 45° SWEEPBACK, ASPECT RATIO 4, TAPER RATIO 0.6, AND NACA 65A006 AIRFOIL SECTION

By Donald L. Loving and Bruce B. Estabrooks

SUMMARY

A pressure-distribution investigation has been made in the Langley 8-foot high-speed tunnel of a wing-fuselage configuration as part of an NACA research program to determine effects of wing geometry on aerodynamic characteristics and to explore the nature of the flow over the configuration and the problem of interference between a wing and fuselage. Measurements were made on a fuselage and a wing-fuselage combination employing a wing with 45° sweepback of the 0.25-chord line, aspect ratio 4, taper ratio 0.6, and NACA 65A006 airfoil sections at Mach numbers from 0.60 to 0.96 and at a Mach number of 1.2.

The results show that pressure distributions indicative of leading-edge separation-vortex flow noted at low speeds were also observed at high Mach numbers; however, this does not mean that the vortex flow was present at these higher speeds. At normal-force coefficients of the order of 0.4, the spanwise loading on the wing shifted slightly outboard at the high Mach numbers. The loading on the fuselage in the presence of the wing shifted rearward with increase in Mach number. An examination of the wing-fuselage interference revealed that the load on the fuselage of the wing-fuselage combination was approximately 10 times greater than the load on the isolated fuselage at the same angle of attack and Mach number and the fuselage carried a large proportion of

the load on the wing-fuselage combination at transonic speeds. The force coefficients and aerodynamic characteristics obtained from the pressure data were in agreement with the results determined from force tests of an identical model.

INTRODUCTION

As part of a systematic transonic flight investigation, several wings have been tested on a fuselage in the Langley 8-foot high-speed tunnel at subsonic Mach numbers from 0.60 to 0.96 and at a Mach number of 1.2. Force-test investigations were conducted to establish the effects of varying the angle of sweepback of the 0.25-chord line of four wings, all having an aspect ratio of 4, a taper ratio of 0.6, and NACA 65A006 airfoil sections parallel to the air stream. The fuselage had a fineness ratio of 10. These results have been presented in references 1, 2, 3, and 4 for configurations having angles of sweepback of 0°, 35°, 45°, and 60°, respectively.

The pressure-distribution investigation reported herein was conducted on the 45° sweptback configuration, which was considered the most representative of this series of swept wings. Data are shown for the same angles of attack and Mach numbers covered in reference 3. Pressure measurements were obtained on the wing-fuselage combination at angles of attack from -2° to 14° at the subsonic Mach numbers and at angles of attack from -2° to 6° at a Mach number of 1.2. Fuselage pressure measurements were obtained at angles of attack from 0° to 14° for all Mach numbers investigated. Complete pressure results for the fuselage and wing-fuselage combination are presented and discussed to explain some of the flow phenomena occurring at these angles of attack and Mach numbers. Comparisons are made with previous results from force tests on an identical model and from free-fall tests on a similar fuselage. These comparisons indicated that all the force coefficients obtained from integrations of the pressure data were in excellent agreement with the force-test results except for the pitching-moment coefficients at high angles of attack.

The Reynolds number for this investigation varied from 1.73×10^6 to 2.02×10^6 when based on the wing mean aerodynamic chord or from 9.4×10^6 to 11.0×10^6 when based on the fuselage length.

SYMBOLS

A	aspect ratio $\left(b^2/S\right)$
B	13.89-percent station of wing semispan, located at fuselage maximum diameter
b	wing span
c	airfoil section chord, parallel to plane of symmetry
$\bar{c}$	average wing chord (S/b)
c'	mean aerodynamic chord $\left(\frac{2}{S}\int_0^{b/2} c^2 dy\right)$
d	fuselage section diameter
d_{max}	fuselage maximum diameter
l	basic fuselage length
M	Mach number
p_o	free-stream static pressure
p	local static pressure
P	pressure coefficient $\left(\frac{p - p_o}{q}\right)$
q	free-stream dynamic pressure $\left(\frac{1}{2}\rho V^2\right)$
R	Reynolds number $\left(\frac{\rho V c'}{\mu}\right)$
r	fuselage section radius
S	total wing area
t	wing thickness
V	velocity in undisturbed stream

x distance measured streamwise from leading edge of section

z distance perpendicular to plane of chord of wing

α angle of attack of fuselage center line

ρ mass density in undisturbed stream

μ coefficient of viscosity in undisturbed stream

Λ angle of sweepback of 0.25-chord line of wing

Subscripts:

ah surface ahead of maximum thickness of airfoil section

bh surface behind maximum thickness of airfoil section

cr critical

f fuselage cross section

F fuselage

L lower surface of airfoil section

T wing-fuselage configuration

U upper surface of airfoil section

w wing

The coefficients are defined as follows:

c_n wing section normal-force coefficient $\left(\frac{1}{c}\int_0^c (P_L - P_U)\,dx\right)$

c_{n_f} fuselage cross-section normal-force coefficient $\left(\frac{1}{2r}\int_{-r}^{r} (P_L - P_U)\,dy\right)$

C_N normal-force coefficient based on total wing area

[redacted]

c_m wing section pitching-moment coefficient about 25-percent-chord station $\left(\frac{1}{c^2}\int_0^c \left(P_U - P_L\right)\left(x - \frac{c}{4}\right)dx\right)$

C_m pitching-moment coefficient about the 25-percent position of the mean aerodynamic chord

C_{c_w} wing section chordwise-force coefficient $\left(\frac{1}{c}\int_0^t \left(P_{ah} - P_{bh}\right)dz\right)$

c_{d_w} wing-section pressure-drag coefficient $\left(C_{c_w} \cos \alpha + c_n \sin \alpha\right)$

C_{D_F} pressure-drag coefficient of fuselage based on total wing area

C_{D_T} pressure-drag coefficient of the wing-fuselage combination based on total wing area

APPARATUS AND METHODS

Tunnel

The investigation was conducted in the Langley 8-foot high-speed tunnel. A plaster liner installed in the tunnel formed the subsonic test section at the geometric minimum and extended downstream to form the supersonic test section. The Mach number was uniform in the subsonic test section and varied by a maximum of 0.02 from the design Mach number of 1.2 in the supersonic test section (reference 5).

Model

The model was a midwing configuration with dimensions identical to the force-test model of reference 3. The wing had 45° sweepback of the 0.25-chord line, an aspect ratio of 4, a taper ratio of 0.6, and NACA 65A006 airfoil sections parallel to the plane of symmetry. Dimensional details are shown in figure 1. The fuselage was designed with the lines of the general transonic fuselage which was the same fuselage used for the other wings in this wing program. The fuselage had circular

[redacted]

cross sections and a basic fineness ratio of 12, although an actual fineness ratio of 10 was obtained after cutting off the rear one-sixth of the fuselage to attach the sting. The fuselage details and ordinates are presented in figure 2. The ratio of the fuselage frontal area to the wing plan-form area, considering the wing extended through the fuselage, was 0.0606. A photograph of the model is presented as figure 3.

The wing was constructed of a mild steel core with a bismuth-tin covering. One hundred and fifteen static-pressure orifices were located in the wings, distributed among five spanwise stations parallel to the free stream, as shown in figure 4. On the actual test model, the 20-, 60-, and 95-percent-semispan stations were located on the left wing and the 40- and 80-percent-semispan stations were located on the right wing. One hundred static-pressure orifices were distributed among six longitudinal rows in the side of the fuselage, as shown in figure 5.

Measurements of the incidence of each half of the wing relative to the fuselage axis showed that the right wing had an incidence of 0.05° and the left wing, -0.1°. These construction inaccuracies were small and no attempt was made to correct the data for them. A close check of the actual machined ordinates of the present wing and the wing previously used in the force tests revealed differences in the airfoil thickness of the order of 0.1 percent. Furthermore, calculations of the deflections of the two wings under load also indicated no appreciable difference. Accordingly, the two wings may be considered essentially equal.

Model Support System

The model was supported by a tapered sting attached to the rear of the fuselage. The tapered sting was mounted on an extensible support tube which was fixed axially in the center of the tunnel by two sets of supports projecting from the tunnel walls. Location of the model in either the subsonic or supersonic test section was accomplished by sliding the support tube forward or rearward on the support bearings. The forward, tapered portion of the support tube was hinged to the rear portion in such a manner that angle-of-attack changes could be accomplished by means of an electric motor driving an actuating screw located within the tube. This mechanism was controlled from outside the test section and therefore permitted angle changes while the tunnel was operating. Details of the model support system and the model locations in the subsonic and supersonic test sections are shown in figures 6 and 7.

Measurements

The attitude of the model was measured by a calibrated optical system consisting of a small mirror mounted on the upper surface of the

fuselage and a point source of light mounted outside the tunnel. To determine the angle, the optical device containing the point source of light was adjusted until the reflected ray from the mirror coincided with the incident ray. The angle of the instrument with respect to the vertical was then measured with a vernier inclinometer. The use of this device in conjunction with the remotely controlled angle-of-attack changing mechanism enabled desired model angles of attack to be set within 0.1° with the tunnel operating at any Mach number.

TESTS

The tests were conducted through a Mach number range from 0.60 to approximately 0.96 with the model in the subsonic test section and at a Mach number of 1.2 with the model in the supersonic test section. The fuselage was tested at angles of attack from 0° to 14° at all Mach numbers. The wing-fuselage combination was tested from -2° to 14° at subsonic Mach numbers and from -2° to 6° at a Mach number of 1.2.

Configurations included the wing-fuselage combination with natural transition and with transition fixed at 10 percent of the chord on the upper and lower surfaces of the wing and at 12 percent of the fuselage length. The transition strip consisted of No. 60 carborundum particles covering approximately 50 percent of a $\frac{1}{8}$-inch-wide layer of an adhesive agent. The fuselage alone was investigated with natural transition only. Unless otherwise noted, the data presented herein are for natural transition only. The model was maintained aerodynamically smooth throughout the investigation.

The variation with Mach number of the approximate test Reynolds number based on a wing mean aerodynamic chord of 6.125 inches is presented in figure 8.

The tunnel choked at the model in the subsonic test section at an uncorrected Mach number of approximately 0.975. Static-pressure measurements made on the tunnel wall gave an indication of any perceptible tendency toward choking at the plane of the model. Data were not obtained for angles of attack and Mach numbers at which such occurrence was noted. At the supersonic Mach number of 1.2, the test angles of attack were limited by the location of the tunnel normal shock at the tail of the model. Visual observations were made of the shock by noting the shadow cast by the shock on the tunnel wall when a parallel light beam was directed across the rear of the model. Previous tests have indicated a detrimental effect on pitching moments especially when the shock is too close to the rear of the model (reference 6). Data are not presented which might be affected by the presence of this shock. Observation of

the tunnel-wall static pressure at a Mach number of 1.2 also indicated that at all angles of attack tested the shock disturbance from the nose of the model was transmitted to the wall sufficiently far downstream from the nose to insure that its reflection did not affect the model.

RESULTS

Accuracy.- The same Mach number corrections determined for the data presented in reference 3 have been applied to the data presented herein, since the dimensions of the models tested were identical. The magnitude of the correction to the Mach number reached 1.5 percent at a Mach number of 0.96. In one instance all known corrections for tunnel Mach number gradient, blockage, and boundary-induced upwash were applied to the pressure data for the upper surface of the fuselage alone at an angle of attack of 0° and Mach numbers of 0.90 and 0.96. At Mach numbers of 0.90 and 0.96 the corrections changed the pressure coefficients 0.01 and 0.015, respectively, in a positive direction. The corrections have not been applied to the remainder of the data.

Figures.- An index of the figures presenting the results is as follows:

Legend:	Figure
The chordwise pressure distributions at five spanwise stations for several angles of attack. $M = 0.60$.	9(a) to 9(d)
The chordwise pressure distributions at five spanwise stations for several Mach numbers. $\alpha = 0^\circ$.	10(a) and 10(b)
The chordwise pressure distributions at five spanwise stations for several Mach numbers. $\alpha = 2^\circ$.	11(a) to 11(c)
The chordwise pressure distributions at five spanwise stations for several Mach numbers. $\alpha = 4^\circ$.	12(a) to 12(c)
The chordwise pressure distributions at five spanwise stations for several Mach numbers. $\alpha = 6^\circ$.	13(a) to 13(c)

[redacted]

[redacted]

The pressure diagrams for an angle of attack of -2° were the same as for an angle of attack of 2° and therefore have not been presented.

Fuselage pressure data for fixed transition have not been presented.

A dashed line has been drawn through the loci of maximum negative pressure coefficient in the pressure contours shown in figure 27. For an angle of attack of 4° the contours of equal pressure coefficients are shown for the fuselage.

The pressure orifices located along the six meridians on the fuselage were so arranged that they also formed rings around the fuselage. The pressure coefficients for each of these rings were plotted against percent radius. Interpolated values of pressure coefficient were obtained from these plots to prepare the data shown in figures 29 and 30 for six fuselage sections parallel to the fuselage vertical plane of symmetry.

The fuselage longitudinal section coefficients, which are based on chord lengths of the wing projected through the fuselage, were obtained by integration of figures 29 and 30.

The pitching-moment coefficients for the fuselage longitudinal sections are based on the 0.25-chord line of the wing extended through the fuselage.

DISCUSSION

In general, the pressure distributions followed trends noted in references 7 to 13. These trends and additional effects may be studied in figures 9 to 17 for the wing, and in figures 18 to 26 for the fuselage. All data presented here for the wing were affected by the presence of the fuselage.

Pressure Distributions on Wing

0.60 Mach number.- The effect on the wing pressures of varying the angle of attack from 0° to 14° at the low-speed Mach number of 0.6 may be seen in figure 9. Here it is shown that when the angle of attack was increased up to 4° a sharp negative pressure-coefficient peak formed on the leading edge of the wing as might be expected. When the angle of attack was increased to 6°, the forms of the pressure diagrams over the wing became similar to those reported in reference 7 in which a separation vortex was shown to exist on the upper surface. The chordwise pressure distributions of the wing indicated high peak negative pressure coefficients at the leading edge for the most inboard station, and these peaks became progressively lower and broader toward the wing tip. The separation vortex was formed as a result of flow separation over the relatively sharp leading edge of the wing. With increasing angle of attack, the extent of the separation vortex increased over the outboard stations until, at an angle of attack between 6° and 8°, the core turned back along the chord and a trailing vortex was shed off the wing between the 80- and 95-percent-semispan stations. The wing stalled on the outboard section, and this stalled region moved inboard with increase in angle of attack. The presence of separation was indicated by the reduction of the peak negative pressure coefficient near the leading edge of the upper surface and the relatively high negative pressure coefficients near the trailing edge.

0° angle of attack.- The effects of changing Mach number for the wing at zero angle of attack, as shown in figure 10, are similar to those reported in reference 8. It may be seen that the inboard and outboard wing sections differed considerably in pressure distribution throughout the Mach number range investigated. Contours of equal pressure coefficient, as shown in figure 27, indicated that at a Mach number of 0.6 the line of maximum negative pressure coefficient occurred across the span from 50-percent chord at 20-percent-semispan station to 40-percent

chord at 80-percent-semispan station, then shifted forward to approximately 11-percent chord at 95-percent-semispan station. As the Mach number was increased to 0.96 the peaks moved rearward. At a Mach number of 1.2, the values of negative pressure coefficient were reduced all along the span and the peak moved considerably rearward to 80 percent of the chord at the tip station. It is also shown that as the peak negative pressure coefficient moved rearward the pressure coefficients became more positive at the leading edge of the inboard stations.

2° angle of attack.- The trends for the wing at various angles of attack are shown in figures 11 to 17. Pressure distributions over the wing at an angle of attack of 2° for Mach numbers from 0.60 to 0.96, as shown in figures 11(a) to 11(c), are similar to two-dimensional data obtained on thin wings at low angles of attack. When the pressure distributions over the midsemispan stations were compared with two-dimensional data reported in reference 9, it was indicated that for comparable Mach numbers and angles of attack (that is, comparing the data herein at an angle of attack of 2° and a Mach number of 0.96 with the two-dimensional data for the NACA 66-006 airfoil at an angle of attack of about 3° and a Mach number of 0.75), changes in pressure distribution occurred at a much lower Mach number than predicted; however, the trends for increase in angle of attack and Mach number were much the same. A peak negative pressure coefficient occurred at the leading edge of the upper surface of the wing indicating the same type of flow in this area. When the Mach number was increased from 0.85 to 0.96 for the wing reported herein (figs. 11(b) and 11(c)), the pressure coefficients decreased over the forward portion of the 20-percent-semispan station and a second minimum-pressure peak developed to the rear of the midchord. The same thing has been predicted in reference 10 for subsonic as well as supersonic wings. As shown in the pressure contours (fig. 27(e)) one peak was located along the wing leading edge and the other lay diagonally across the span from 80 percent of the chord on the 20-percent-semispan station to 25 percent of the chord at the 95-percent-semispan station. However, the second peak negative pressure coefficient was considerably more rearward on the sweptback wing than might be expected from the two-dimensional data. Similar variations have been reported in reference 11. At a Mach number of 0.90 (fig. 11(b)), a pressure gradient became evident following the second minimum-pressure peak indicating the presence of a weak normal shock extending from about 80 percent of the chord at the 20-percent-semispan station and diminishing in strength out to the 60-percent-semispan station. At the same Mach number and angle of attack an abrupt change in pressure coefficient was noted over the forward portion of the 95-percent-semispan station. This discontinuity was associated with a disturbance originating at the wing tip. At a Mach number of 0.96 this disturbance merged with the normal shock as it extended across the wing tip (fig. 11(c)).

At a Mach number of 1.2, the minimum-pressure-coefficient peaks at the leading edge were considerably reduced all along the span. The

pressure contours (figs. 27(g), 27(h), and 27(i)) were similar to those obtained for a Mach number of 0.96 except that the minimum-pressure peak near the trailing edge shifted rearward toward the tip and located itself along the 70-percent-chord line.

4° angle of attack.- At an angle of attack of 4° the same type of pressure distribution and flow phenomena are shown as for an angle of attack of 2° up to a Mach number of 0.85, as shown in figures 12(a) and 12(b). Thereafter, when the Mach number was increased to 0.875 the first indication of the appearance of the separation-vortex phenomenon is shown in figure 12(b) by the broadening of the negative-pressure-coefficient peaks over the leading edge of the 80- and 95-percent-semispan station. Since the local pressure coefficients for these peaks indicated local Mach numbers greater than unity and the component of local Mach number perpendicular to the contour lines was greater than 1.00, it is believed that an oblique shock appeared at the trailing boundary of the vortex. The severe adverse gradient behind the minimum-pressure peak appeared to be associated with the redirection of the flow as it reattached itself to the airfoil behind the leading-edge separation-vortex bubble. Because of the strong separation-vortex flow on the outer wing stations the pressure distributions for a Mach number of 0.93, as shown in figure 12(c), did not indicate any discontinuity due to a disturbance originating at the wing tip.

The pressure gradient following the second minimum-pressure peak became more severe with increase in angle of attack to 4° and was noted at stations farther outboard (fig. 12(b)). This indicated that increasing the angle of attack increased the strength of the normal shock, extended it farther outboard on the wing, and at the same time increased the chordwise extent of the relatively high negative pressure coefficients. However, as shown by the chordwise location of the second minimum-pressure peak, the chordwise position of the normal shock was only slightly affected by change in angle of attack and was influenced mostly by increase in Mach number. It may also be seen that as the angle of attack was increased the peak of the separation-vortex core moved inboard and the broadened peak pressures spread over more of the outboard stations. The flow may have been approaching that described for supersonic airfoils at high subsonic speeds in reference 9. The wings actually had similar pressure distributions, but the precise nature of the transition from vortex flow to that indicated in reference 9 cannot be definitely stated at the present time. At a Mach number of 1.2 the upper-surface pressure coefficients became more negative and had the same forms usually present when either separated flow existed or the shock moved to the wing trailing edge (fig. 12(c)). The discontinuity in the negative-pressure-coefficient distributions extending obliquely across the semispan on the upper surface at a Mach number of 1.2, which apparently originated at the leading edge of the wing-fuselage juncture (fig. 12(c)), was similar to the discontinuity predicted by supersonic theory for the case when the Mach line is

swept behind the leading edge. It is not known at the present time whether the discontinuity shown herein was due to a discontinuity in nonviscous linear supersonic flow or to the separation vortex present at subsonic Mach numbers. Additional information must await the results of proposed tuft surveys and wake measurements for this wing.

6° angle of attack.- At an angle of attack of 6° the broadening pressure peaks at the leading edge of the inboard stations of the wing indicated that the separation-vortex flow began very near the fuselage at a Mach number of 0.60 (fig. 13(a)) and spread outboard along the semispan. At all Mach numbers up to 0.96 the failure of the upper-surface pressures to return to free-stream conditions at the trailing edge of the outer stations indicated separated flow over the wing tip. The trailing boundary of the vortex was shed off the wing trailing edge between the 80- and 95-percent-semispan stations. As in the case of angles of attack of 2° and 4°, it is noted that when the angle of attack was increased the separation vortex became more pronounced and its effects moved inboard. The normal shock became stronger and may have extended out to the wing tip but was masked in the region of the vortex flow and was not evident due to the softening effect of the separation over the outer sections of the wing (fig. 13(b)). At a Mach number of 1.2 the trends shown for 2° and 4° angles of attack were evident. Increasing the angle of attack increased the angle of the oblique discontinuity in negative-pressure-coefficient distribution originating at the wing-fuselage juncture. Moreover, the strength of the wing-tip disturbance was increased to such an extent that a discontinuity in the level of the pressure distribution became evident over the 95-percent-semispan station.

8° to 14° angle of attack.- The significant factors shown by the pressure distributions in figures 14(a) to 17(b) for angles of attack from 8° to 14° are that, as the angle of attack was increased, the vortex-flow region on the wing expanded inboard and separation on the outboard sections increased in intensity and extent. As the Mach number was increased, however, the spread of the separation was delayed. At the highest angle of attack tested (14°), the pressure distributions indicated that the vortex flow had spread over almost the entire wing with the trailing boundary being shed off somewhere between the 20- and 40-percent-semispan stations (figs. 17(a) and 17(b)). Because of this separation, the pressure distribution on the upper surface of the wing outer sections became nearly flat.

An examination of the pressure distributions for the wing with natural transition, presented in figure 13(a), indicated a small region of high negative pressure coefficient at the leading edge of the 80-percent-semispan station. This peak pressure may have been caused by a local irregularity in the leading-edge surface of the right wing. It should be remembered that the 40- and 80-percent-semispan stations were on the right wing and the remaining stations on the left wing. Therefore, it appears

that the leading-edge surface irregularity disrupted the outward spread of the vortex flow on the right wing until a Mach number between 0.85 and 0.875 was reached at an angle of attack of 6° as shown in figure 13(b). By the time the transition strip was fixed on the wing, the surface irregularity seemed to have been eliminated and the flow phenomenon was the same on both wings, except at an angle of attack of 8° and a Mach number of 0.6, as shown in figure 14(a). Here it may be seen that fixing the point of transition delayed the angle of attack at which the trailing boundary of the vortex flow was shed off the wing trailing edge.

Pressure Distributions on Fuselage

The pressure distributions for the fuselage (figs. 18 to 26) did not reveal any large changes in the flow due to changes in angle of attack or Mach number with the exception of the development of a minimum-pressure-coefficient peak on the rear part of the fuselage upper surface at a Mach number of 1.2. Increases in Mach number increased the level of negative pressure coefficient. Increases in angle of attack changed the pressure coefficients in a negative direction on the upper surface at the nose and on the lower surface at the rear of the fuselage.

Pressure Distributions on Fuselage with Wing

When the wing was added to the fuselage, a considerable interference effect appears, as shown by the pressure diagrams in figures 18 to 26, 29, and 30. The negative pressure coefficients on the fuselage plane of symmetry at the midchord of the wing-fuselage juncture were increased approximately 200 percent by the presence of the wing at a Mach number of 0.60 and an angle of attack of only 4° (fig. 18(a)). The maximum negative pressure coefficient at the plane of symmetry of the fuselage with wing was approximately 55 percent of the negative pressure coefficient at the 20-percent-semispan station on the wing, excluding the negative-pressure-coefficient peak at the leading edge (fig. 29).

The negative pressure coefficients on the fuselage with wing exhibited a greater influence from the pressures on the rear portion of the wing chords nearest the fuselage than from the leading-edge pressures. The longitudinal pressures along the fuselage reflected the sharp rise in negative pressure coefficient toward the trailing edge of the wing. For example, at an angle of attack of 4° and a Mach number of 0.96, two negative-pressure-coefficient peaks were apparent on the inboard station of the wing (figs. 12(c) and 29). One was located at the leading edge and the other was found near the trailing edge. The pressures on the fuselage near the wing-fuselage juncture at the 11.6-percent station indicated almost the same minimum pressures as the wing near the rear

of the chord (fig. 29). However, the minimum pressures on the fuselage in the region of the wing leading edge indicated only a fraction of the pressure peak shown for the wing. The fuselage pressures along the streamwise stations closer to the plane of symmetry displayed even less influence from the leading-edge peak.

A definite rearward shift in the location of maximum negative pressure coefficient on the fuselage with wing was noted as Mach number was increased. Beginning at a Mach number of approximately 0.93 it is noted that the rearward shift along the upper meridian was farther rearward than at the side of the fuselage. At a Mach number of 1.2 and an angle of attack of 4° the peak negative pressure coefficient was located at about 61 percent fuselage length near the wing-fuselage juncture and at about 71 percent fuselage length on the fuselage upper meridian. The contours of equal pressure in figures 27(f) and 27(i) also illustrate this phenomenon for an angle of attack of 4° at Mach numbers of 0.96 and 1.2, respectively.

In figure 28 an indication of the change in pressure coefficient over the fuselage at zero lift is shown when all available corrections to the data had been applied at Mach numbers of 0.90 and 0.96. At a Mach number of 0.90 the corrections changed all the pressure coefficients by about 0.01 in a positive direction. At a Mach number of 0.96 the change was approximately 0.015 in a positive direction. Also shown is the comparison between theoretical (reference 12) and measured pressure coefficients for data obtained in the Langley 8-foot high-speed tunnel and by the free-fall technique (reference 13). The corrected wind-tunnel data are seen to be in excellent agreement with theory for Mach numbers of 0.90, 0.96, and 1.2. However, the data from the free-fall investigation, in general, appear to be slightly more positive than those predicted by theory.

The divergence of the wind-tunnel data and free-fall data near the tail of the model was the result of differences in sting interference. The sting for the tunnel model was considerably larger in cross section. The slight increase in pressure over the nose of the tunnel model at a Mach number of 1.2 (fig. 28(c)) is believed to be the result of a slight axial Mach number gradient in the region of the nose of the model in the supersonic test section. It should be noted, however, that a velocity gradient did not exist in the region of the wing at a Mach number of 1.2.

Section Loading Characteristics

The span load distributions, in general, were elliptical in shape at angles of attack up to 8°. At angles of attack from 0° to 6° and at Mach numbers from 0.60 to 0.93, the section normal-force coefficients (fig. 32) exhibited the type of trend shown in reference 14. The section

normal-force coefficient near the root of the wing was less than that farther outboard. It is also shown that in the angle-of-attack range from 0° to 8° the loading of all the sections increased by the same relative amount with increasing Mach number up to 0.90 (figs. 32(a) to 32(e)) without any appreciable shift in lateral center of pressure (fig. 48). At higher Mach numbers the trend of reference 14 was not followed. Further increase in Mach number to 0.96 resulted in decreased section normal-force coefficients over the inner portion of the wing and an increase in loading over the outer portion. This led to an outboard shift in the center of pressure (fig. 48) and gave rise to greater bending moments at the root. The spanwise distribution of normal-force coefficient at a Mach number of 1.2 indicated the same trend noted at a Mach number of 0.96. With reference to figures 9 to 17, it is noted that at a Mach number of 0.60 stall developed on the outer portion of the wing at angles of attack between 6° and 8° and progressed toward the root with increase in angle of attack.

At the higher angles of attack from 8° to 14°, the spanwise variation of normal-force coefficient exhibited the general trend experienced by sweptback wings with stall conditions at the outer sections. The peak load coefficient increased and moved inboard due to the inboard spread of separated flow.

In figure 31, it is noted that at a Mach number of 0.60 and an angle of attack of 6°, the section normal-force coefficient at the 80-percent-semispan station obtained with natural transition was somewhat less than that obtained with transition fixed. The difference in the section load can be attributed to the leading-edge surface irregularity as explained in the discussion of pressure distributions. The difference in section normal-force coefficient for the outboard stations at 8° angle of attack is due to the fact that the influence of the transition strip delayed the separation of the flow over the wing. This also has been mentioned in the pressure distribution discussion.

Reference 15 pointed out that adding a fuselage to a sweptback wing to make a midwing configuration increased the lift near the wing root due to the local upwash around the fuselage. Figure 33 shows that the same effect may be indicated by the data presented herein. Results for the isolated wing were not obtained, but if the trend for the loading over the inboard wing sections of reference 15 is followed, as shown in figure 33, with consideration given to the theoretical distribution suggested in reference 16, an indication of the fuselage-interference effect on the wing is apparent. On this basis it may be seen that the loading on the wing-fuselage combination was greater than for the wing alone, assuming the wing extended through the fuselage. It was also greater than the individual loadings of the fuselage and wing added together.

Comparing the contribution of the load on the fuselage alone with the total load on the fuselage in the presence of the wing, at an angle of attack of 4°, revealed the fact that the load on the fuselage of the wing-fuselage combination was approximately 10 times greater than the load on the isolated fuselage at the same angle of attack and Mach number. The fuselage loading in the presence of the wing varied with Mach number much the same as the wing loading. In figure 32(c) for an angle of attack of 4° a dip, or loss, in fuselage spanwise normal-force coefficient occurred on the fuselage and appeared to shift toward the wing-fuselage juncture with increase in Mach number. The shape of the spanwise-loading curve was due primarily to the shape of the spanwise loading on the fuselage alone (fig. 33).

The fuselage loading in the presence of the wing indicated that the load on the fuselage was affected both in front of and behind the wing-fuselage juncture by the pressures of the wing at subsonic Mach numbers (fig. 34). When the Mach number was increased to 1.2, the wing had little effect on the fuselage ahead of the wing-fuselage juncture. The center of pressure of the incremental loading on the fuselage due to the wing appeared to move rearward with increase in Mach number from 0.60 to 1.2.

The loading on the 20-percent-semispan station revealed that the center of pressure on the inboard sections of the wing moved rearward when the Mach number was increased from 0.60 to 0.96 (fig. 35). When the Mach number was increased to 1.2, a further center-of-pressure shift on the inboard wing sections was not noted. The longitudinal center-of-pressure displacement indicated by the fuselage loading at a Mach number of 1.2 may be attributed to a rearward displacement of the effect of the wing on the pressures along the mean spanwise station of the fuselage at a Mach number of 1.2.

The spanwise distributions of normal-loading coefficient $c_n c/C_N \bar{c}$ have been compared with theoretical distributions for the incompressible case (M = 0) and for a Mach number of 0.85, from charts in reference 16 (figs. 36 and 37). The theory used in reference 16 takes account only of the additional loading due to angle of attack. Close agreement would be expected between the experiment and theory, since the wing investigated was without camber or twist. Because of the unusual flow over the wing as a result of the shocks or the action of the separation vortex near the leading edge, it can be seen that the measured span-load distribution was only in fair agreement with the loading predicted by the theoretical method based on potential flow. Poor agreement was noted at the high angles of attack near that at which stall occurred at the tip.

Normal-Force Characteristics

The variation of normal-force coefficient with Mach number and angle of attack proved to be almost identical to the force-test results of reference 3 (fig. 38). The normal-force coefficients for the isolated fuselage (fig. 39) were also in agreement with reference 3. The reason for the change in the normal-force-curve slope between normal-force coefficients of 0.2 and 0.4 (fig. 40) has been pointed out in the discussion of the pressure distributions. The increase in chordwise extent of relatively high negative pressure coefficients near the leading edge of the wing upper surface resulted in the increase in normal-force-curve slope. This increase may be assumed to be caused by the fact that the stream must flow about an effectively thick, highly cambered airfoil. This increase was noted up to an angle of attack of 10°. Thereafter, the normal-force-curve slope decreased due to the loss in normal force associated with more severe separation near the tip.

It should be noted that the data presented herein are for relatively low Reynolds numbers, and the same phenomena may not exist at the higher Reynolds numbers encountered in actual flight.

It is evident from the normal-force data in figure 40 that the flow over the wing at low values of normal force was not appreciably influenced by the transition strip. There was some indication of a change at the high normal-force coefficients. However, the shape of the normal-force curves, obtained with fixed transition, agreed closely with that obtained for the smooth wing of the force test at the same Mach number.

The normal-force-curve slopes from pressure data and force tests were in agreement with theory up to a Mach number of 0.80 as shown in figure 41. The deviation of the experimental data from theory at the higher Mach numbers has been noted in other investigations for wings (reference 14) but the deviation usually was not so rapid as shown in figure 41. There is a possibility that the fuselage may have contributed to the rapid rise.

With reference to figure 42, it is noted that at normal-force coefficients up to 0.7 and Mach numbers up to 0.90, approximately 16.5 percent of the total load on the wing-fuselage combination was carried by the fuselage. Approximately 16.5 percent of the total wing area was blanketed by the fuselage. At normal-force coefficients up to 0.4, the fuselage carried 14.5 precent of the total load at a Mach number of 1.2.

Pitching-Moment Characteristics

The region of maximum negative section pitching-moment coefficient moved inboard from the tip with increase in angle of attack (fig. 43).

This resulted from an increase in the chordwise extent of relatively high negative pressure coefficients over the forward portion of the wing upper surface as shown in figures 9 to 17. The negative section pitching-moment coefficients increased in magnitude until the flow over the sections separated. Thereafter, change in angle of attack had little effect on change in pitching-moment coefficient of the stalled sections (fig. 44).

The variation with Mach number of pitching-moment coefficient for the wing-fuselage combination and the isolated fuselage at all angles of attack and Mach numbers tested (figs. 45 and 46) indicated that Mach number effects on the fuselage were negligible. At the high Mach numbers and angles of attack, the transition data indicated a less negative pitching-moment coefficient. The variation of pitching-moment coefficient with normal-force coefficient exhibited the same effect (fig. 47). Data from the force test (reference 3) were compared with the pressure data in figure 47 and excellent agreement was noted except at the high lift coefficients. The discrepancy may be partially due to differences in surface roughness of the models. Similar deviations have been reported in reference 14.

Associated with the pitching-moment characteristics, the center of pressure on the wing, with wing-fuselage interference present, moved rearward 3 to 4 percent of the mean aerodynamic chord with an increase in normal-force coefficient from 0.2 to 0.4, as shown in figure 48. When the normal-force coefficient was increased to 0.7, the center of pressure moved forward 1 to 2 percent of the mean aerodynamic chord. For a normal-force coefficient of 0.4 at a Mach number of 1.2, the increase in spread of the high-negative-pressure-coefficient region over the chord resulted in the center of pressure being located at 53 percent of the mean aerodynamic chord.

The fuselage longitudinal center of pressure was located in front of the fuselage at low angles of attack and shifted rearward with increase in angle of attack (fig. 49). As the Mach number was increased, the center of pressure moved forward. A large variation in the longitudinal position of the center of pressure was noted at a Mach number of 1.2. For this Mach number and an angle of attack of 4°, the center of pressure was located 61.5 percent fuselage length in front of the fuselage; however, when the angle of attack was increased to 14°, the center of pressure was located 14.5 percent fuselage length to the rear of the fuselage nose. With reference to figure 50, at a normal-force coefficient of 0, the aerodynamic center of the wing-fuselage combination shifted from 20 percent mean aerodynamic chord at a Mach number of 0.60 to 32.5 percent mean aerodynamic chord at a Mach number of 0.96, and to 36 percent mean aerodynamic chord at $M = 1.2$. At a normal-force coefficient of 0.4, the aerodynamic center shifted from 27 percent mean

aerodynamic chord at a Mach number of 0.60 to 45.5 percent mean aerodynamic chord at a Mach number of 0.96 and to 46 percent mean aerodynamic chord at M = 1.2. This rearward movement was probably due to the increase in chordwise extent of the minimum pressures over the forward portion of the wing upper surface as mentioned in the discussion of the pressure distributions. At normal-force coefficients in excess of 0.6, the flow over the wing tip separated completely, and the center of pressure moved forward and inboard (fig. 48).

In general, increases in Mach number tended to decrease the magnitude of the wing interference on the fuselage pitching-moment coefficients (fig. 51). At a Mach number of 0.8, the wing interference accounted for about 47 percent of the positive pitching-moment coefficient of the fuselage in the presence of the wing. At a Mach number of 0.93 only 24 percent can be attributed to the presence of the wing. With reference to figure 34, the center of pressure of the incremental loading on the fuselage due to the wing moved rearward toward the pitching-moment axis (the 0.25-chord position of the mean aerodynamic chord) with increase in Mach number and tended to decrease the fuselage positive pitching-moment coefficients.

Pressure-Drag Characteristics

The pressure-drag coefficient on the outboard section of the wing at an angle of attack of 4° was much less than the coefficient for the inboard section at subsonic Mach numbers (fig. 52). The variation at a Mach number of 0.60 was in agreement with the prediction from nonviscous flow theory (reference 10). As pointed out in reference 11, these pressure forces were associated with potential flow and were not a manifestation of losses. They were compensated in potential flow by thrust on the outboard sections. At a Mach number of 1.2, the section pressure-drag coefficient was nearly uniform for the entire semispan. The theory predicted that the pressure drag for the inboard sections at supersonic speeds should be considerably greater than for the outboard sections. The difference was due to the fact that the separation for the outboard sections was more severe than inboard (see figs. 9 to 17 and reference 11).

The pressure-drag coefficient for the isolated fuselage exhibited very little change with increase in Mach number up to 0.96 throughout the angle-of-attack range investigated. The pressure-drag-coefficient rise appeared to take place between Mach numbers of 0.96 and 1.2 (fig. 53). The pressure-drag coefficients of the wing-fuselage combination indicated the same effects of Mach number as in reference 3. For example, the force break at an angle of attack of 4° occurred approximately at a Mach number of 0.90 as shown in figure 54.

[redacted]

The fuselage pressure-drag coefficient at zero lift was compared with the drag determined from free-fall data (reference 13) and wind-tunnel force tests (reference 3) in figure 55. A fuselage base-pressure correction was subtracted from the tunnel force-test data so those data would be directly comparable with that obtained by integrating the external pressures of the present investigation. Although the body in the free-fall tests had a shorter portion cut off at the rear, the data were in agreement. The data also have been compared with theoretical pressure drag computed from reference 17. Although this theoretical value is independent of Mach number at supersonic Mach numbers, it was considered to be in satisfactory agreement with the experimental data from a Mach number of 1.05 up to the highest velocities tested.

Fuselage Skin-Friction Drag

The variation with Mach number of skin-friction drag for the fuselage was determined as the difference between the Langley 8-foot high-speed-tunnel force-test drag-coefficient and the Langley 8-foot high-speed-tunnel pressure-drag-coefficient curves of figure 55 and is presented in figure 56. The skin-friction drag coefficient did not vary appreciably with Mach number. The experimental values of skin-friction drag coefficient are compared with theoretical values calculated by the method of reference 17, for the case of transition at the nose. Also included are the skin-friction-drag-coefficient values obtained from free-fall tests. Agreement was obtained between the theoretical result for transition at the nose and the experimental data up to the highest Mach number tested. Further comparison was impossible because the point of transition was not known.

The free-fall data were obtained at Reynolds numbers between 1×10^6 and 6×10^6. The pressure data for the tunnel model were obtained at a Reynolds number of about 2×10^6.

CONCLUSIONS

The pressure-distribution investigation of a fuselage and a wing-fuselage combination employing a wing with 45° sweepback of the 0.25-chord line, aspect ratio 4, taper ratio 0.6, and NACA 65A006 airfoil sections at high subsonic Mach numbers and at a Mach number of 1.2 indicated that:

1. Pressure distributions indicative of leading-edge separation-vortex flow noted at low speeds were also observed at the high subsonic Mach numbers. Separation over the outboard sections of the wing spread inboard with increase in angle of attack. Increasing the Mach number delayed the spread of this separation.

2. The spanwise loading shifted slightly outboard at angles of attack below 8° when the Mach number was increased from 0.90 to 1.2. At higher angles of attack, the peak load coefficient increased and shifted inboard due to inboard spread of the separation region at the wing tip.

3. The pressures on the rear portion of the chord of the wing stations nearest the fuselage exerted the most influence on the fuselage pressure distributions. The minimum-pressure peaks on the wing leading edge near the wing-fuselage juncture appeared to be localized on the wing.

4. The load on the fuselage was affected by the wing in front of and behind the wing-fuselage juncture at subsonic speeds with the majority of the load in the region directly above the juncture. The center of the load increment on the fuselage produced by the wing moved rearward with increase in Mach number.

5. The load on the fuselage in the wing-fuselage combination was approximately 10 times greater than the load on the isolated fuselage at the same angle of attack and Mach number. At normal-force coefficients up to 0.7 and Mach numbers up to 0.90, approximately 16.5 percent of the total load on the wing-fuselage combination was carried by the fuselage. At normal-force coefficients up to 0.4, the fuselage carried about 14.5 percent of the total load at a Mach number of 1.2.

Langley Aeronautical Laboratory
National Advisory Committee for Aeronautics
Langley Field, Va.

[redacted]

REFERENCES

1. Cahn, Maurice S., and Bryan, Carroll R.: A Transonic-Wing Investigation in the Langley 8-Foot High-Speed Tunnel at High Subsonic Mach Numbers and at a Mach Number of 1.2. Wing-Fuselage Configuration Having a Wing of 0° Sweepback, Aspect Ratio 4.0, Taper Ratio 0.6, and NACA 65A006 Airfoil Section. NACA RM L51A02, 1951.

2. Henry, Beverly Z., Jr.: A Transonic Wing Investigation in the Langley 8-Foot High-Speed Tunnel at High Subsonic Mach Numbers and at a Mach Number of 1.2. Wing-Fuselage Configuration Having a Wing of 35° Sweepback, Aspect Ratio 4, Taper Ratio 0.6, and NACA 65A006 Airfoil Section. NACA RM L50J09, 1950.

3. Osborne, Robert S.: A Transonic-Wing Investigation in the Langley 8-Foot High-Speed Tunnel at High Subsonic Mach Numbers and at a Mach Number of 1.2. Wing-Fuselage Configuration Having a Wing of 45° Sweepback, Aspect Ratio 4, Taper Ratio 0.6, and NACA 65A006 Airfoil Section. NACA RM L50H08, 1950.

4. Wood, Raymond B., and Fleming, Frank F.: A Transonic-Wing Investigation in the Langley 8-Foot High-Speed Tunnel at High Subsonic Mach Numbers and at a Mach Number of 1.2. Wing-Fuselage Configuration Having a Wing of 60° Sweepback, Aspect Ratio 4, Taper Ratio 0.6, and NACA 65A006 Airfoil Section. NACA RM L50J25, 1951.

5. Ritchie, Virgil S., Wright, Ray H., and Tulin, Marshall P.: An 8-Foot Axisymmetrical Fixed Nozzle for Subsonic Mach Numbers up to 0.99 and for a Supersonic Mach Number of 1.2. NACA RM L50A03a, 1950.

6. Ritchie, Virgil S.: Effects of Certain Flow Nonuniformities on Lift, Drag, and Pitching Moment for a Transonic-Airplane Model Investigated at a Mach Number of 1.2 in a Nozzle of Circular Cross Section. NACA RM L9E20a, 1949.

7. Lange, Roy H., Whittle, Edward F., Jr., and Fink, Marvin P.: Investigation at Large Scale of the Pressure Distribution and Flow Phenomena over a Wing with the Leading Edge Swept Back 47.5° Having Circular-Arc Airfoil Sections and Equipped with Drooped-Nose and Plain Flaps. NACA RM L9G15, 1949.

8. Johnston, J. Ford, and Danforth, Edward C. B.: Some Pressure-Distribution Measurements on a Swept Wing at Transonic Speeds by the NACA Wing-Flow Method. NACA RM L7D22, 1947.

9. Lindsey, W. F., Daley, Bernard N., and Humphreys, Milton D.: The Flow and Force Characteristics of Supersonic Airfoils at High Subsonic Speeds. NACA TN 1211, 1947.

10. Jones, Robert T.: Subsonic Flow over Thin Oblique Airfoils at Zero Lift. NACA Rep. 902, 1948.

11. Whitcomb, Richard T.: An Experimental Study at Moderate and High Subsonic Speeds of the Flow over Wings with 30° and 45° of Sweepback in Conjunction with a Fuselage. NACA RM L50K27, 1951.

12. Thompson, Jim Rogers: A Rapid Graphical Method for Computing the Pressure Distribution at Supersonic Speeds on a Slender Arbitrary Body of Revolution. NACA TN 1768, 1949.

13. Thompson, Jim Rogers: Measurements of the Drag and Pressure Distribution on a Body of Revolution throughout Transition from Subsonic to Supersonic Speeds. NACA RM L9J27, 1950.

14. Edwards, George G., and Boltz, Frederick W.: An Analysis of the Forces and Pressure Distribution on a Wing with the Leading Edge Swept Back 37.25°. NACA RM A9K01, 1950.

15. Tunnel Staff of Aero. Dept.: Low Speed Pressure Distributions on a 59° Swept Wing and Comparison with High Speed Results on a 45° Swept Wing. Rep. No. Aero. 2311, British R.A.E., Feb. 1949.

16. DeYoung, John: Theoretical Additional Span Loading Characteristics of Wings with Arbitrary Sweep, Aspect Ratio, and Taper Ratio. NACA TN 1491, 1947.

17. Young, A. D.: The Calculation of the Total and Skin Friction Drags of Bodies of Revolution at Zero Incidence. R. & M. No. 1874, British A.R.C., 1939.

[redacted]

[redacted]

Wing Details

Airfoil section (parallel to plane of symmetry)	NACA 65A006
Area, sq ft	1
Aspect ratio	4
Taper ratio	0.6
Incidence, deg	0
Dihedral, deg	0
Geometric twist, deg	0

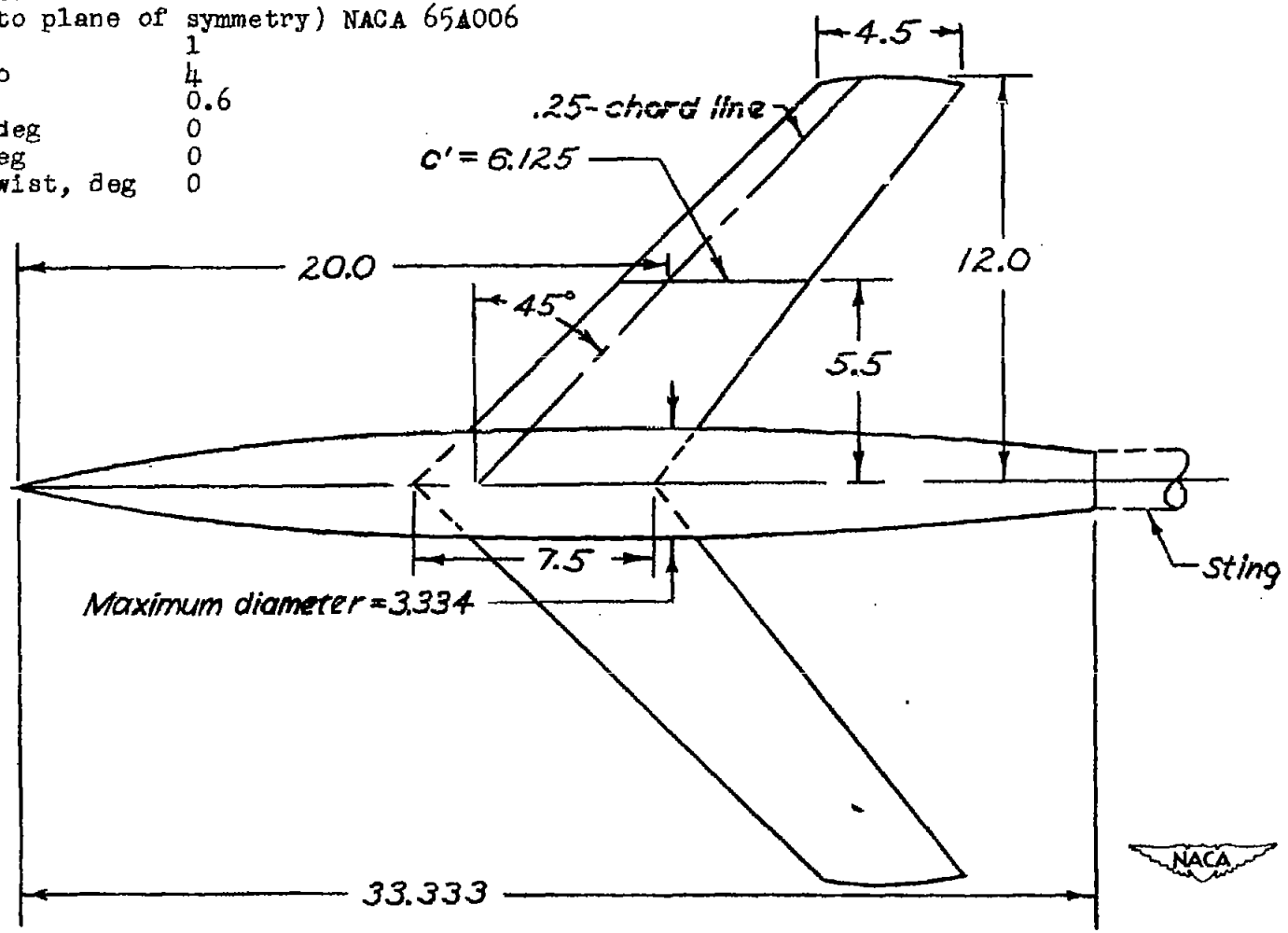

Figure 1.- Model details. All dimensions are in inches.

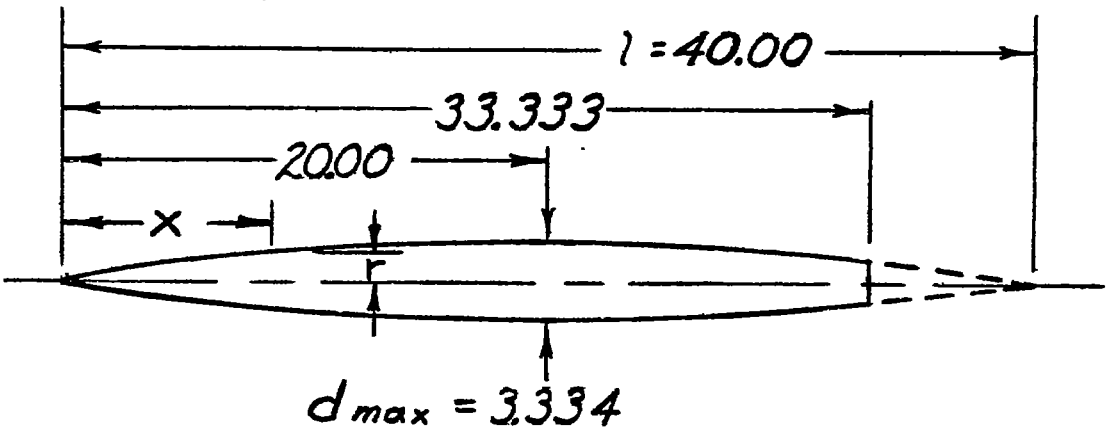

ORDINATES			
x/l	r/l	x/l	r/l
0	0		
.0050	.00231	.4500	.04143
.0075	.00298	.5000	.04167
.0125	.00428	.5500	.04130
.0250	.00722	.6000	.04024
.0500	.01205	.6500	.03842
.0750	.01613	.7000	.03562
.1000	.01971	.7500	.03128
.1500	.02593	.8000	.02526
.2000	.03090	.8333	.02083
.2500	.03465	.8500	.01852
.3000	.03741	.9000	.01125
.3500	.03933	.9500	.00439
.4000	.04063	1.0000	0
L.E. radius = 0.0005l			

NACA

Fineness ratio 10

$\frac{c'}{4}$ located at d_{max}

Figure 2.- Fuselage details. All dimensions are in inches.

Figure 3.- Photograph of the model as tested in the Langley 8-foot high-speed tunnel.

Orifice locations	
Percent chord	
Upper surface	Lower surface
0	0
2.5	2.5
7.5	7.5
15	15
25	25
35	35
45	45
55	55
65	65
75	75
85	85
95	95

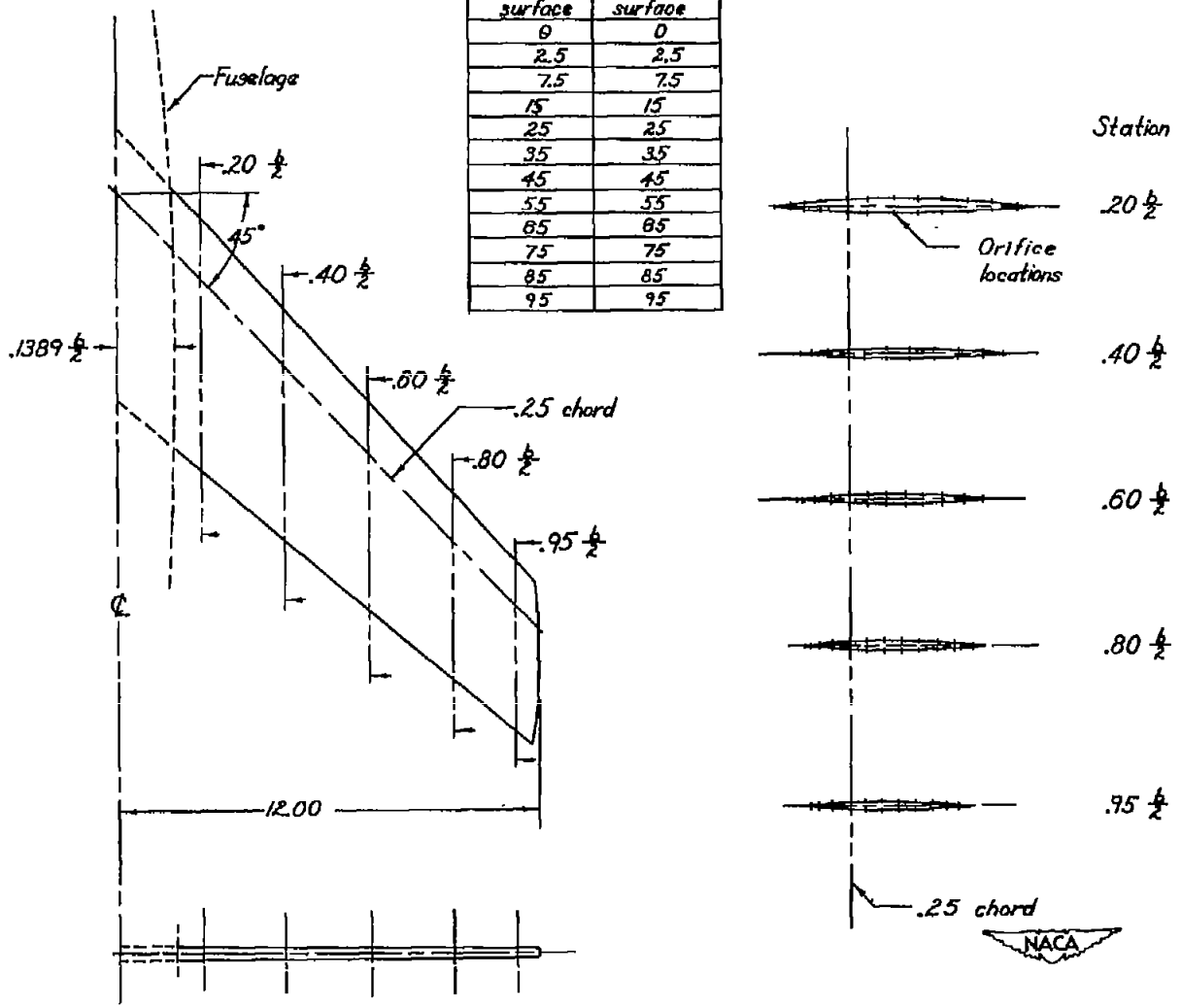

Figure 4.- Location of orifices and dimensions of wing. All dimensions are in inches.

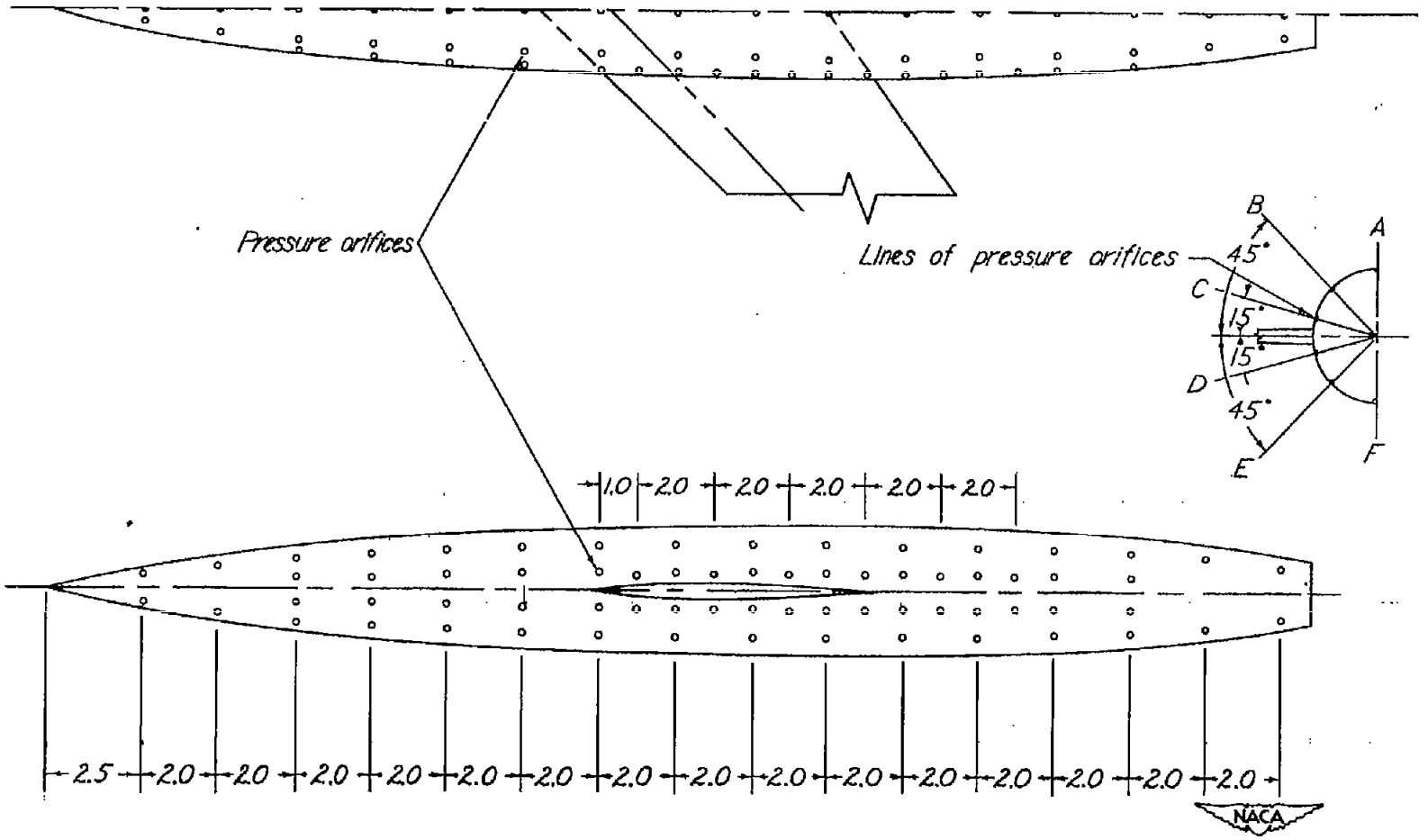

Figure 5.- Location of orifices on fuselage. All dimensions are in inches.

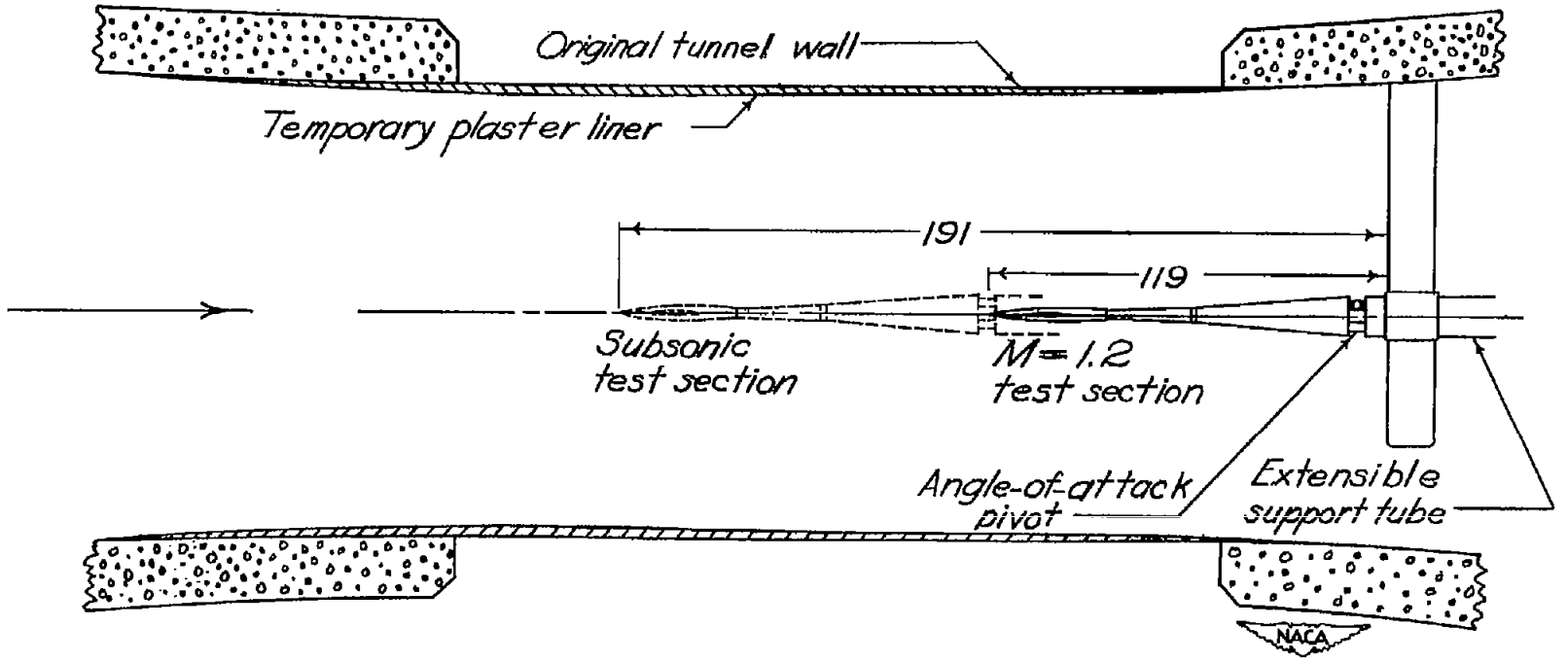

Figure 6.- Diagram showing test-section setup for pressure-model investigation. All dimensions are in inches.

Figure 7.- Photograph of the model and the model support system in the Langley 8-foot high-speed tunnel.

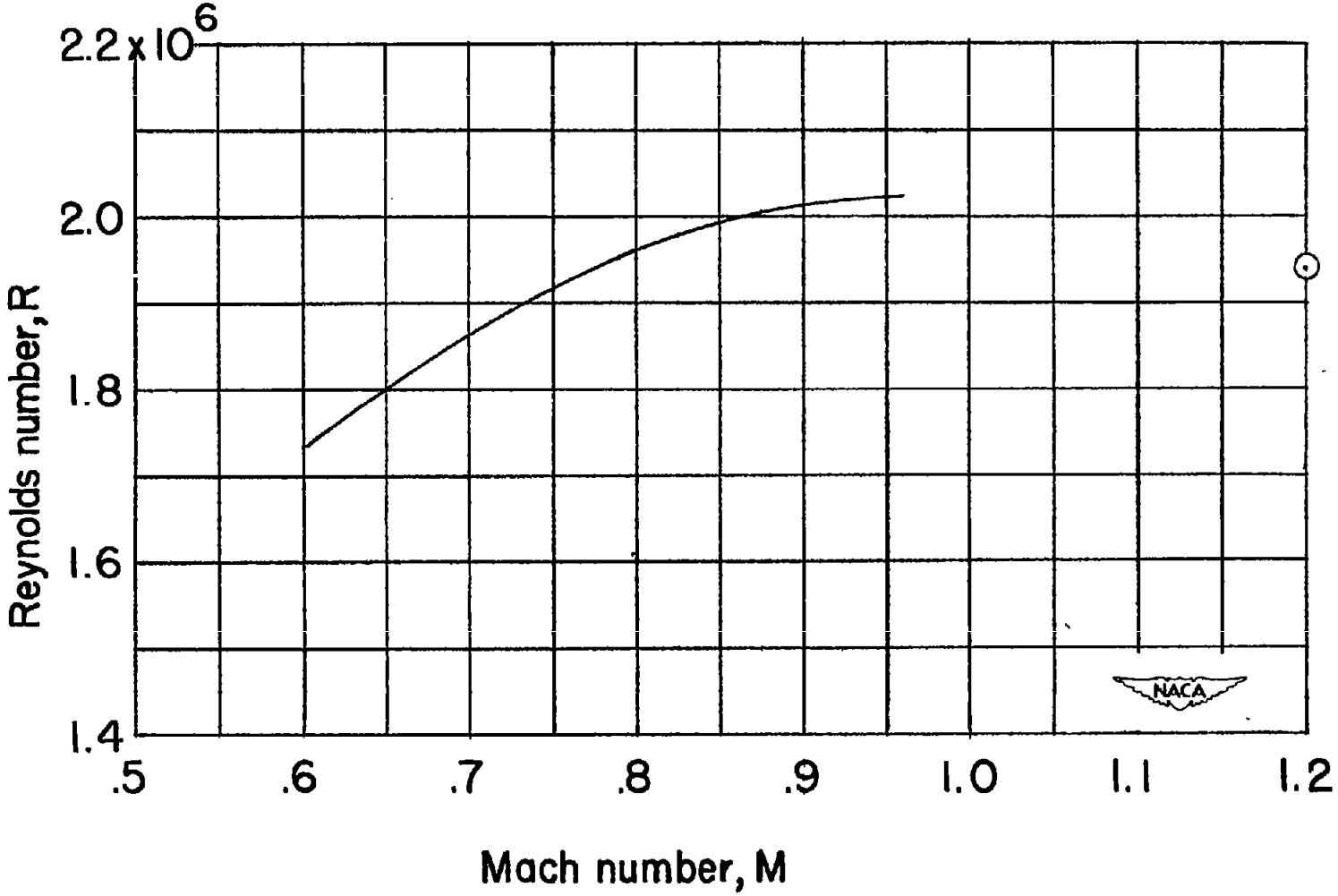

Figure 8.- Variation with Mach number of test Reynolds number based on a mean aerodynamic chord of 6.125 inches.

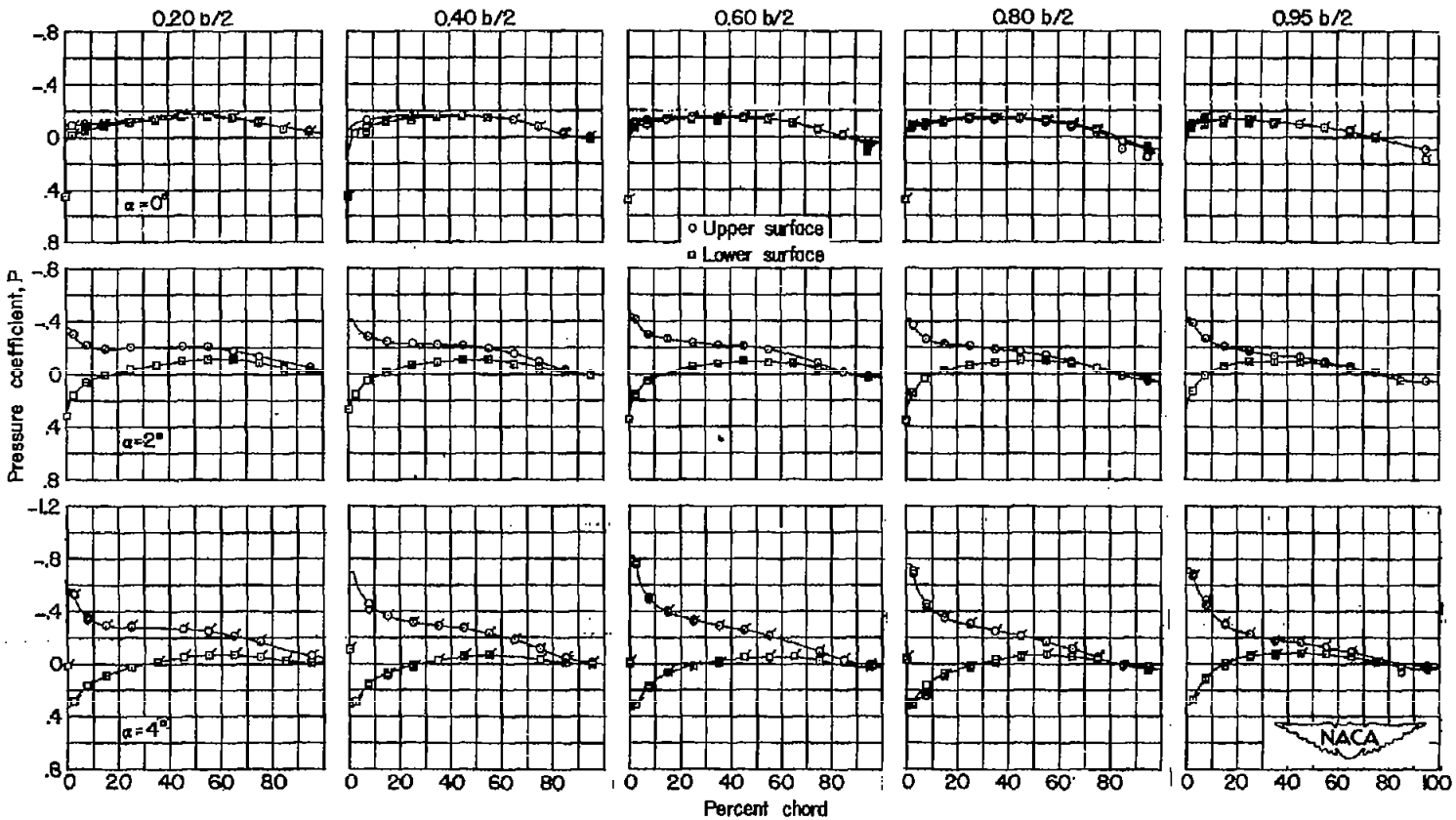

(a) M = 0.60; $\alpha = 0^\circ$, 2°, and 4°.

Figure 9.- The chordwise pressure distributions at five spanwise stations for several angles of attack. (Plain symbols indicate transition natural and flagged symbols indicate transition fixed.)

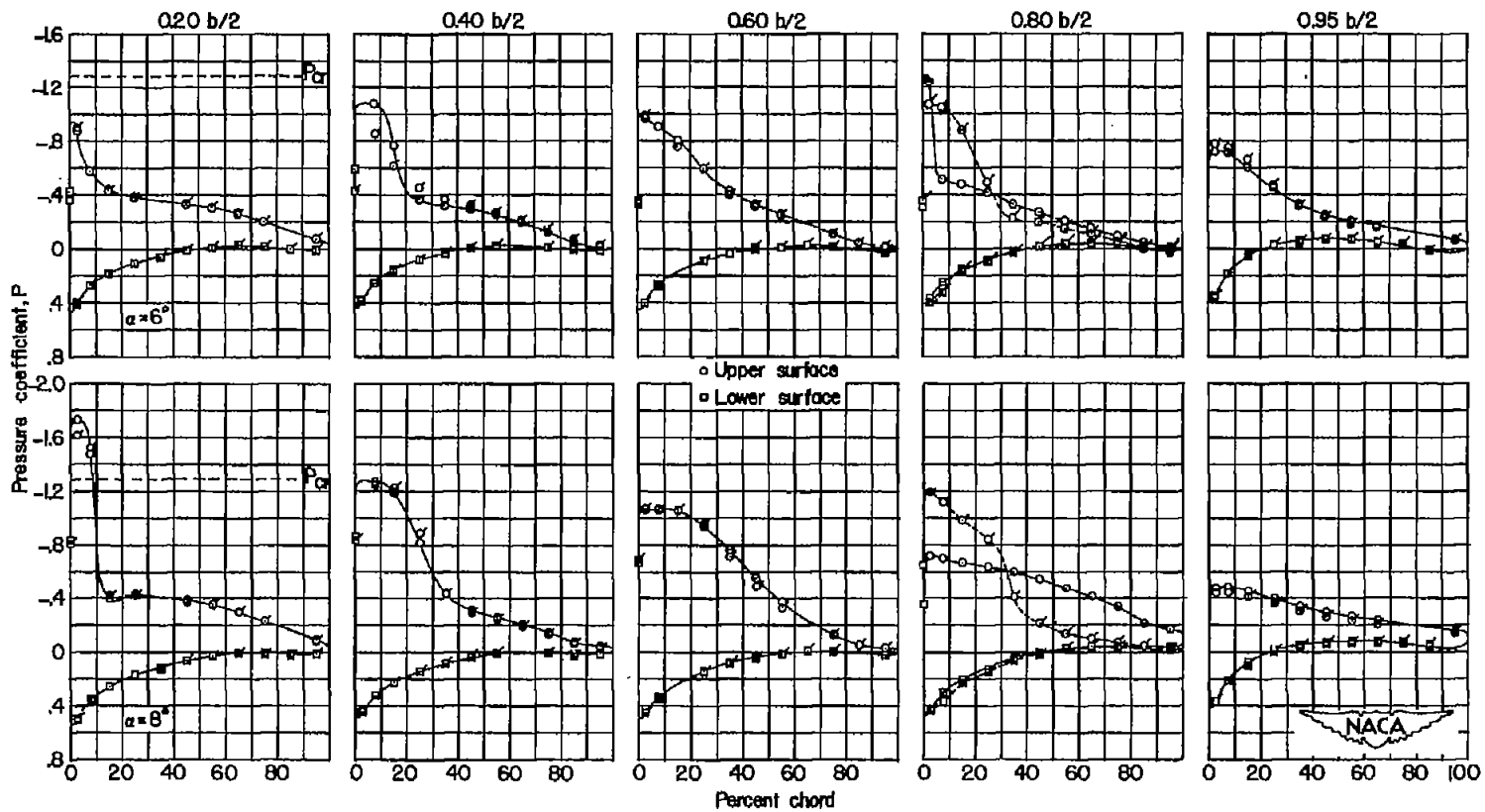

(b) M = 0.60; $\alpha = 6^{\circ}$ and 8°.

Figure 9.- Continued.

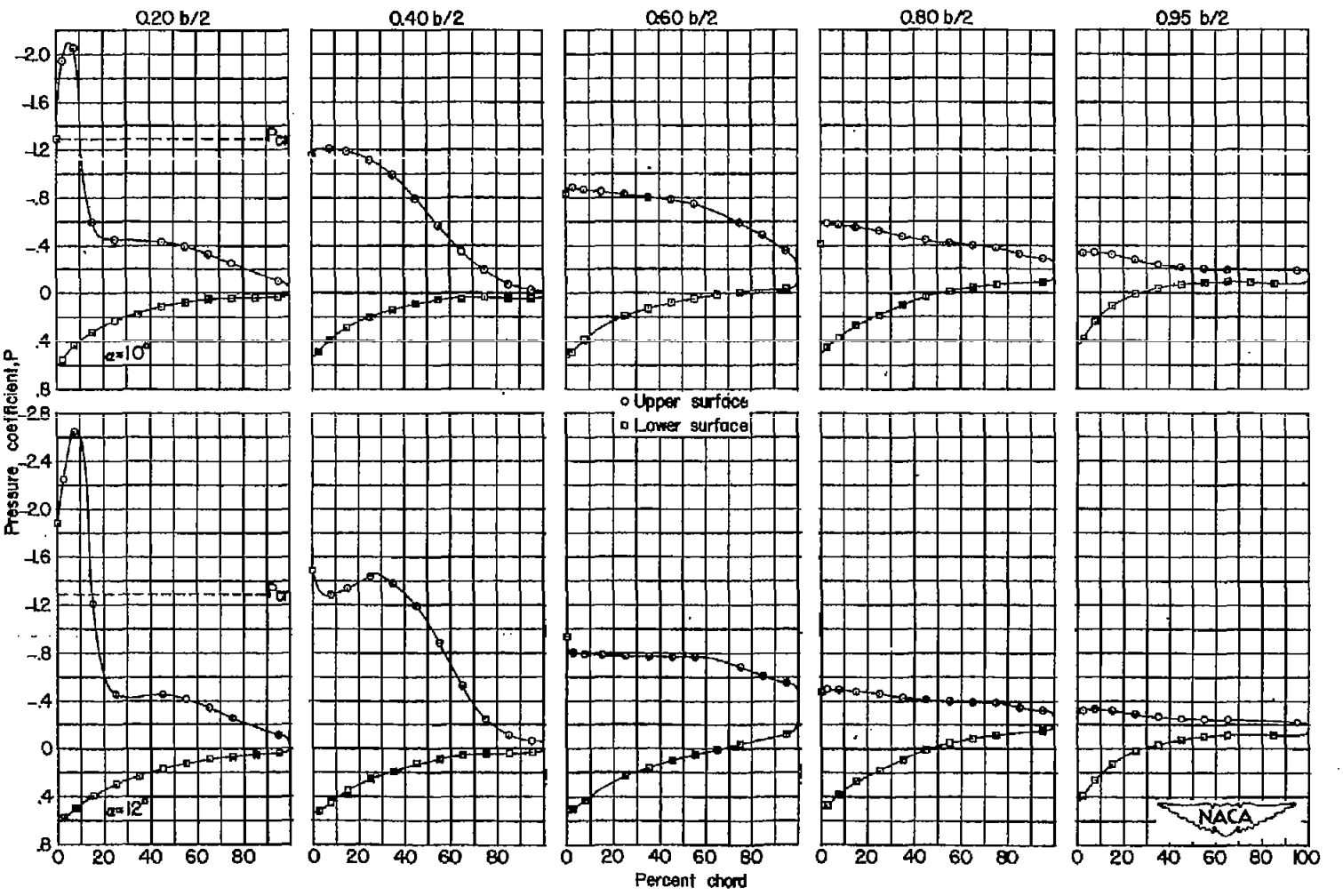

(c) M = 0.60; $\alpha = 10^{\circ}$ and 12°.

Figure 9.- Continued.

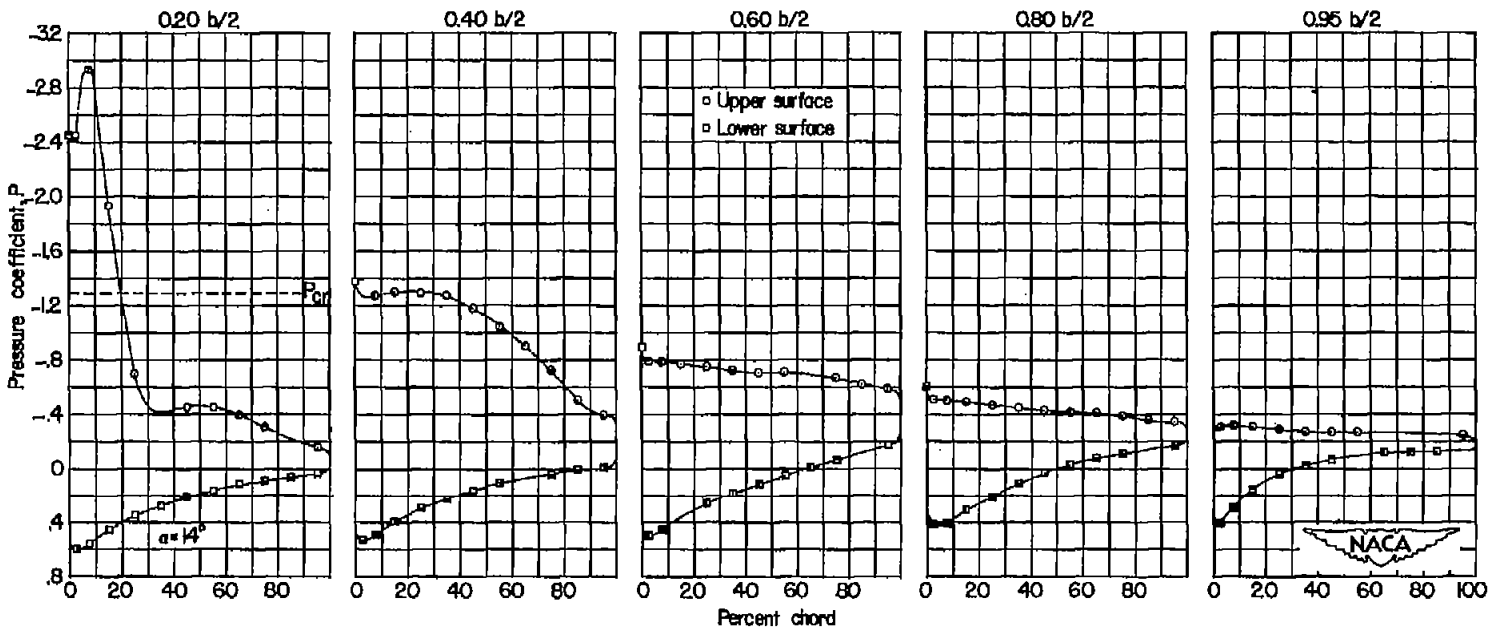

(d) $M = 0.60$; $\alpha = 14^{\circ}$.

Figure 9.- Concluded.

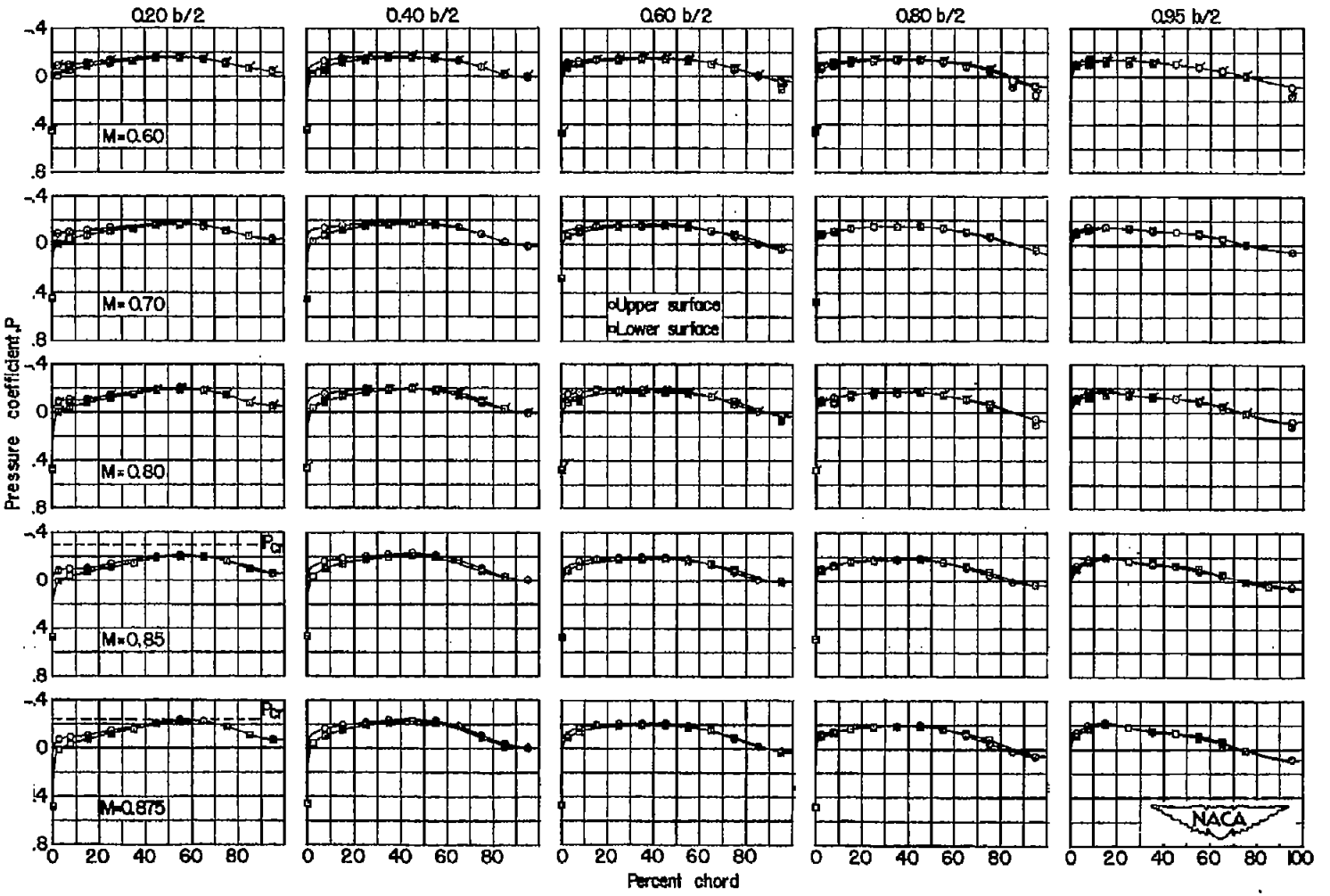

(a) $\alpha = 0^{\circ}$; M = 0.60, 0.70, 0.80, 0.85, and 0.875.

Figure 10.- The chordwise pressure distributions at five spanwise stations for several Mach numbers. (Plain symbols indicate transition natural and flagged symbols indicate transition fixed.)

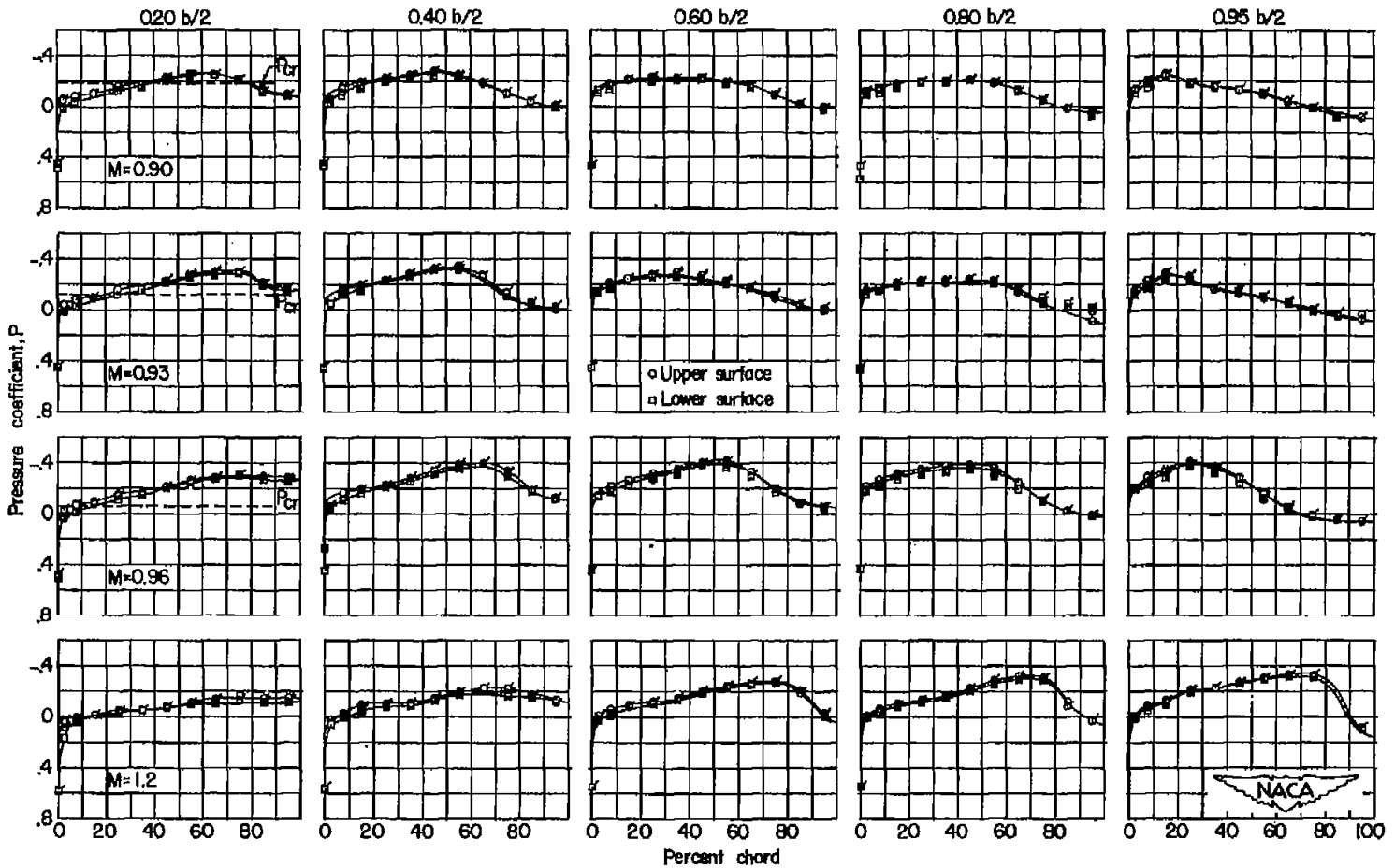

(b) $\alpha = 0^{\circ}$; M = 0.90, 0.93, 0.96, and 1.2.

Figure 10.- Concluded.

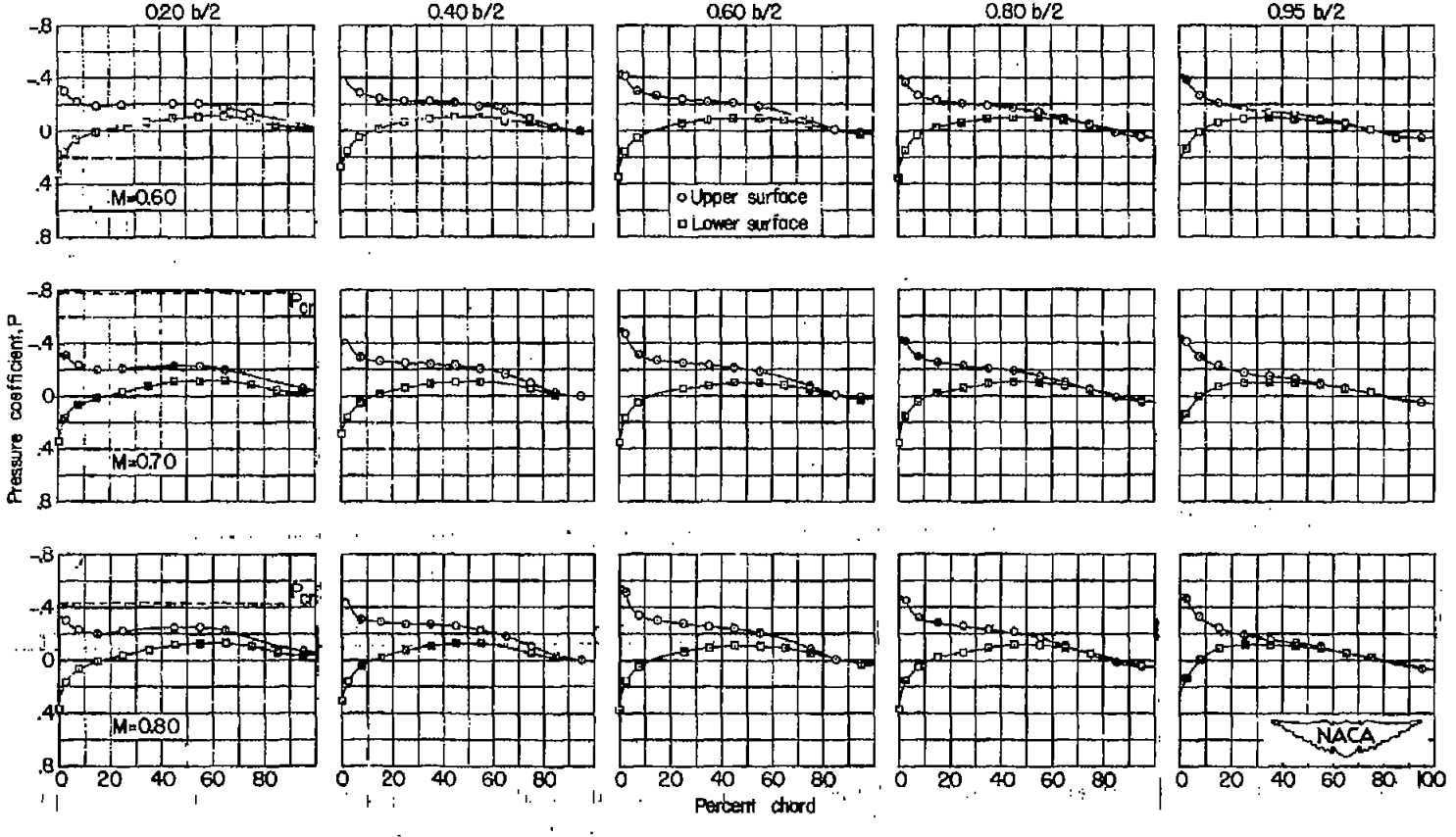

(a) $\alpha = 2^{\circ}$; M = 0.60, 0.70, and 0.80.

Figure 11.- The chordwise pressure distributions at five spanwise stations for several Mach numbers.

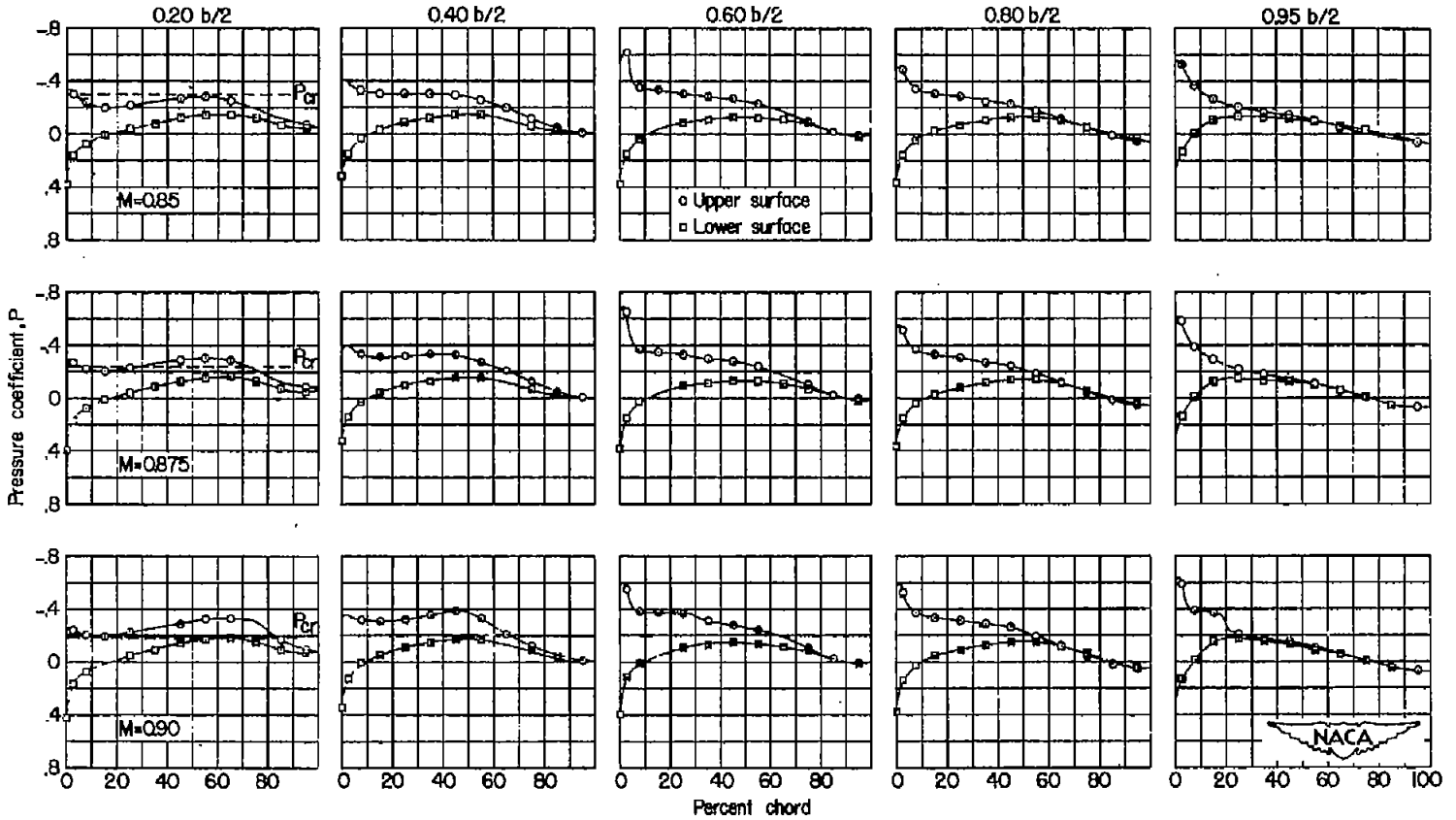

(b) $\alpha = 2^{\circ}$; M = 0.85, 0.875, and 0.90.

Figure 11.- Continued.

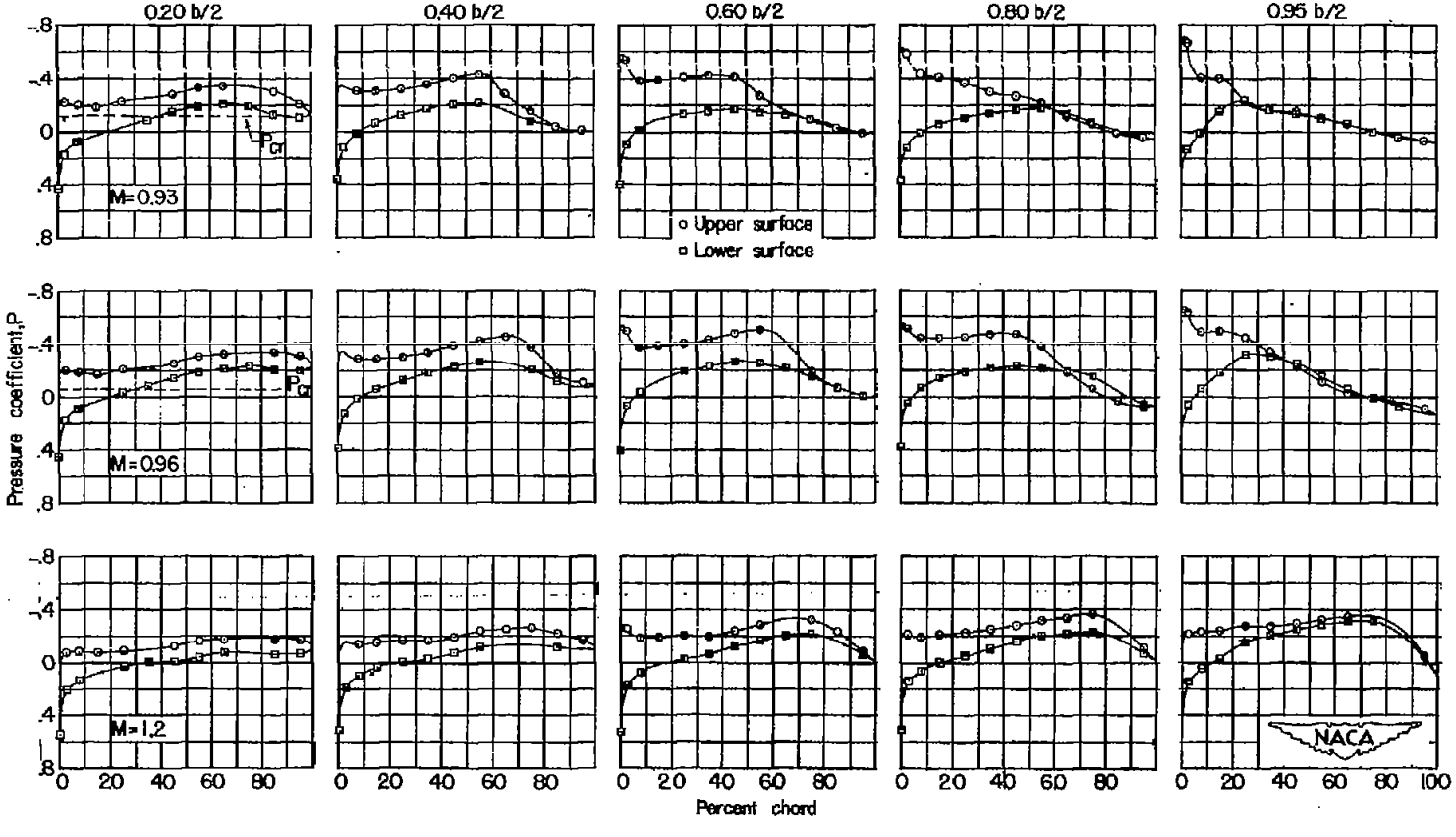

(c) $\alpha = 2^{\circ}$; M = 0.93, 0.96, and 1.2.

Figure 11.- Concluded.

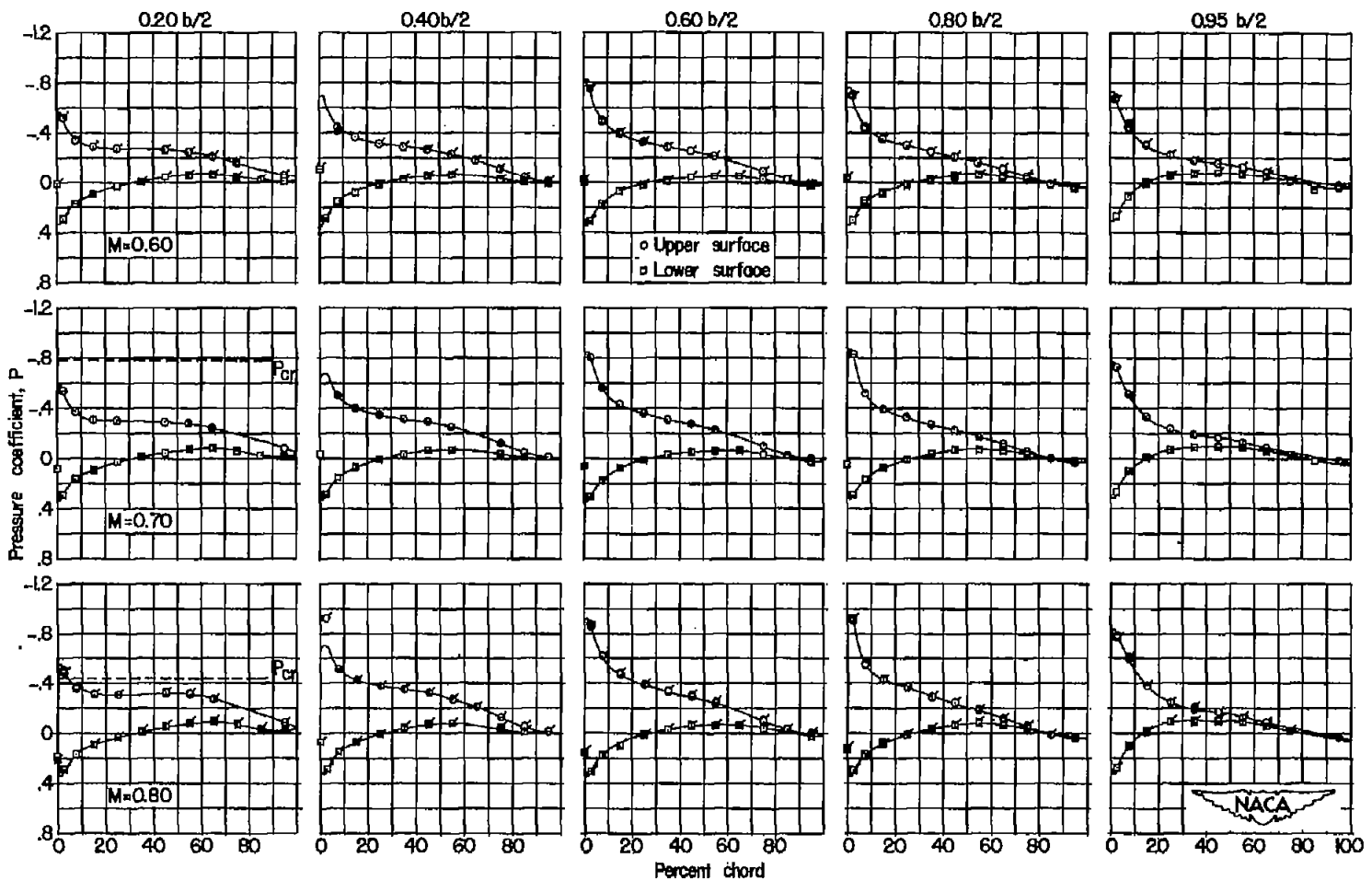

(a) $\alpha = 4^{\circ}$; M = 0.60, 0.70, and 0.80.

Figure 12.- The chordwise pressure distributions at five spanwise stations for several Mach numbers. (Plain symbols indicate transition natural and flagged symbols indicate transition fixed.)

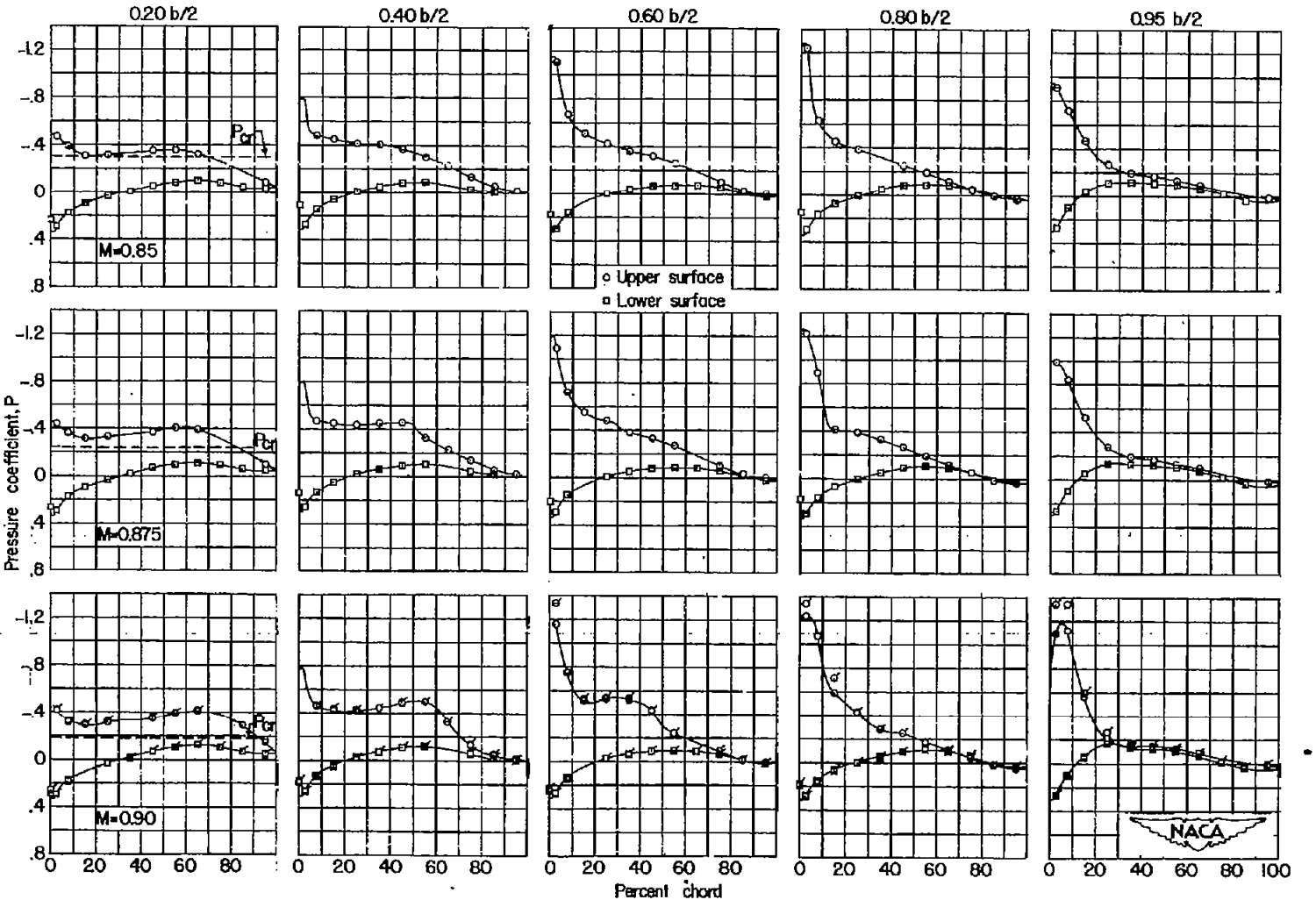

(b) $\alpha = 4^{\circ}$; M = 0.85, 0.875, and 0.90.

Figure 12.- Continued.

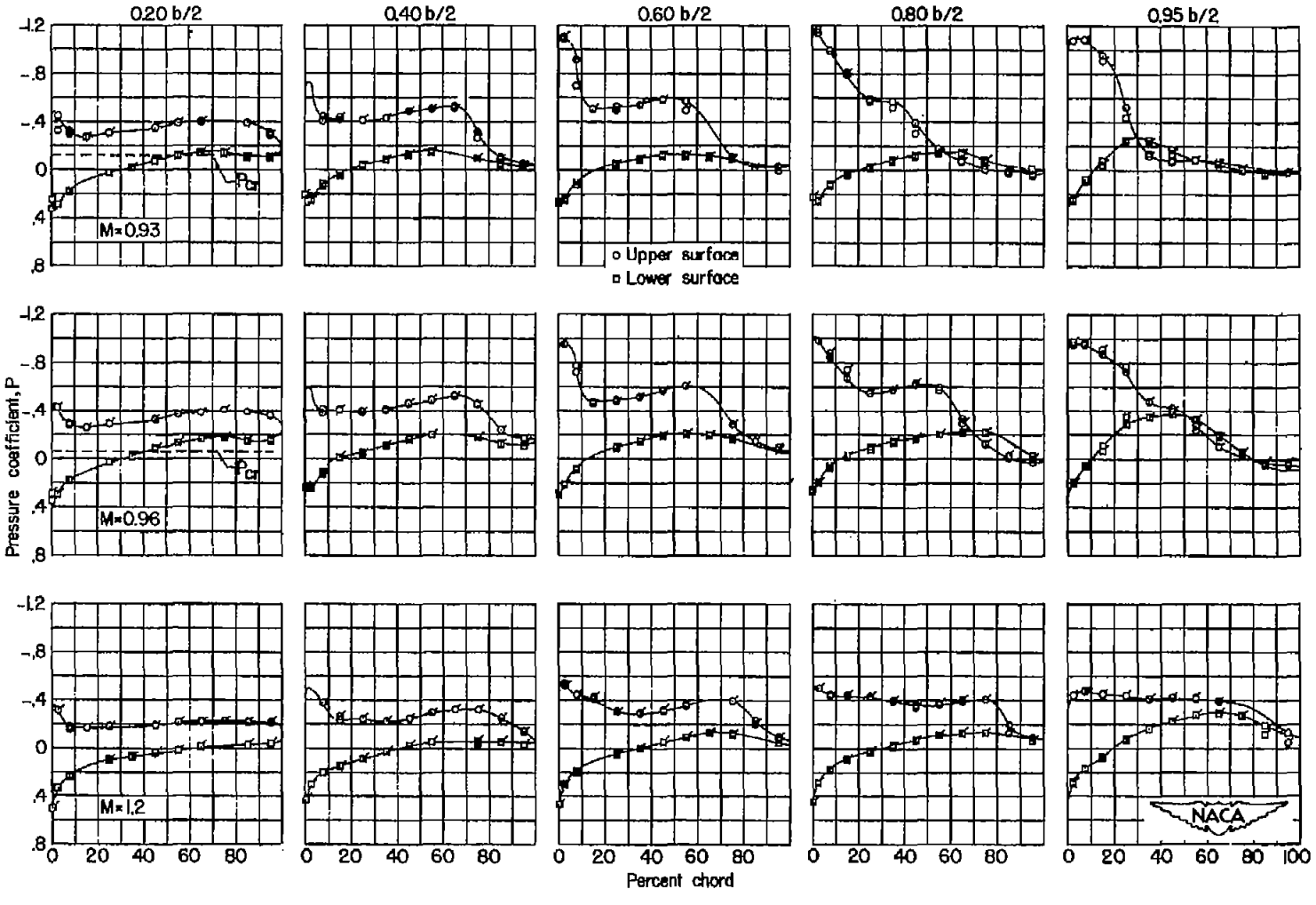

(c) $\alpha = 4^{\circ}$; M = 0.93, 0.96, and 1.2.

Figure 12.- Concluded.

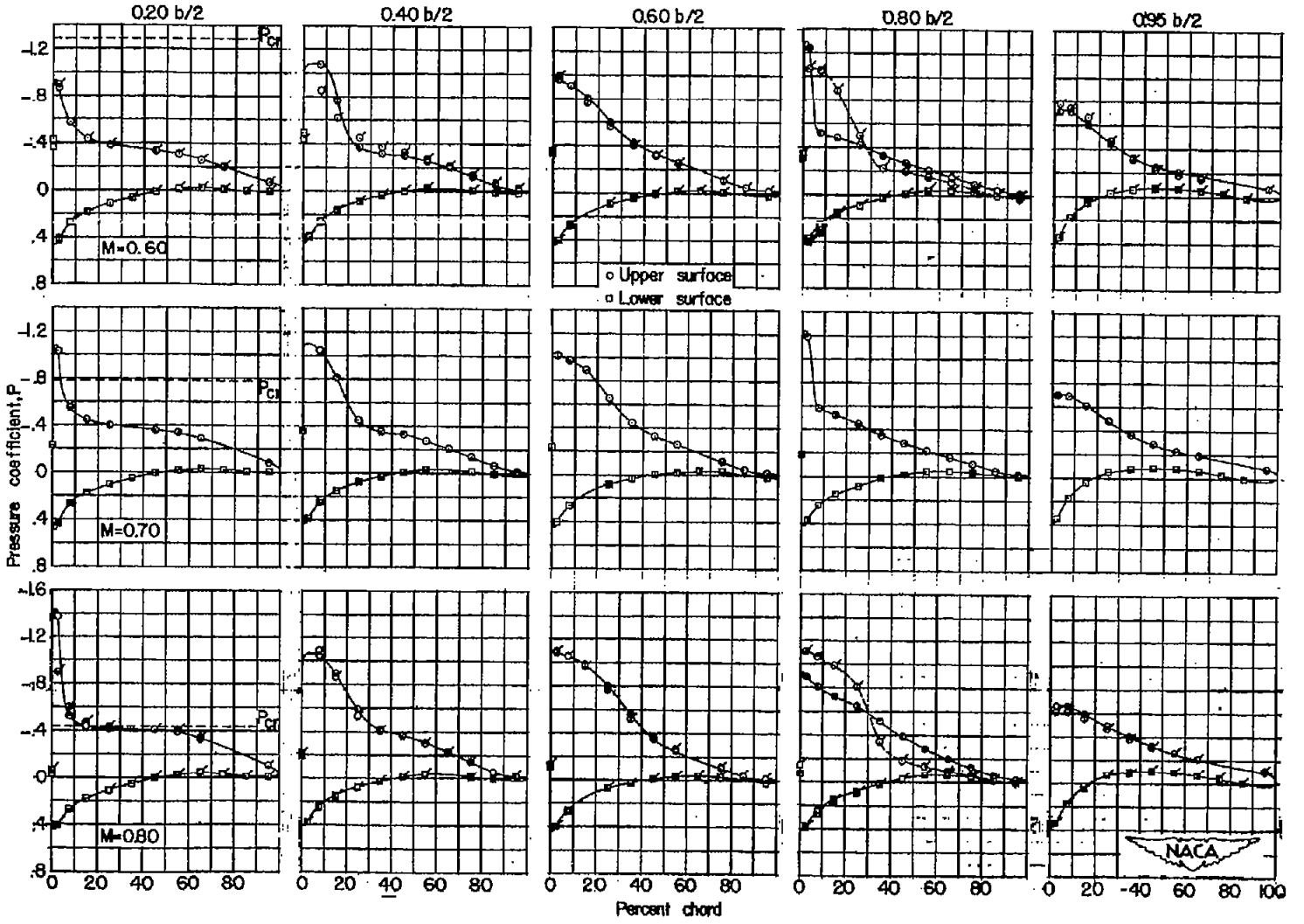

(a) $\alpha = 6^{\circ}$; M = 0.60, 0.70, and 0.80.

Figure 13.- The chordwise pressure distributions at five spanwise stations for several Mach numbers. (Plain symbols indicate transition natural and flagged symbols indicate transition fixed.)

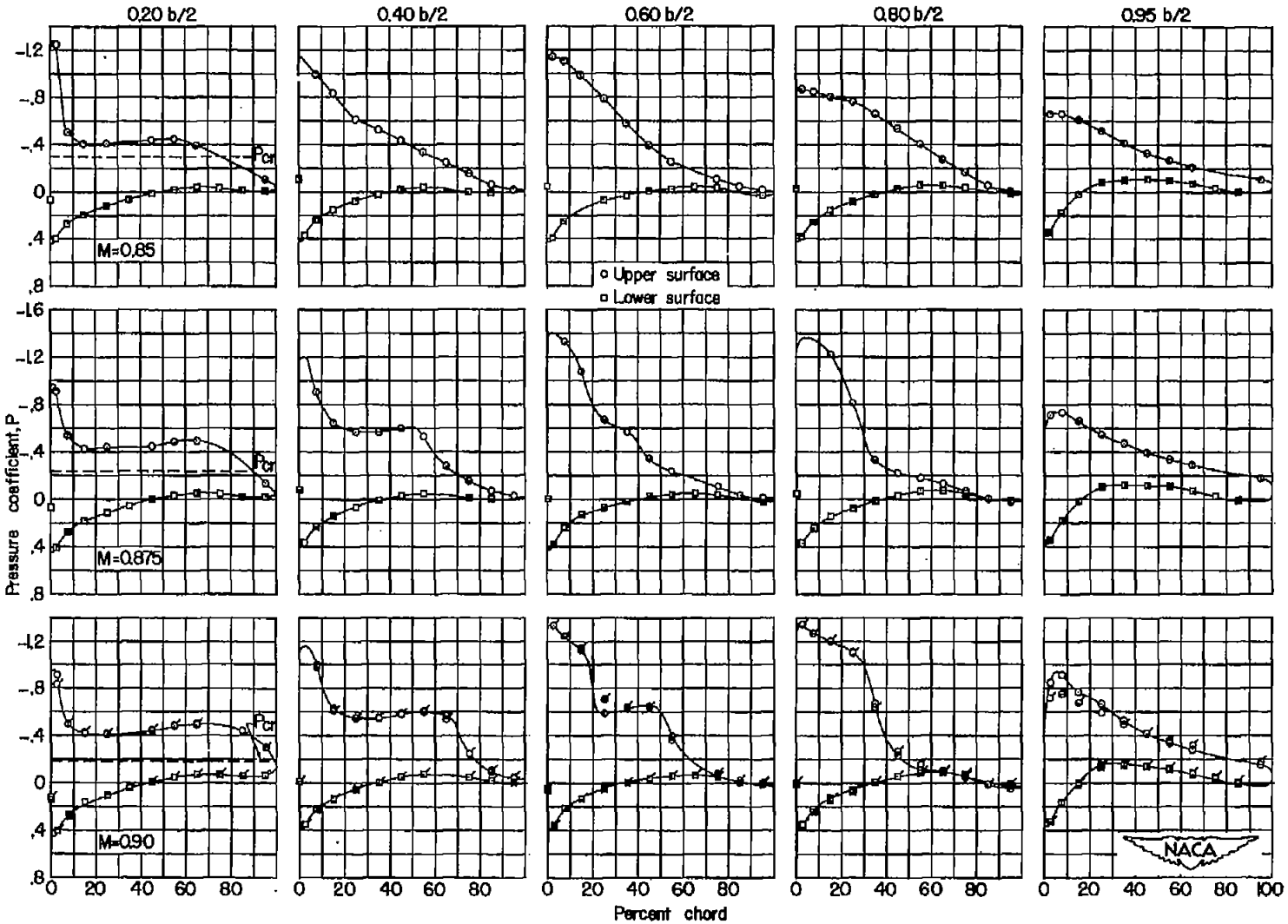

(b) $\alpha = 6^{\circ}$; M = 0.85, 0.875, and 0.90.

Figure 13.- Continued.

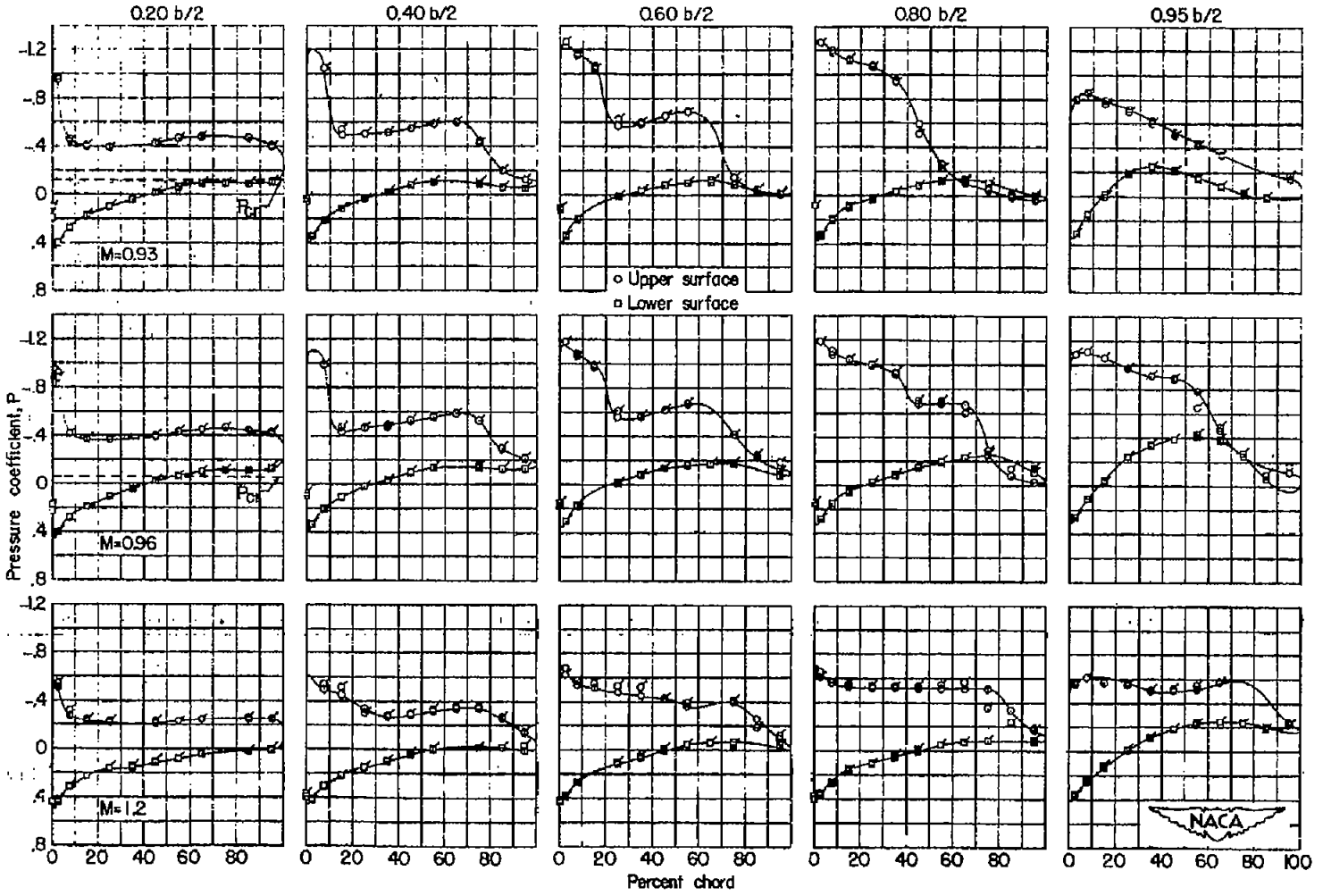

(c) $\alpha = 6^{\circ}$; M = 0.93, 0.96, and 1.2.

Figure 13.- Concluded.

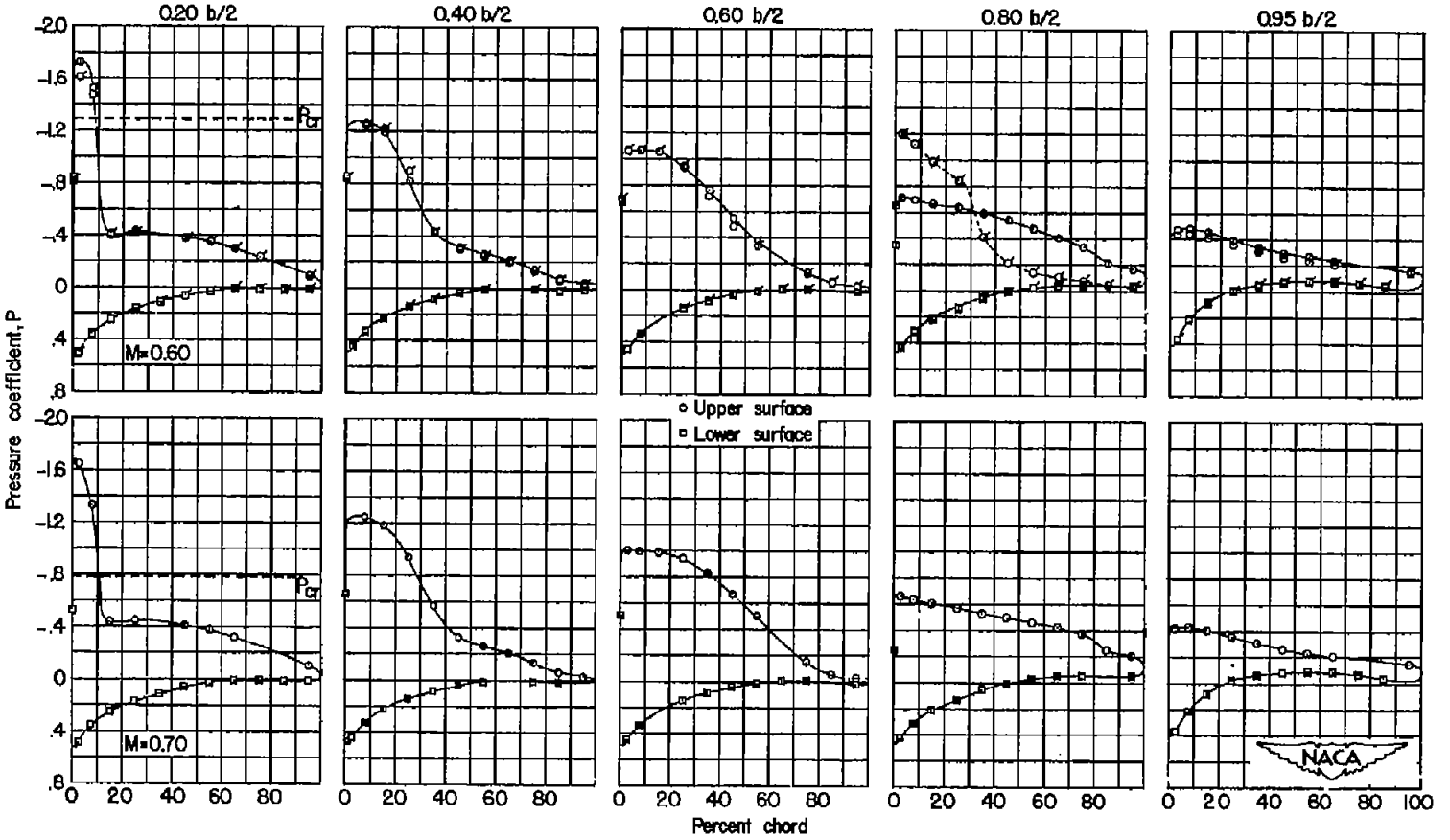

(a) $\alpha = 8^{\circ}$; M = 0.60 and 0.70.

Figure 14.- The chordwise pressure distributions at five spanwise stations for several Mach numbers. (Plain symbols indicate transition natural and flagged symbols indicate transition fixed.)

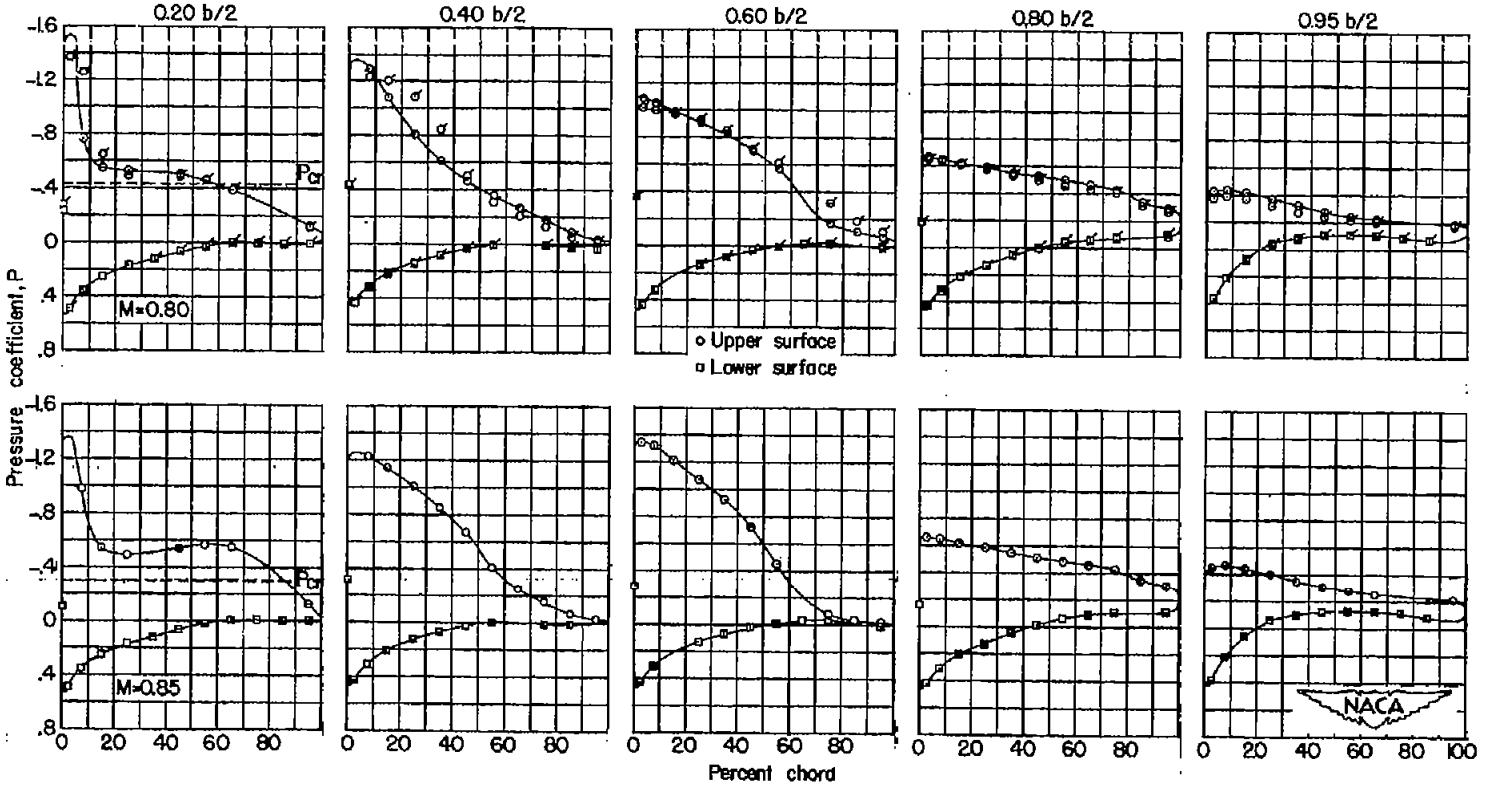

(b) $\alpha = 8^{\circ}$; M = 0.80 and 0.85.

Figure 14.- Continued.

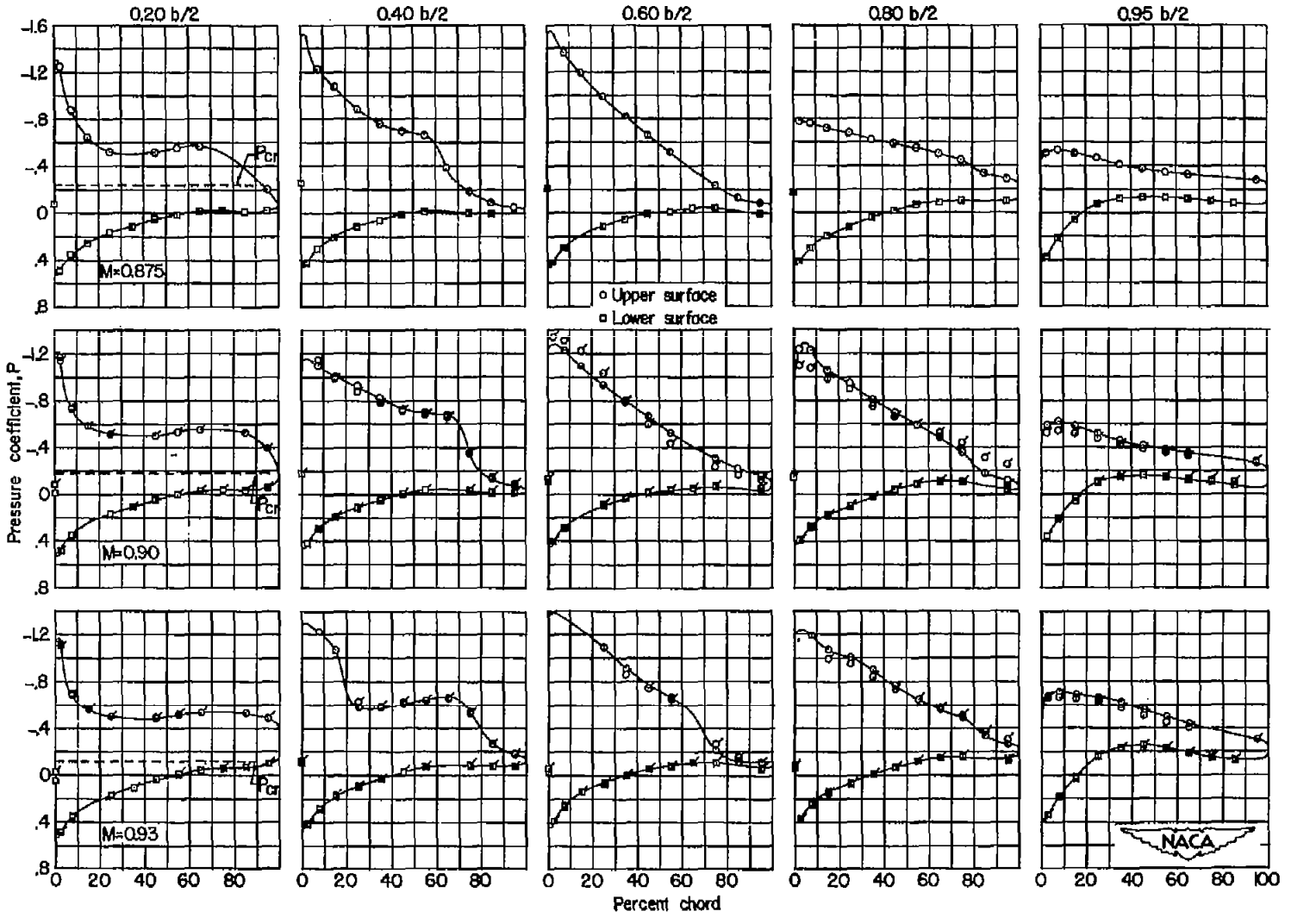

(c) $\alpha = 8^{\circ}$; M = 0.875, 0.90, and 0.93.

Figure 14.- Concluded.

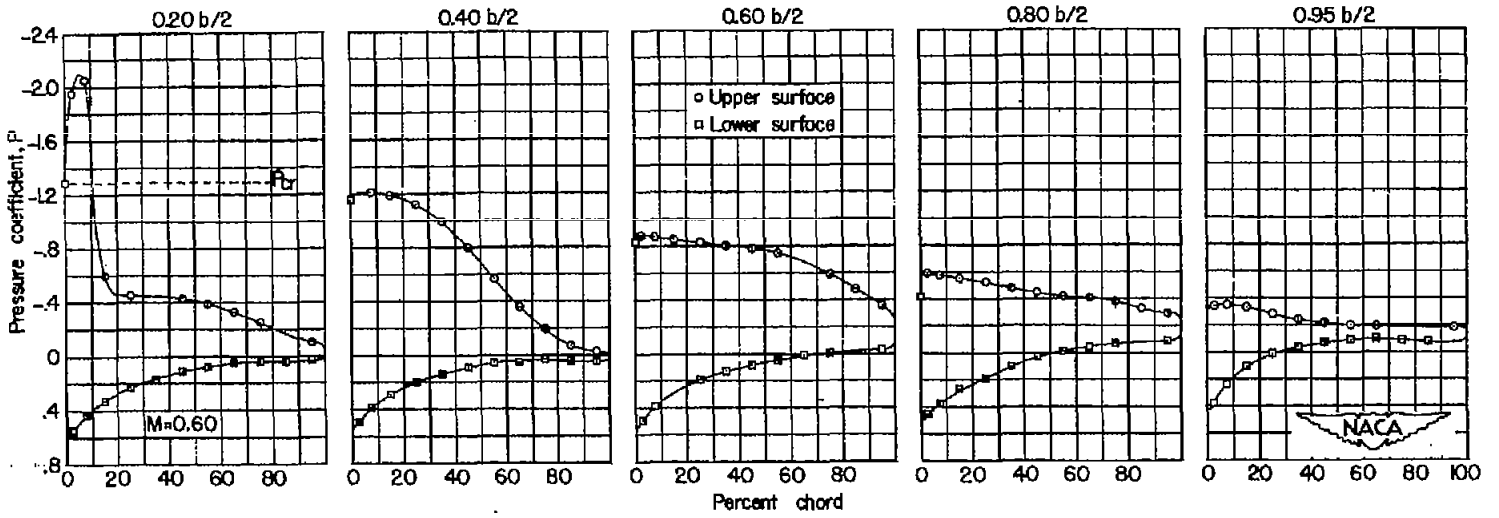

(a) $\alpha = 10^\circ$; $M = 0.60$.

Figure 15.- The chordwise pressure distributions at five spanwise stations for several Mach numbers.

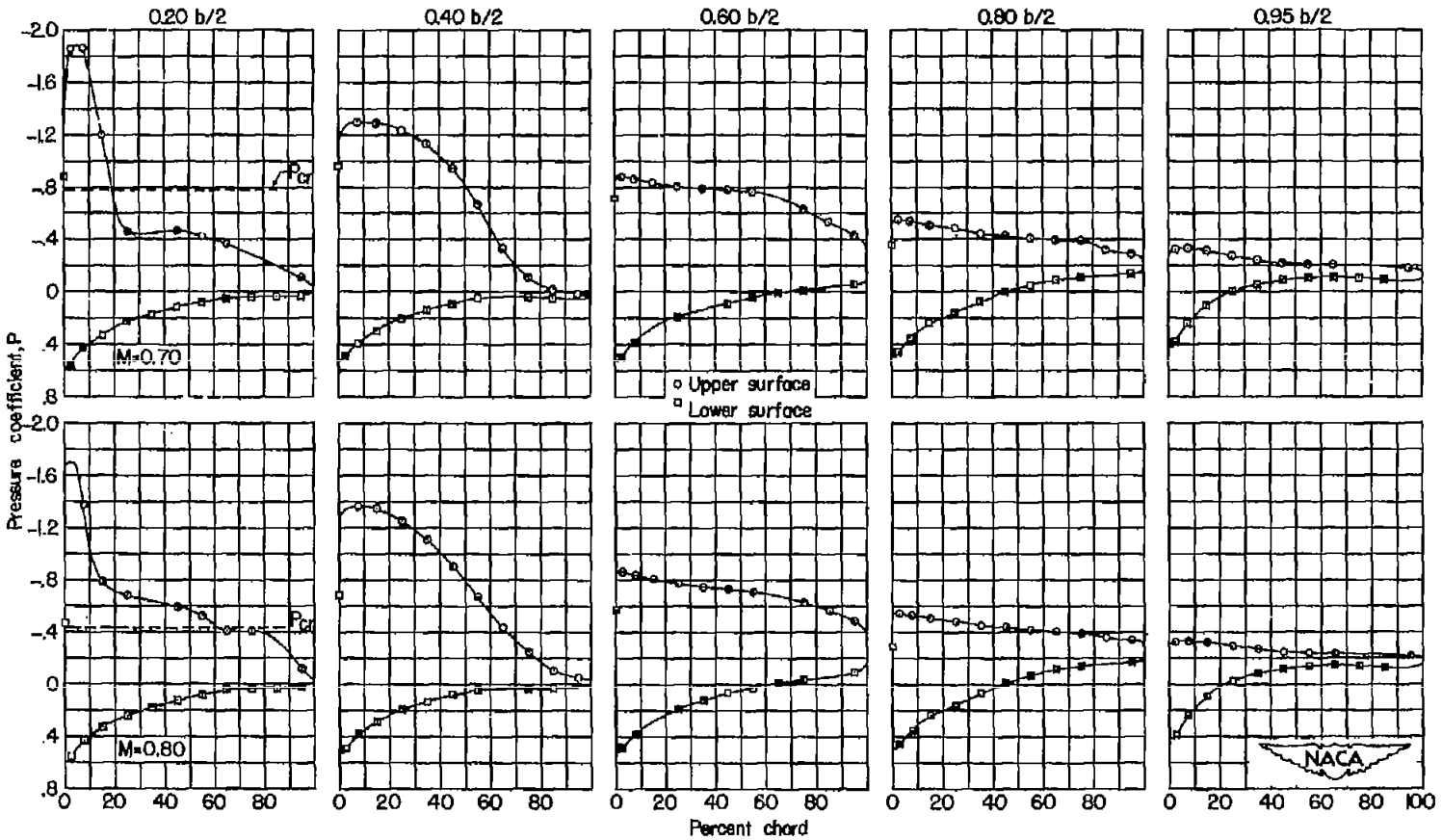

(b) $\alpha = 10^{\circ}$; M = 0.70 and 0.80.

Figure 15.- Continued.

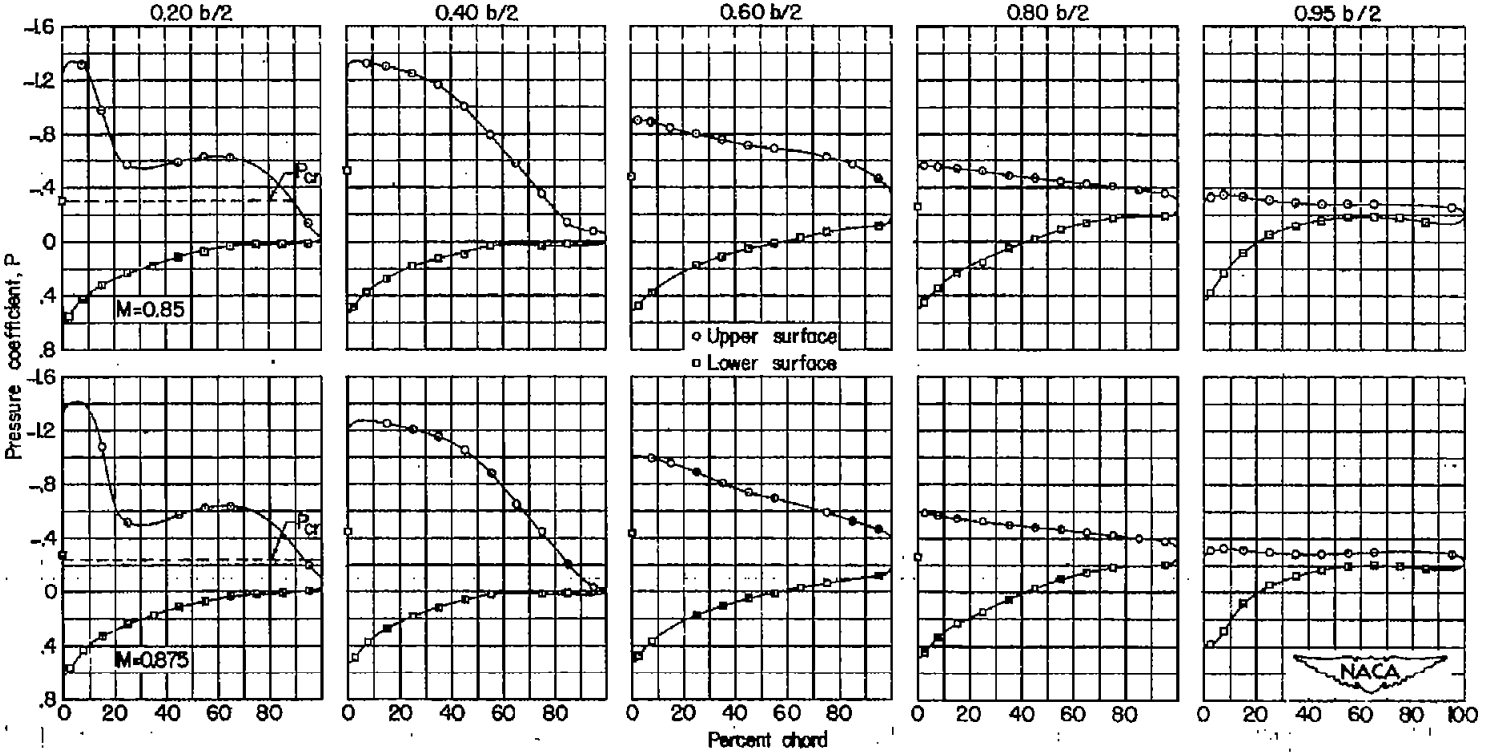

(c) $\alpha = 10^{\circ}$; M = 0.85 and 0.875.

Figure 15.- Continued.

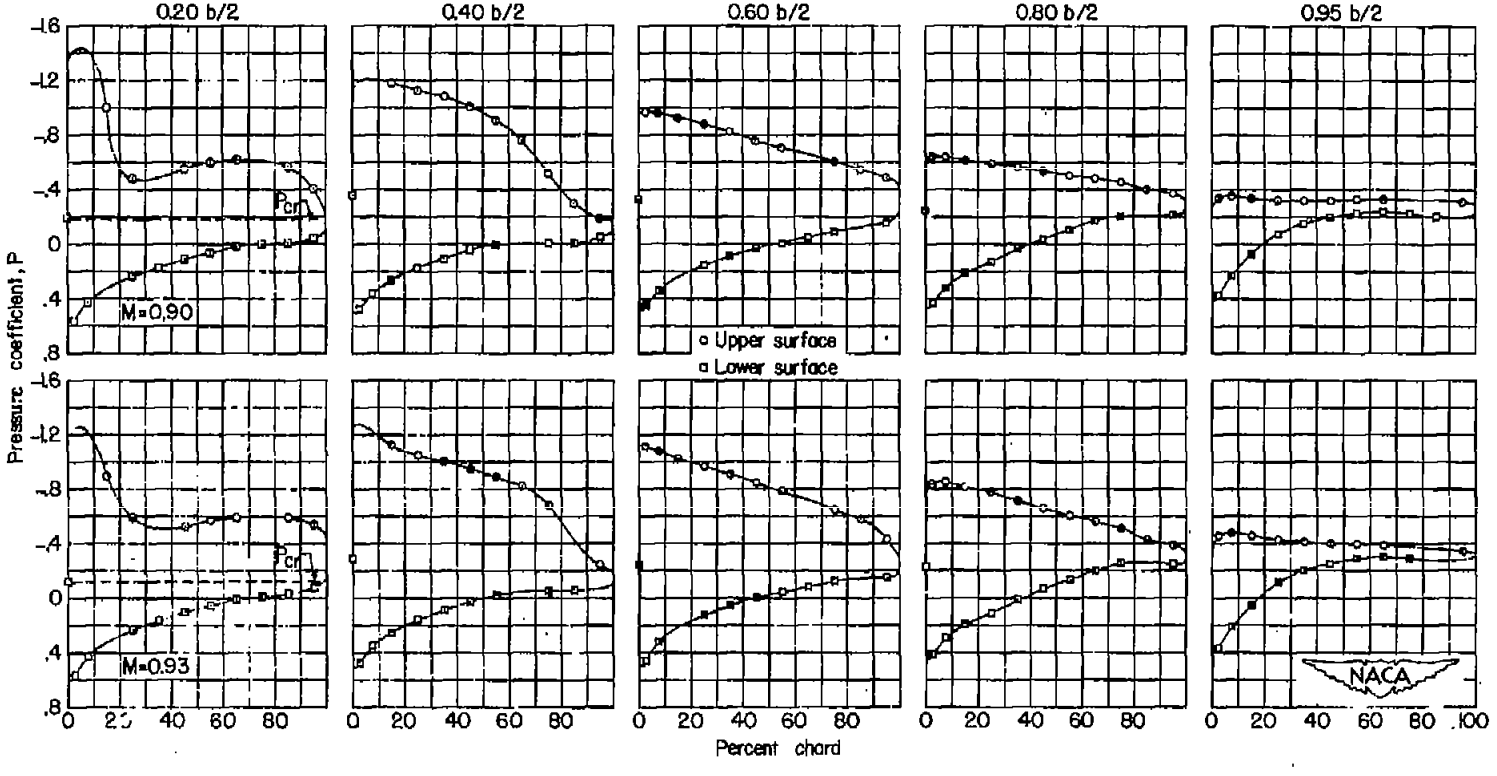

(d) $\alpha = 10^{\circ}$; M = 0.90 and 0.93.

Figure 15.- Concluded.

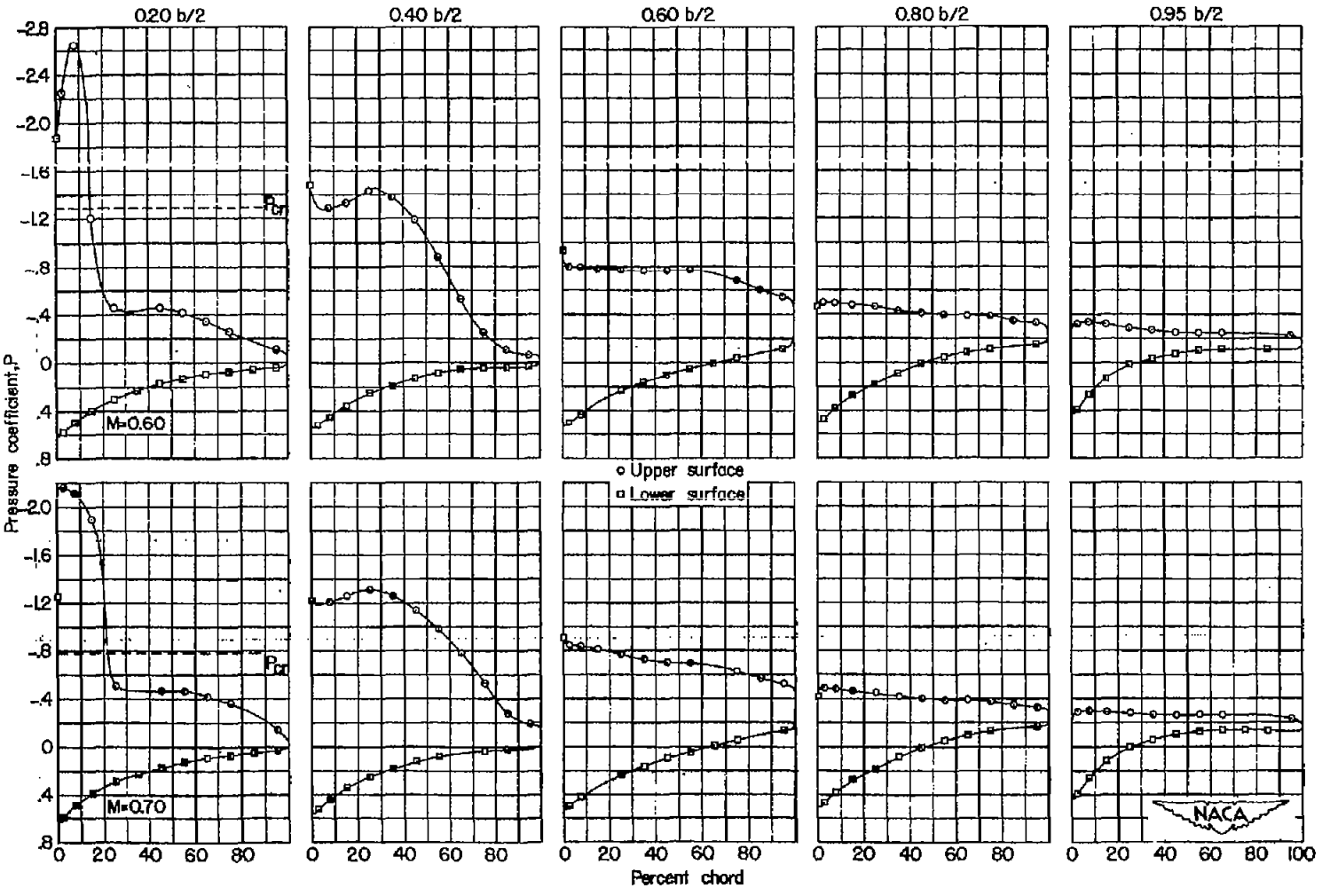

(a) $\alpha = 12^{\circ}$; M = 0.60 and 0.70.

Figure 16.- The chordwise pressure distributions at five spanwise stations for several Mach numbers.

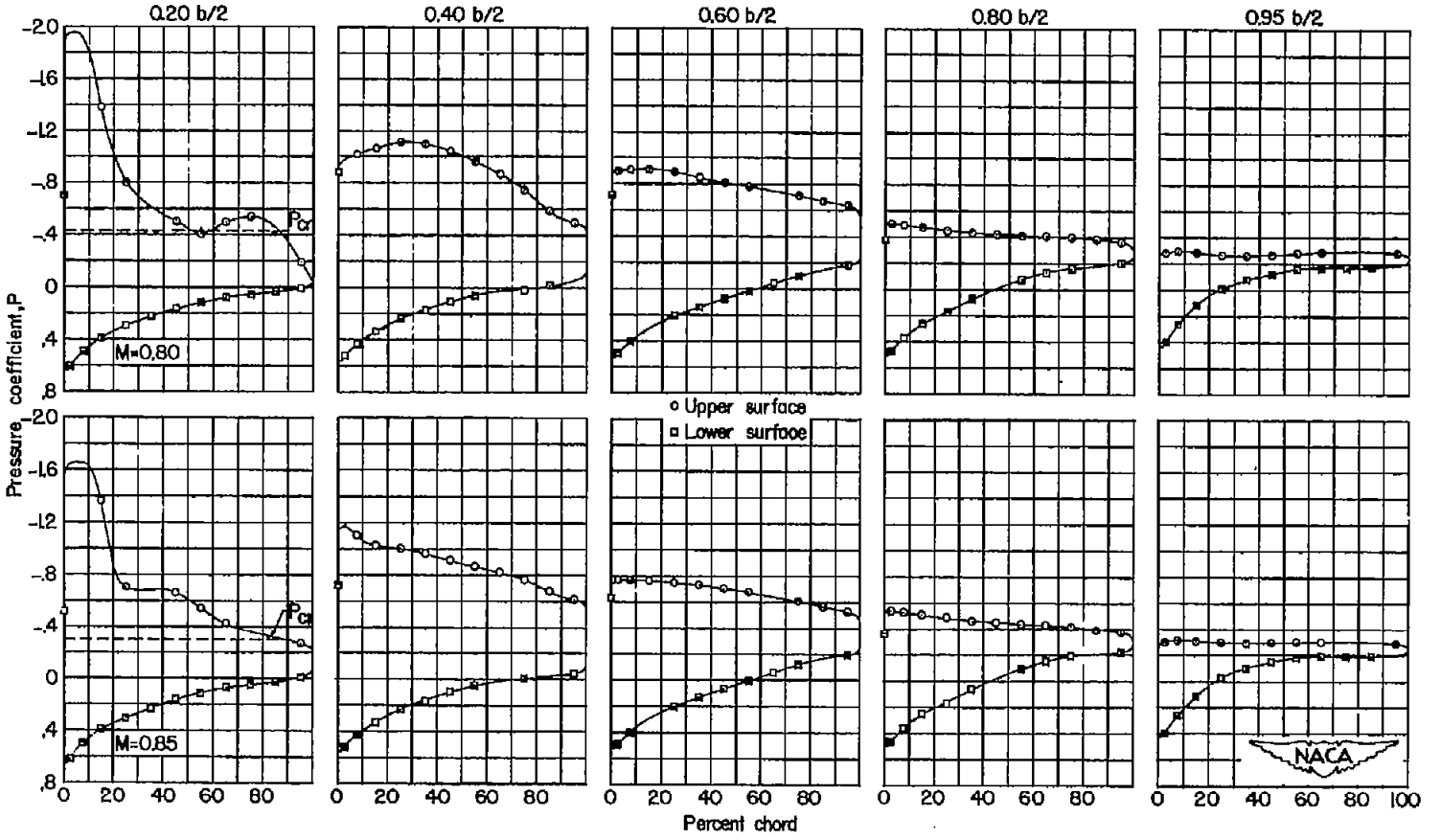

(b) $\alpha = 12^{\circ}$; M = 0.80 and 0.85.

Figure 16.- Concluded.

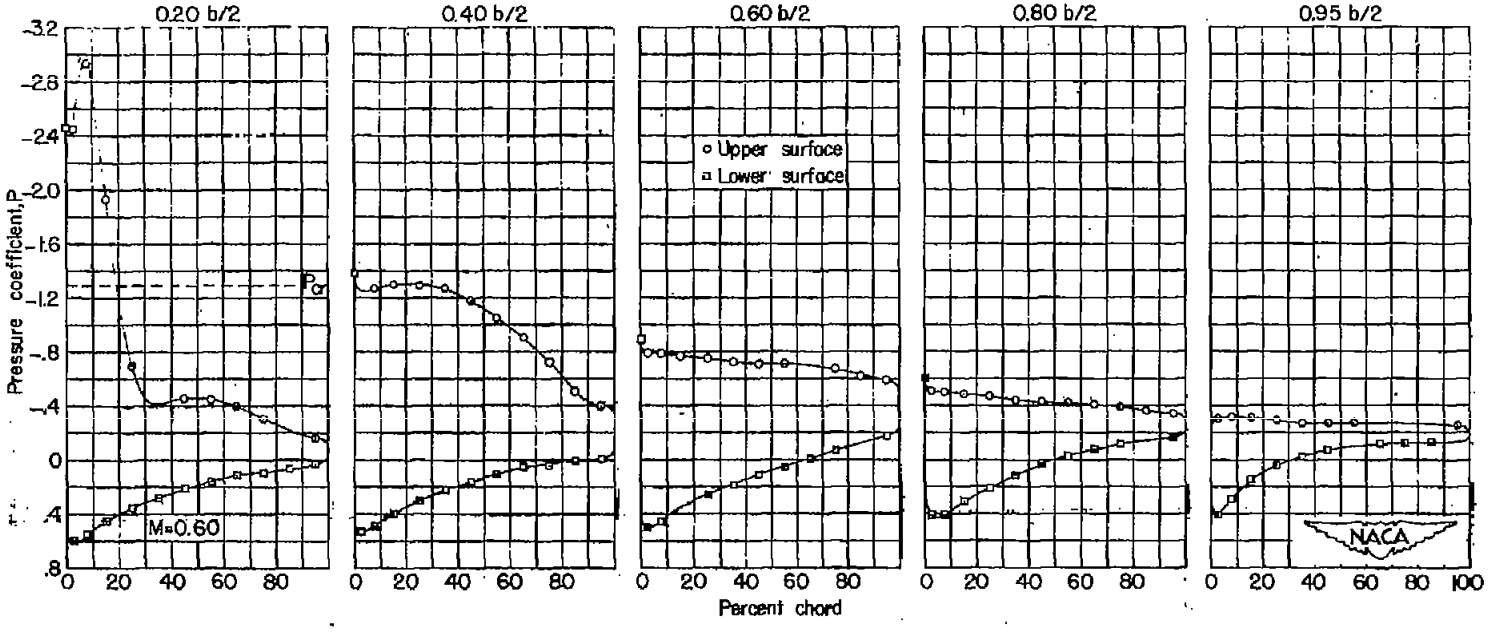

(a) $\alpha = 14^{\circ}$; M = 0.60.

Figure 17.- The chordwise pressure distributions at five spanwise stations for several Mach numbers.

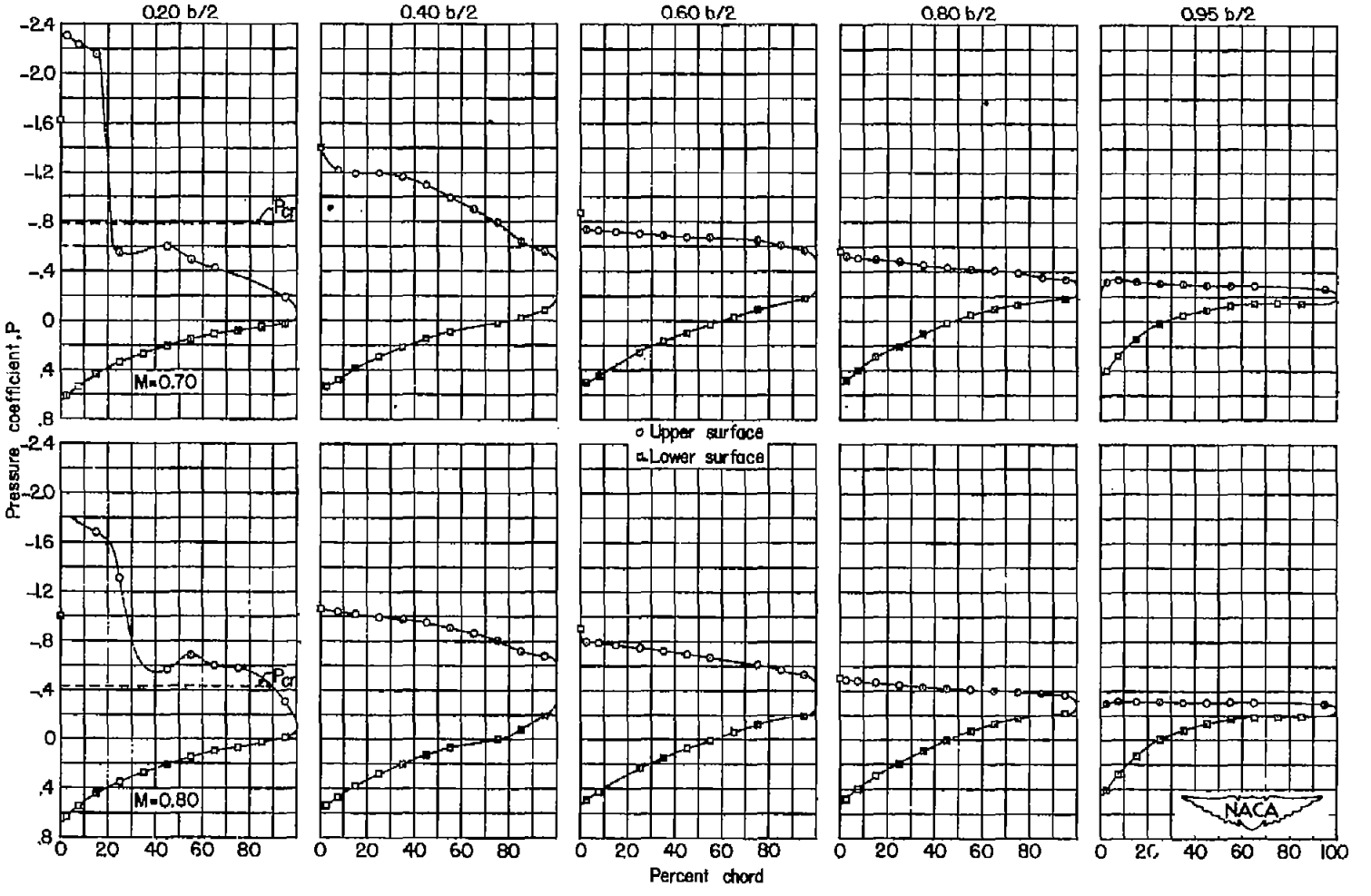

(b) $\alpha = 14^{\circ}$; M = 0.70 and 0.80.

Figure 17.- Concluded.

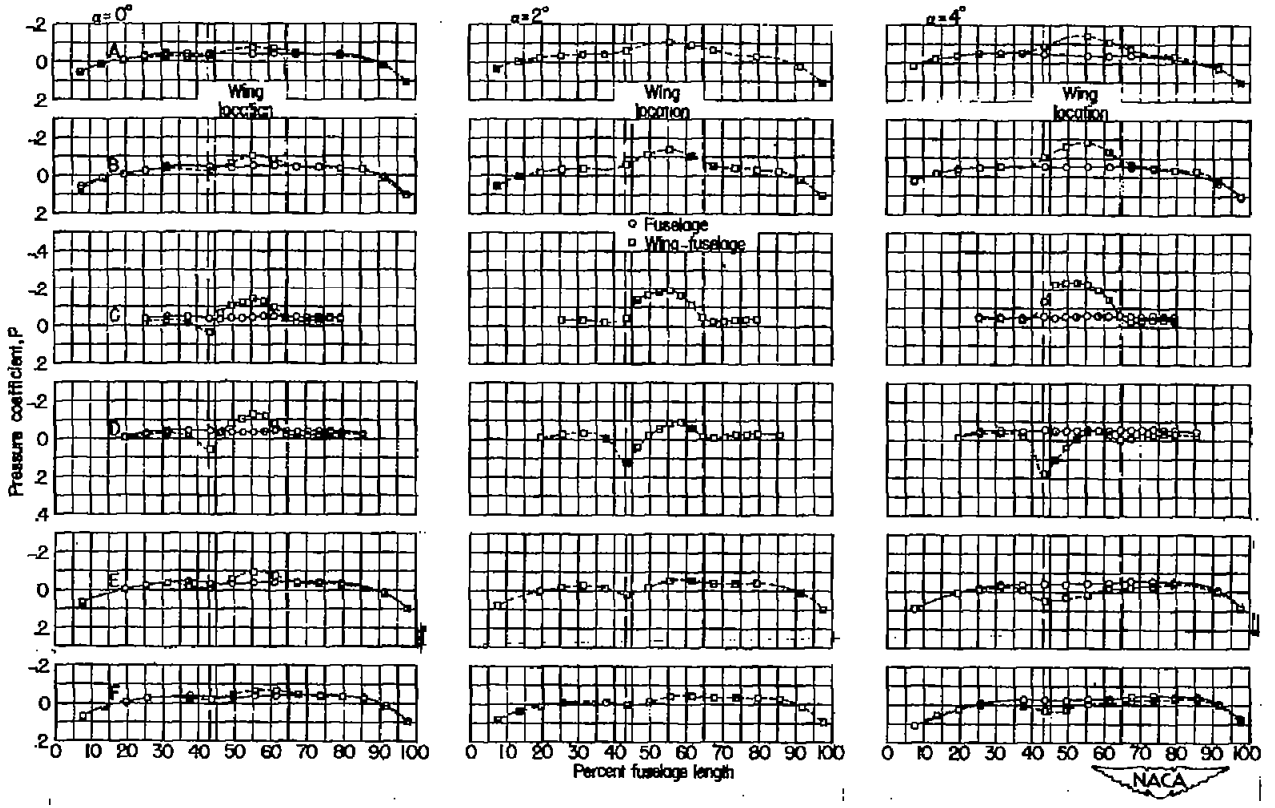

(a) M = 0.60; $\alpha = 0^\circ$, 2°, and 4°.

Figure 18.- The longitudinal pressure distributions at six radial locations for the fuselage and wing-fuselage configuration at several angles of attack.

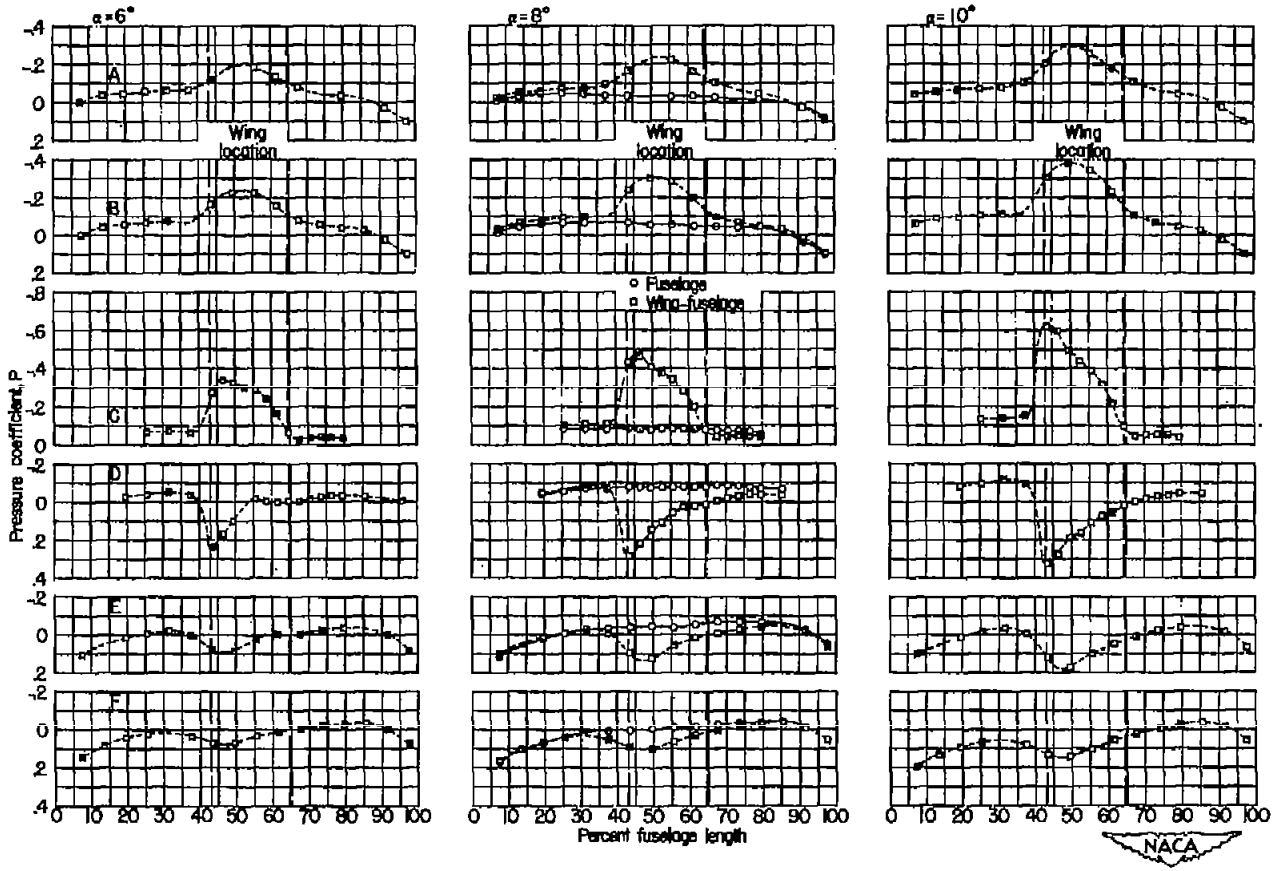

(b) M = 0.60; $\alpha = 6^{\circ}$, 8°, and 10°.

Figure 18.- Continued.

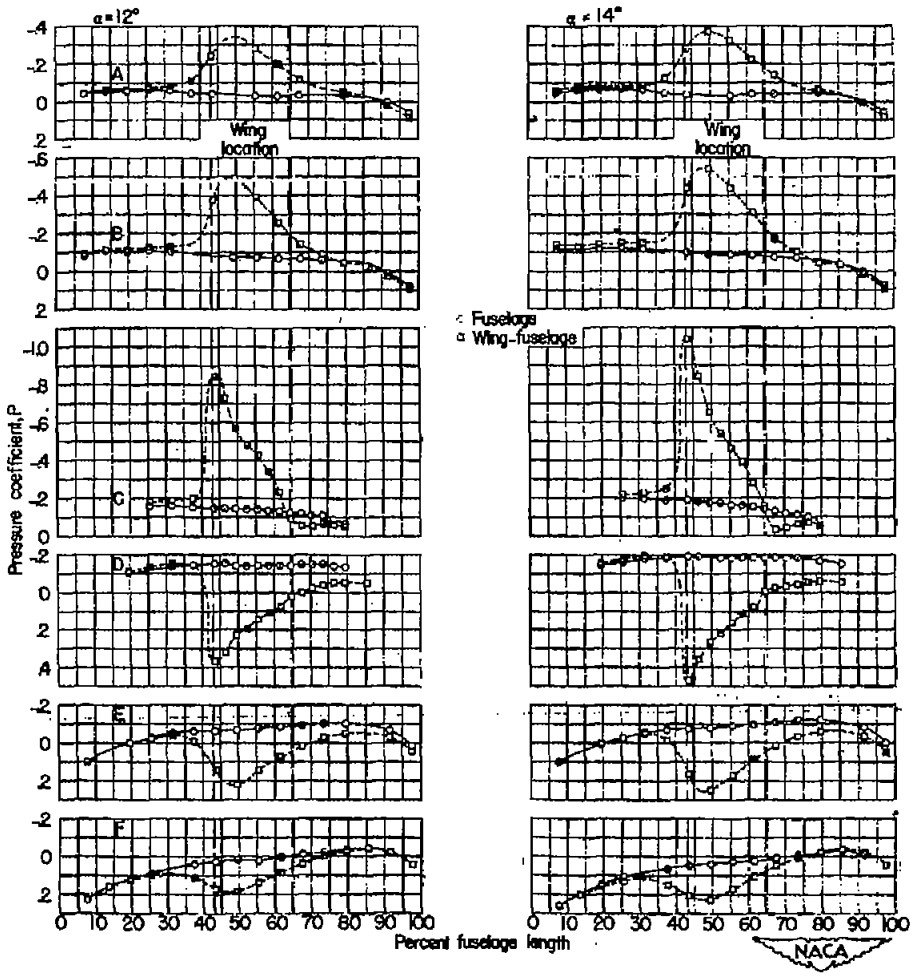

(c) M = 0.60; $\alpha = 12^{\circ}$ and 14°.

Figure 18.- Concluded.

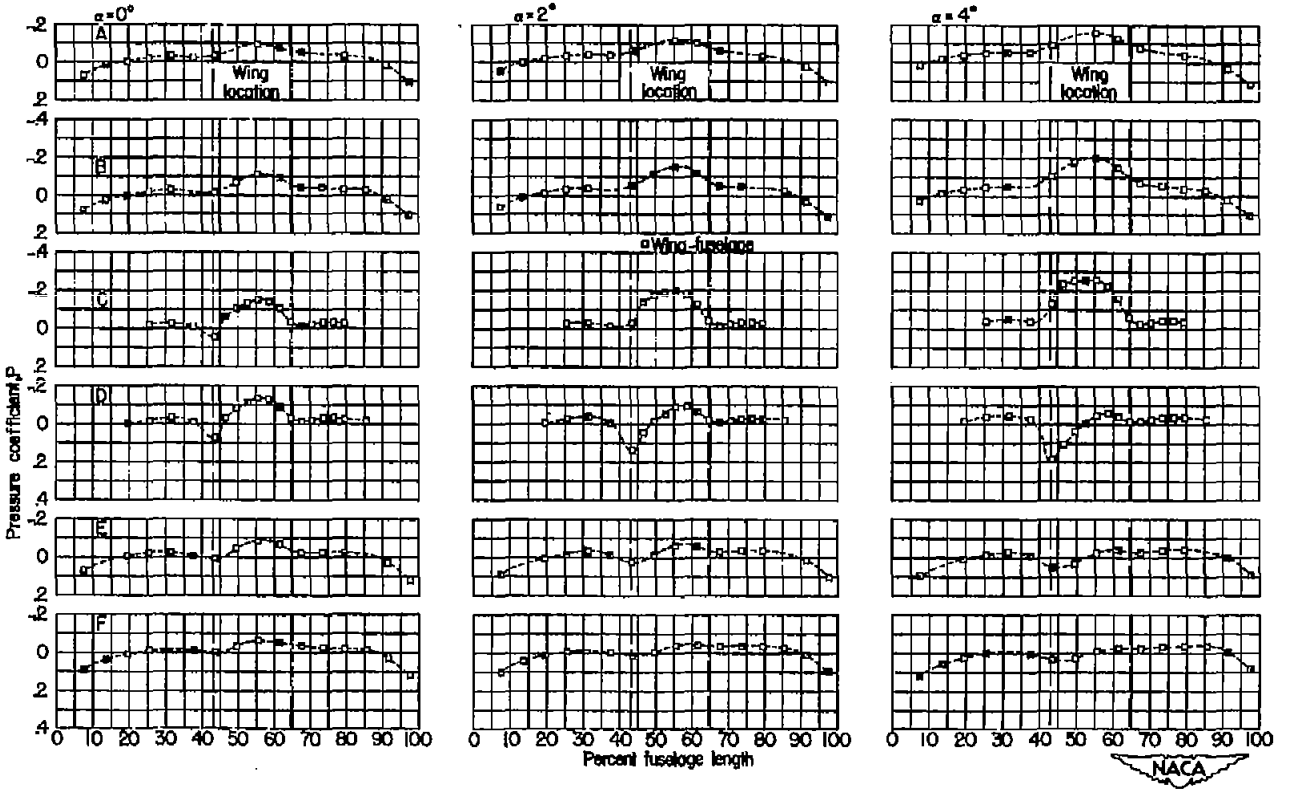

(a) M = 0.70; $\alpha = 0^{\circ}$, 2°, and 4°.

Figure 19.- The longitudinal pressure distributions at six radial locations for the wing-fuselage configuration at several angles of attack.

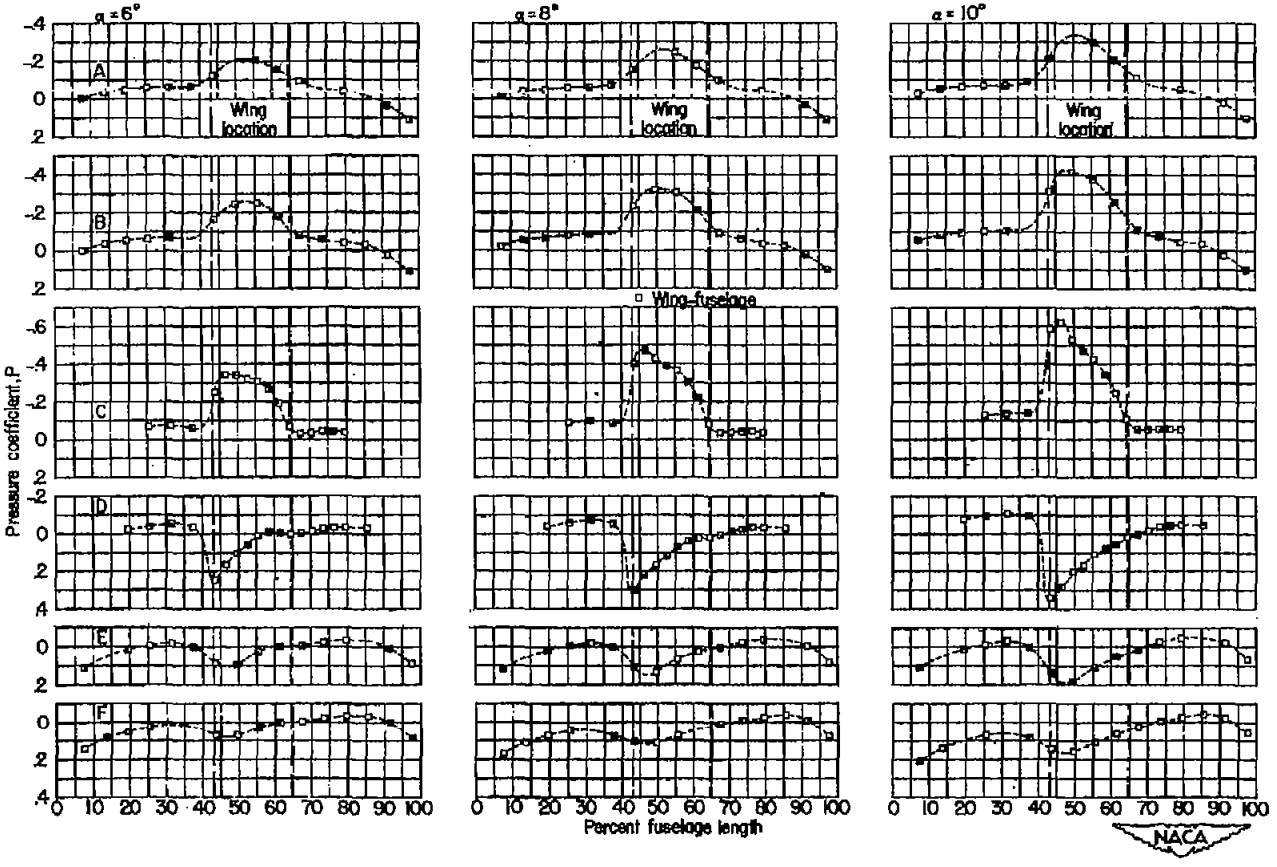

(b) M = 0.70; $\alpha = 6^{\circ}$, 8°, and 10°.

Figure 19.- Continued.

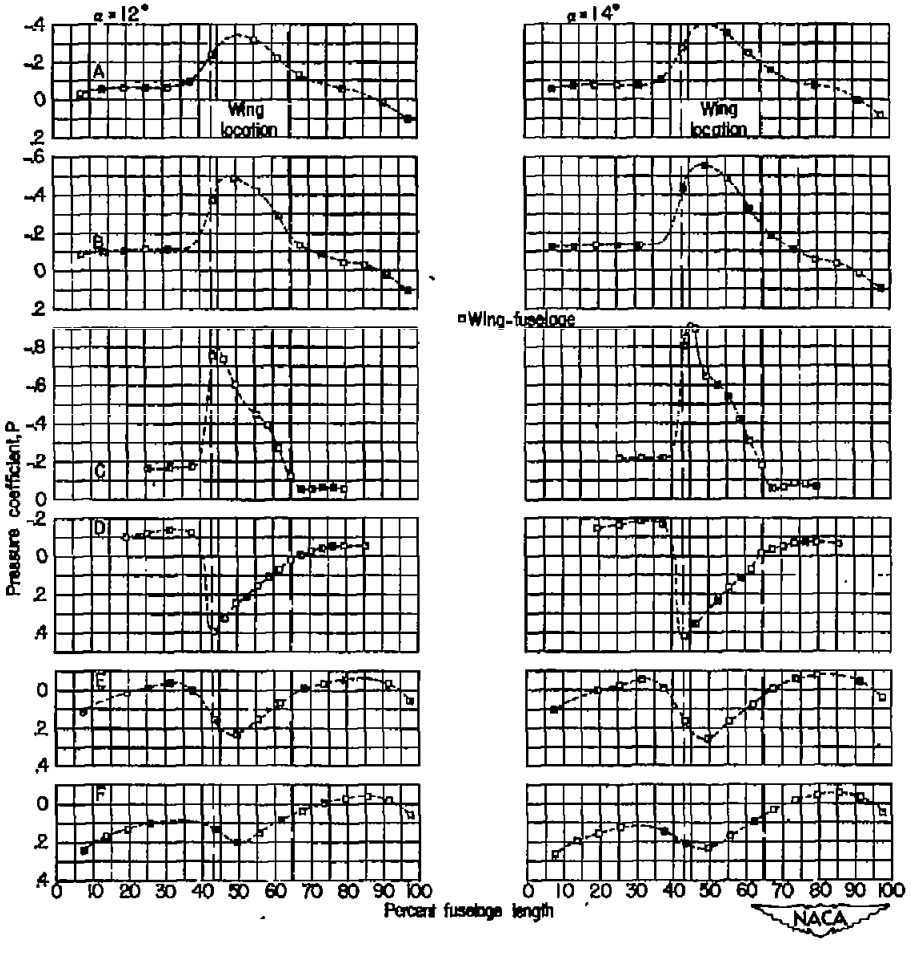

(c) M = 0.70; $\alpha = 12^{\circ}$ and 14°.

Figure 19.- Concluded.

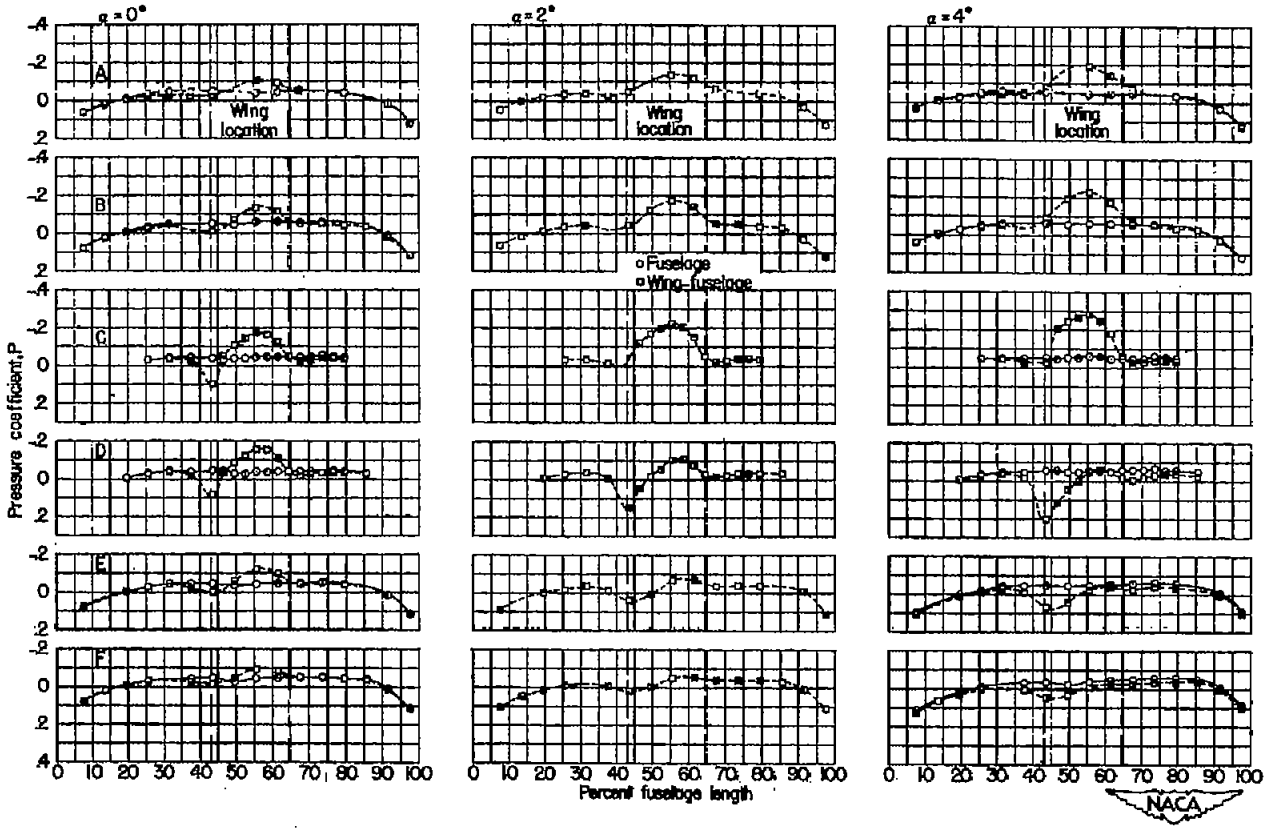

(a) M = 0.80; $\alpha = 0^{\circ}$, 2°, and 4°.

Figure 20.- The longitudinal pressure distributions at six radial locations for the fuselage and wing-fuselage configuration at several angles of attack.

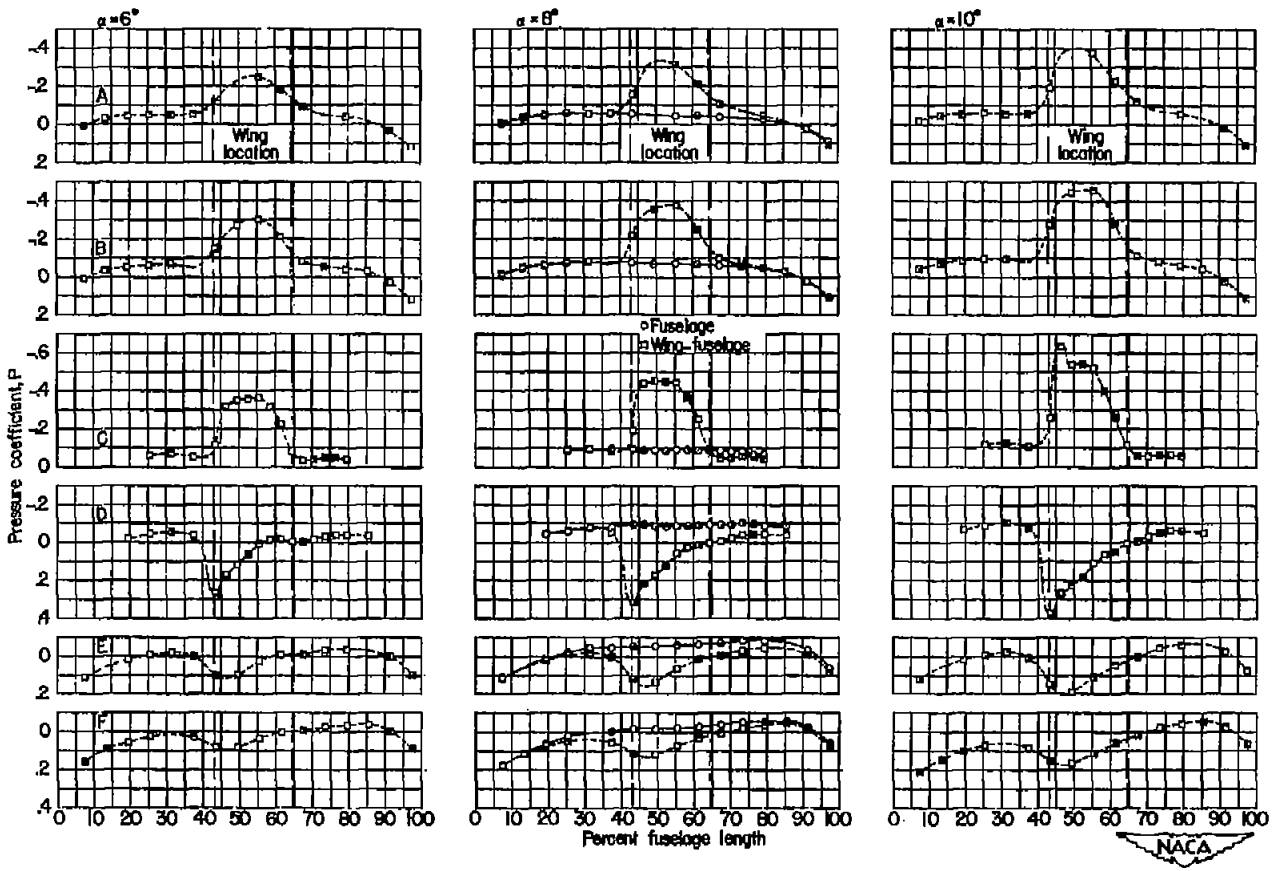

(b) M = 0.80; $\alpha = 6^{\circ}$, 8°, and 10°.

Figure 20.- Continued.

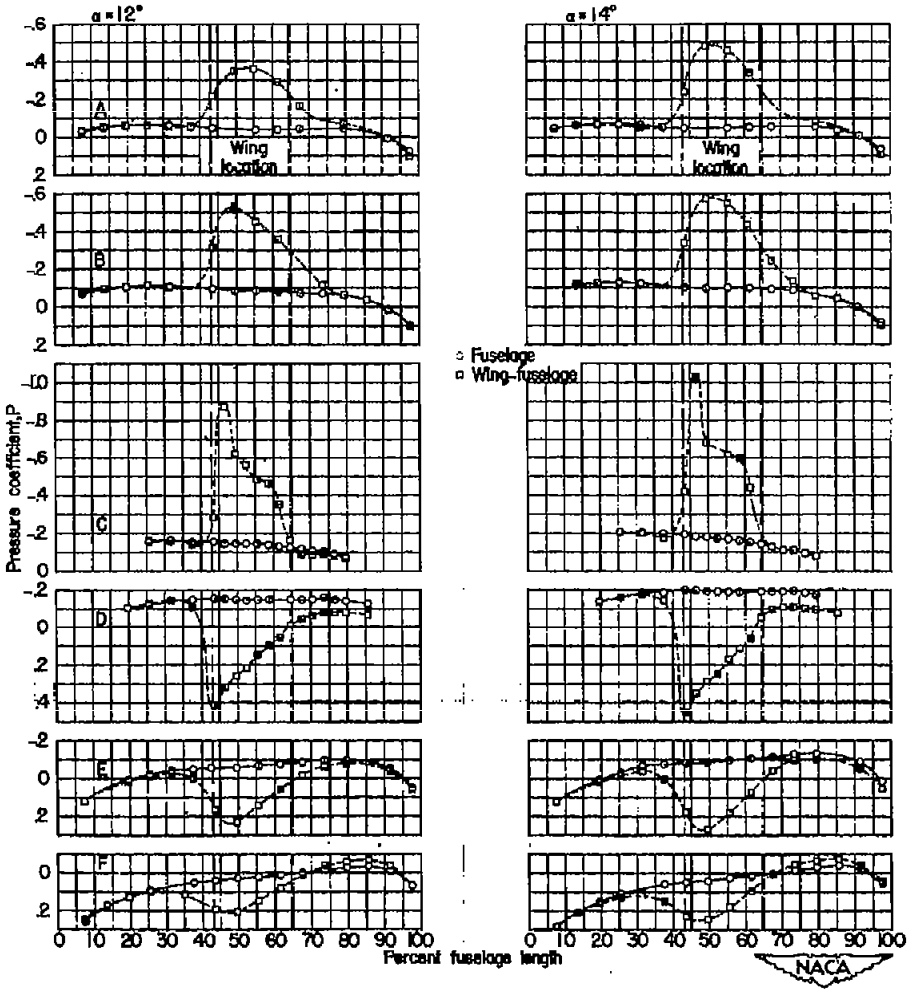

(c) M = 0.80; $\alpha = 12^{\circ}$ and 14°.

Figure 20.- Concluded.

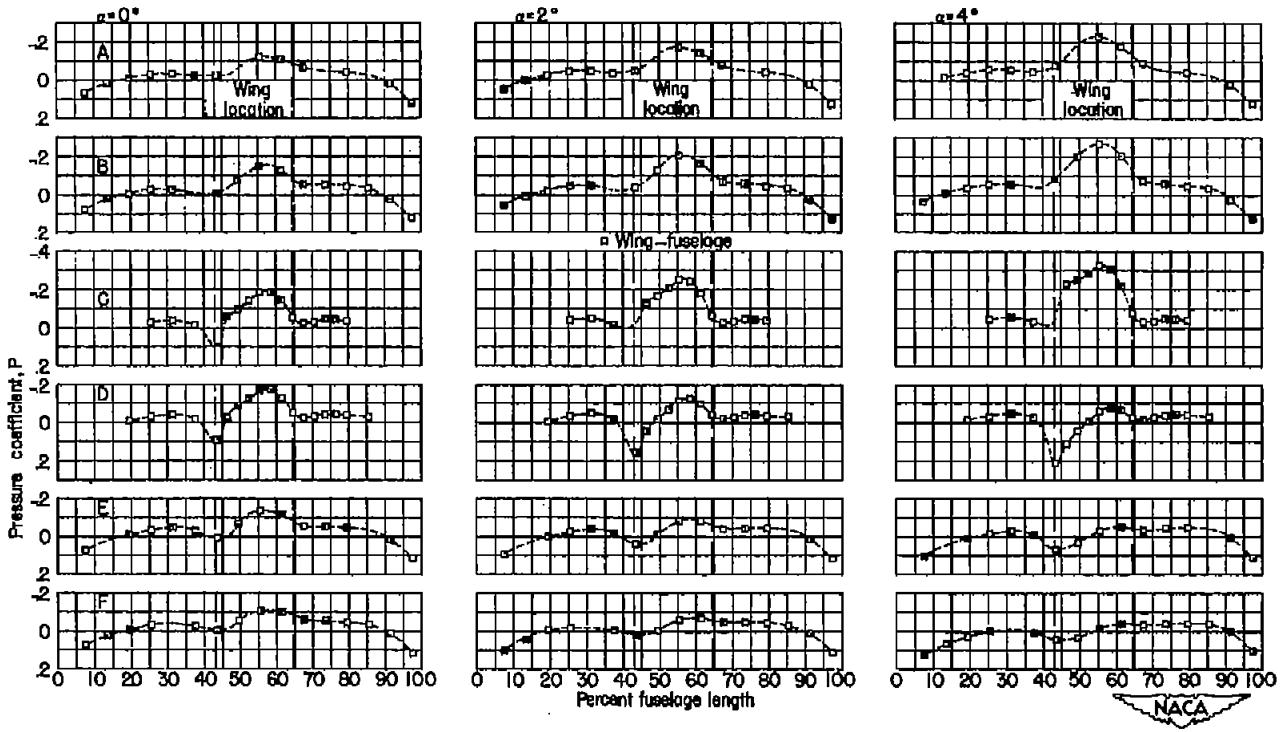

(a) $M = 0.85$; $\alpha = 0^{\circ}$, 2°, and 4°.

Figure 21.- The longitudinal pressure distributions at six radial locations for the wing-fuselage configuration at several angles of attack.

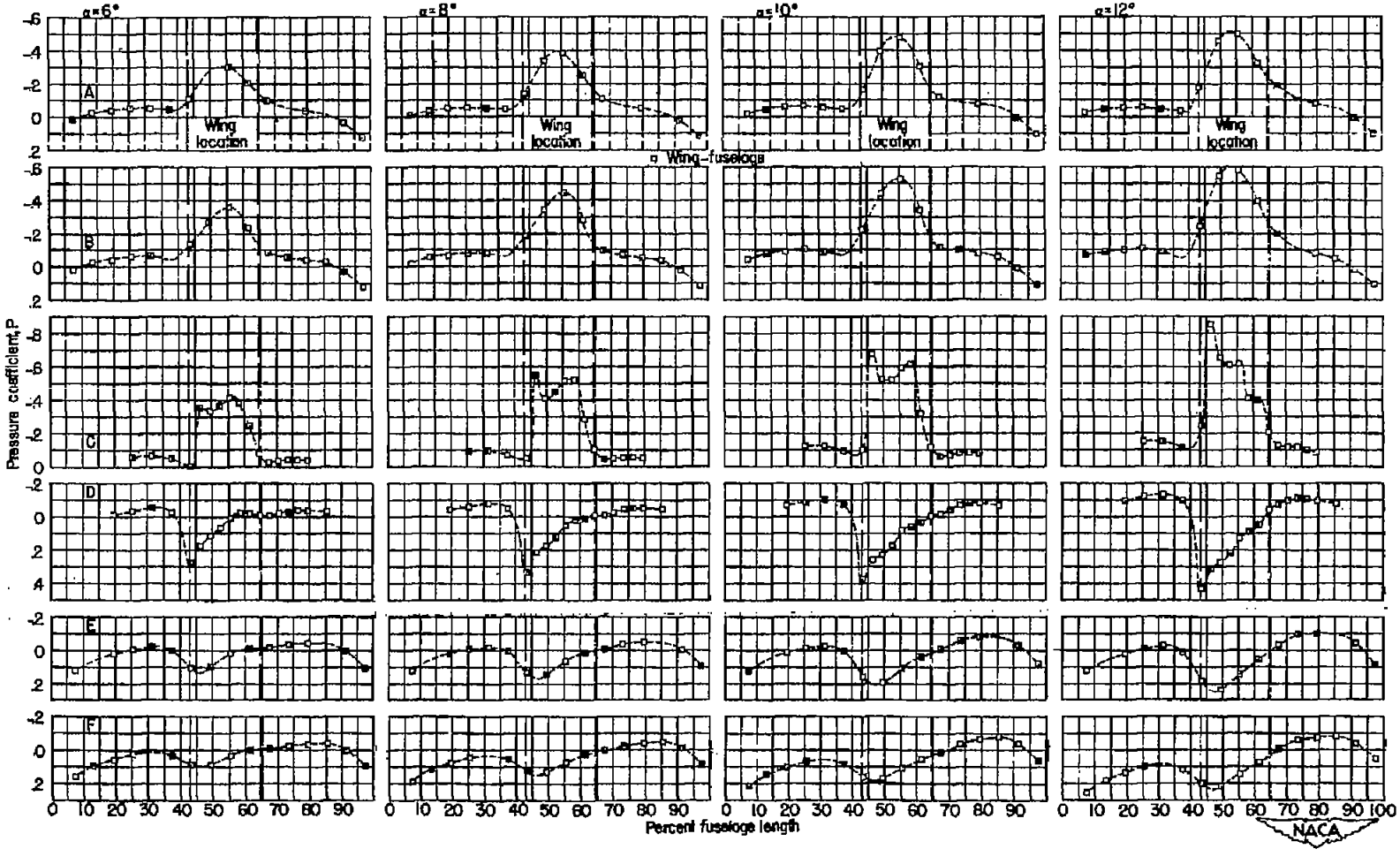

(b) M = 0.85; $\alpha = 6^\circ$, 8°, 10°, and 12°.

Figure 21.- Concluded.

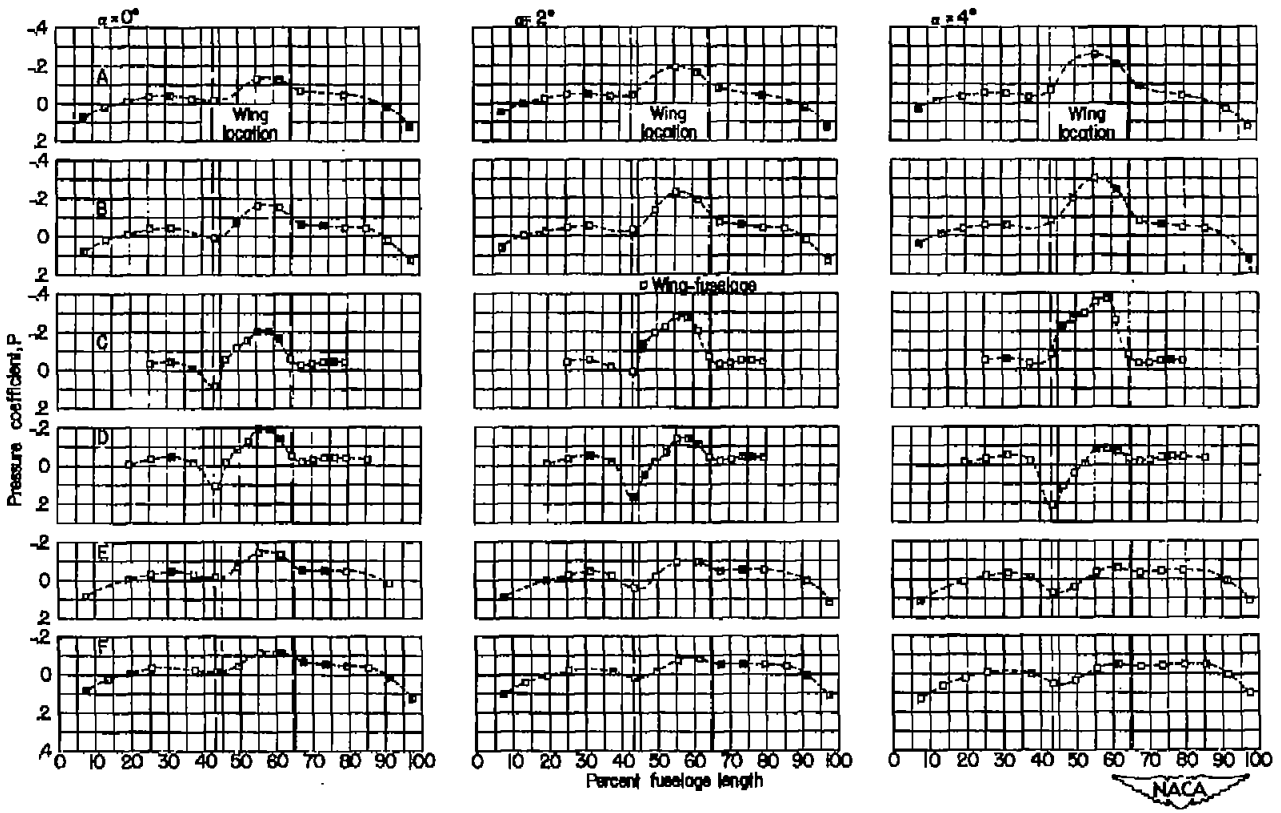

(a) M = 0.875; $\alpha = 0^\circ$, 2°, and 4°.

Figure 22.- The longitudinal pressure distributions at six radial locations for the wing-fuselage configuration at several angles of attack.

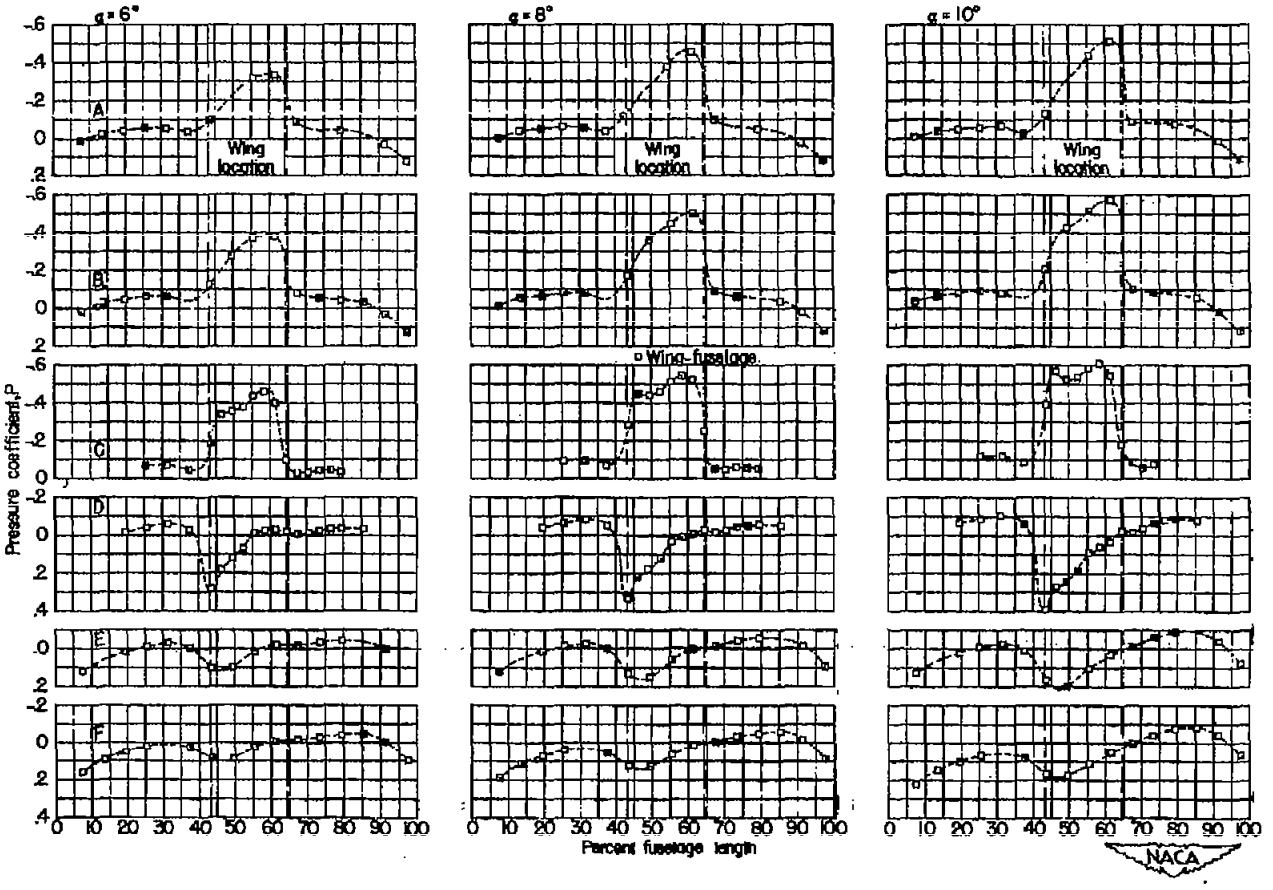

(b) M = 0.875; $\alpha = 6^{\circ}$, 8°, and 10°.

Figure 22.- Concluded.

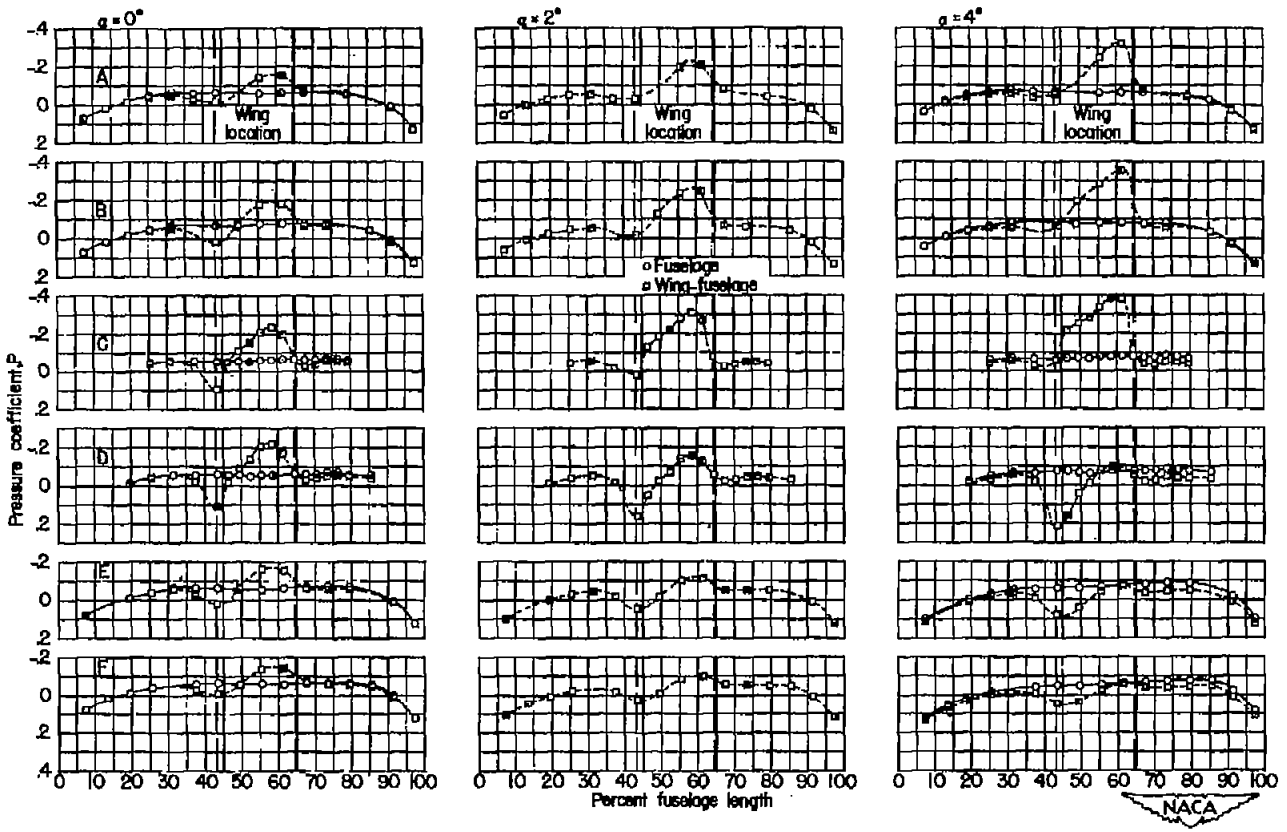

(a) M = 0.90; $\alpha = 0^\circ$, 2°, and 4°.

Figure 23.- The longitudinal pressure distributions at six radial locations for the fuselage and wing-fuselage configuration at several angles of attack.

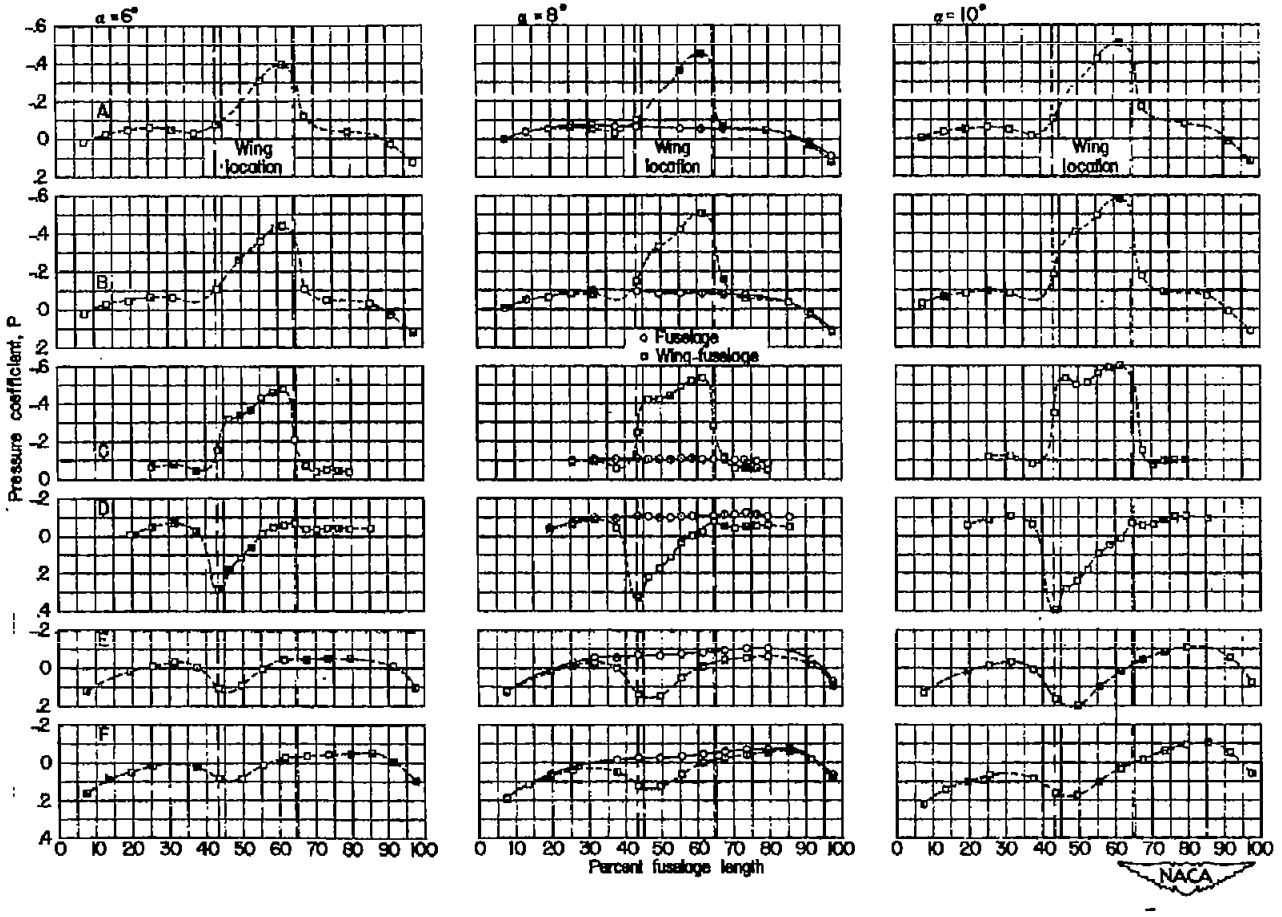

(b) M = 0.90; $\alpha = 6^\circ$, 8°, and 10°.

Figure 23.- Continued.

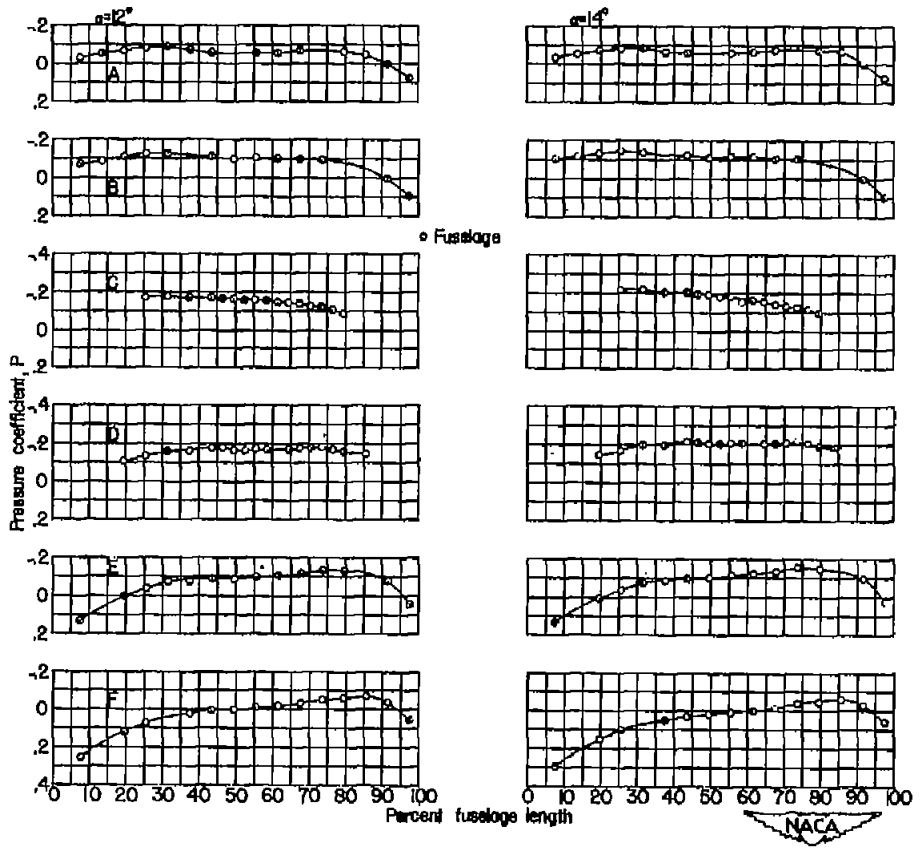

(c) M = 0.90; $\alpha = 12^{\circ}$ and 14°.

Figure 23.- Concluded.

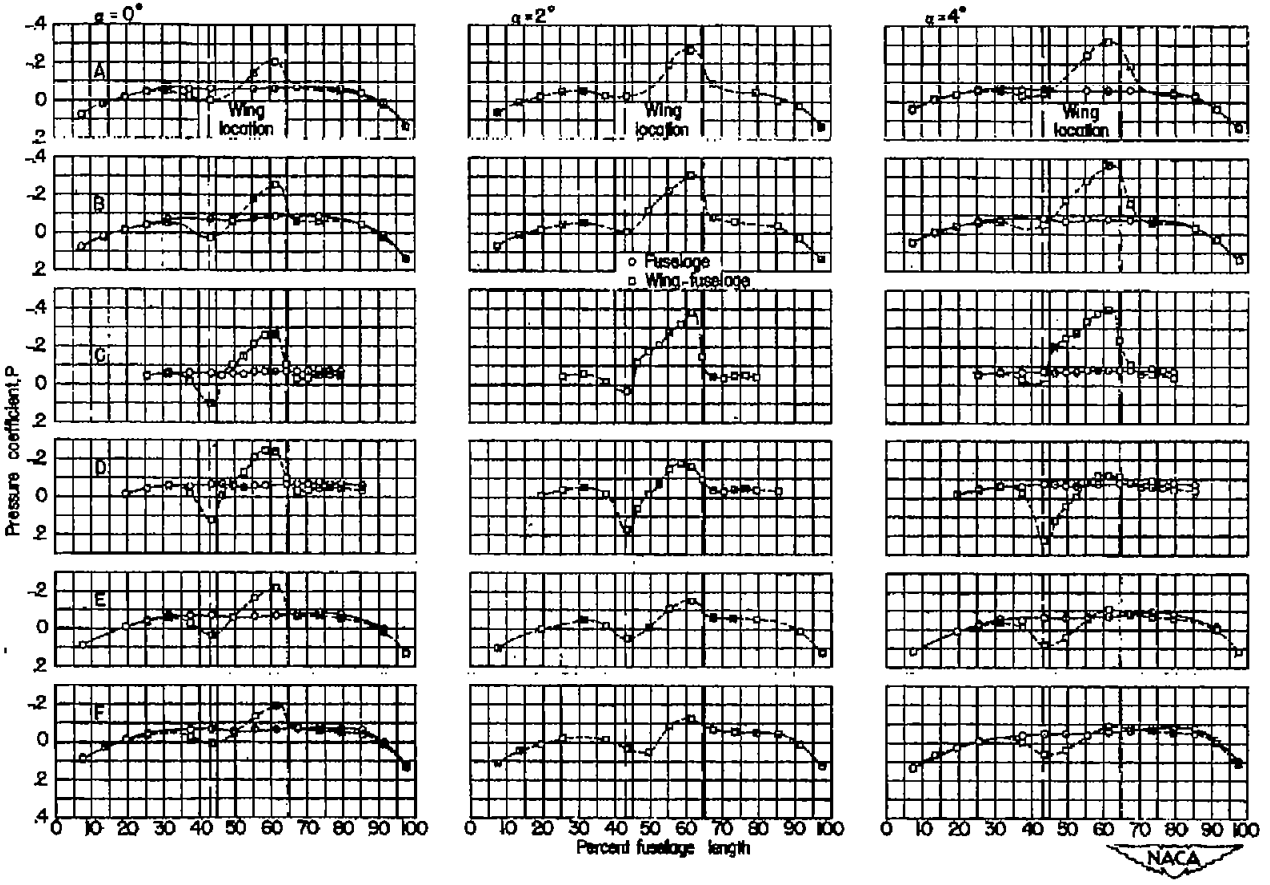

(a) M = 0.93; $\alpha = 0^{\circ}$, 2°, and 4°.

Figure 24.- The longitudinal pressure distributions at six radial locations for the fuselage and wing-fuselage configuration at several angles of attack.

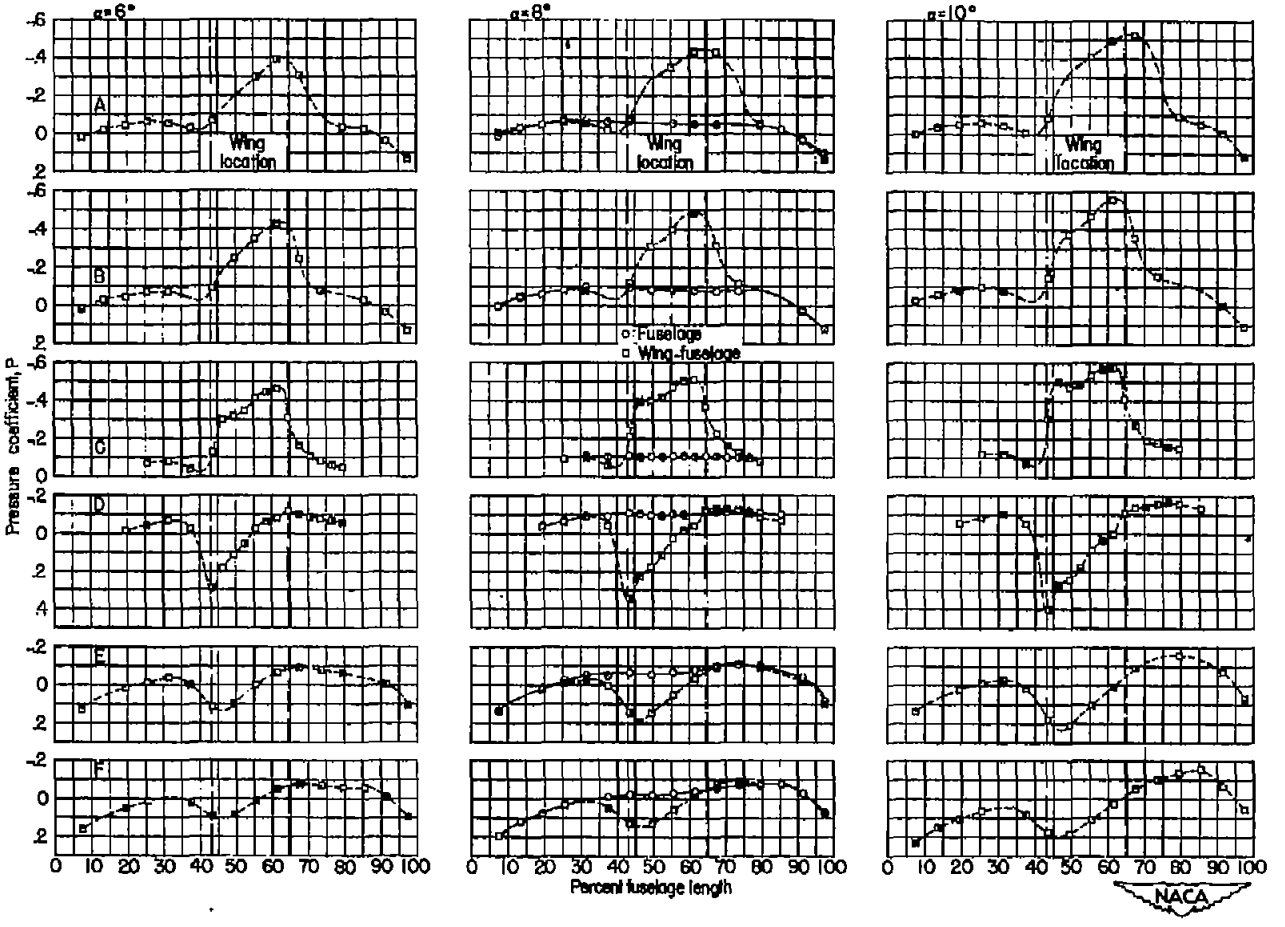

(b) M = 0.93; $\alpha = 6^{\circ}$, 8°, and 10°.

Figure 24.- Continued.

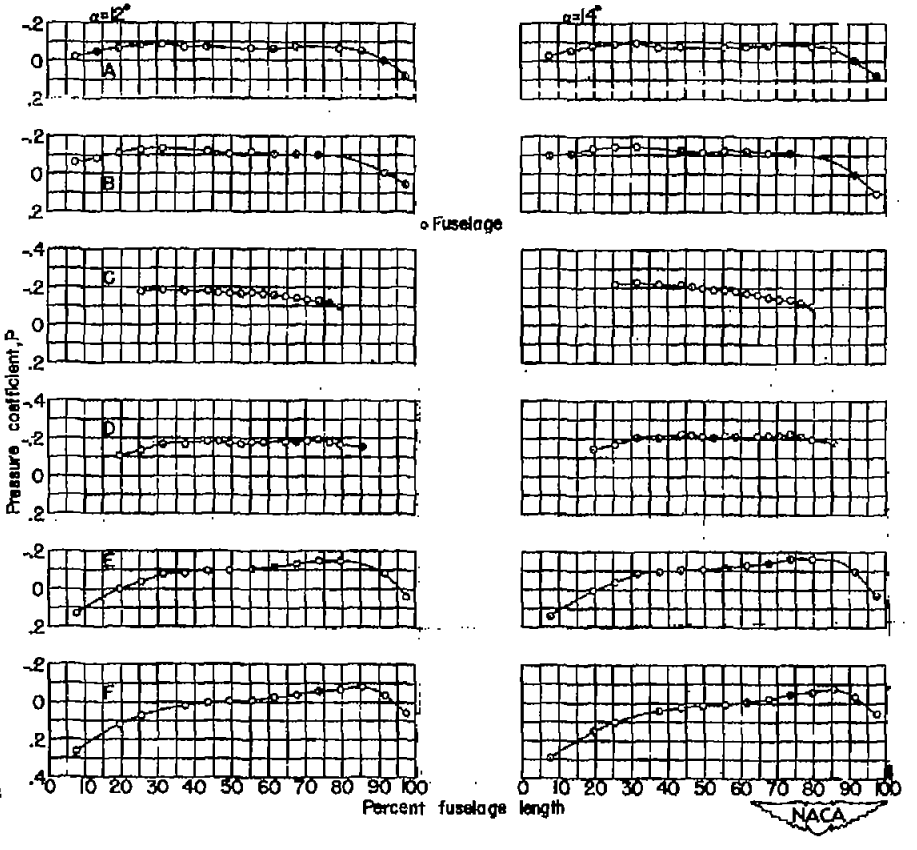

(c) M = 0.93; $\alpha = 12^{\circ}$ and 14°.

Figure 24.- Concluded.

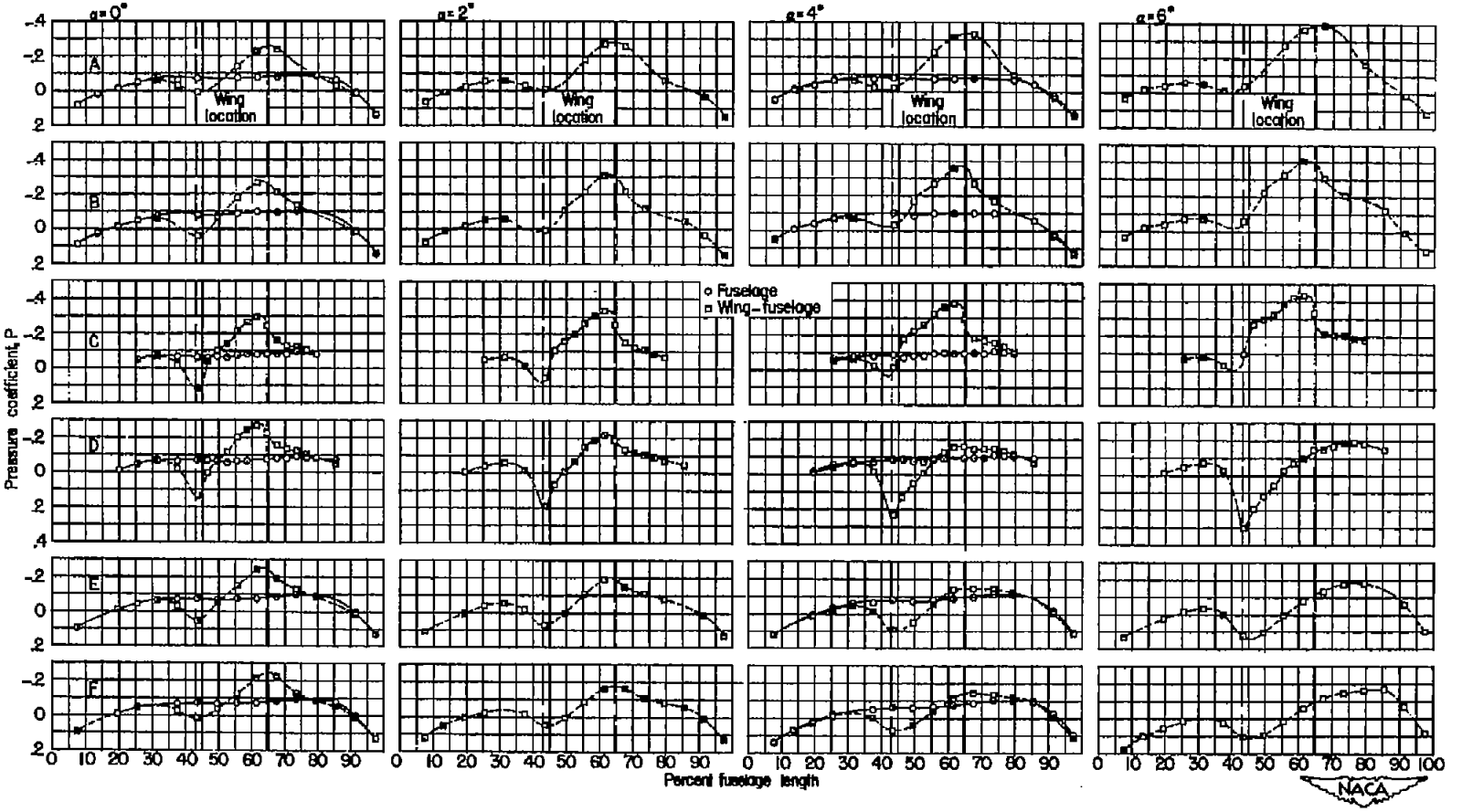

(a) M = 0.96; $\alpha = 0^\circ$, 2°, 4°, and 6°.

Figure 25.- The longitudinal pressure distributions at six radial locations for the fuselage and wing-fuselage configuration at several angles of attack.

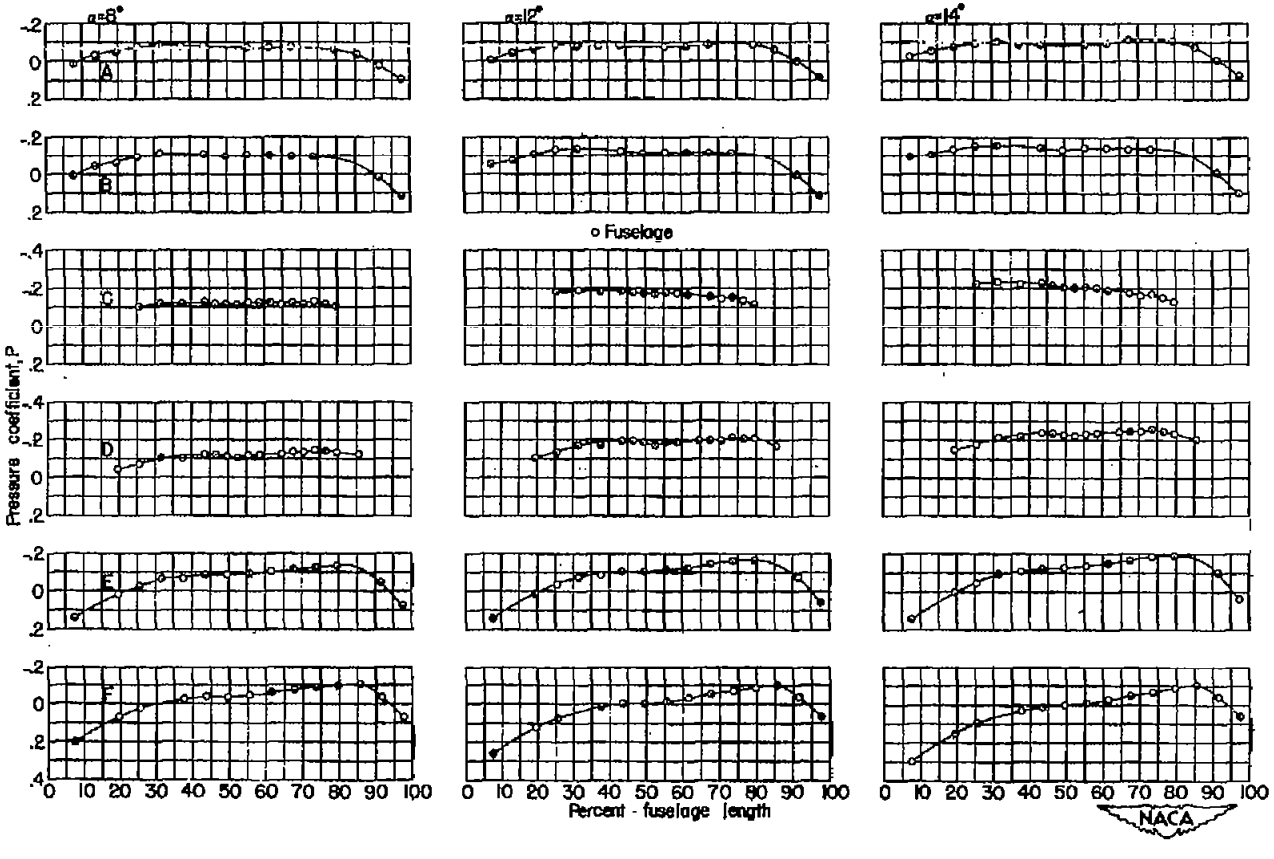

(b) M = 0.96; $\alpha = 8^{\circ}$, 12°, and 14°.

Figure 25.- Concluded.

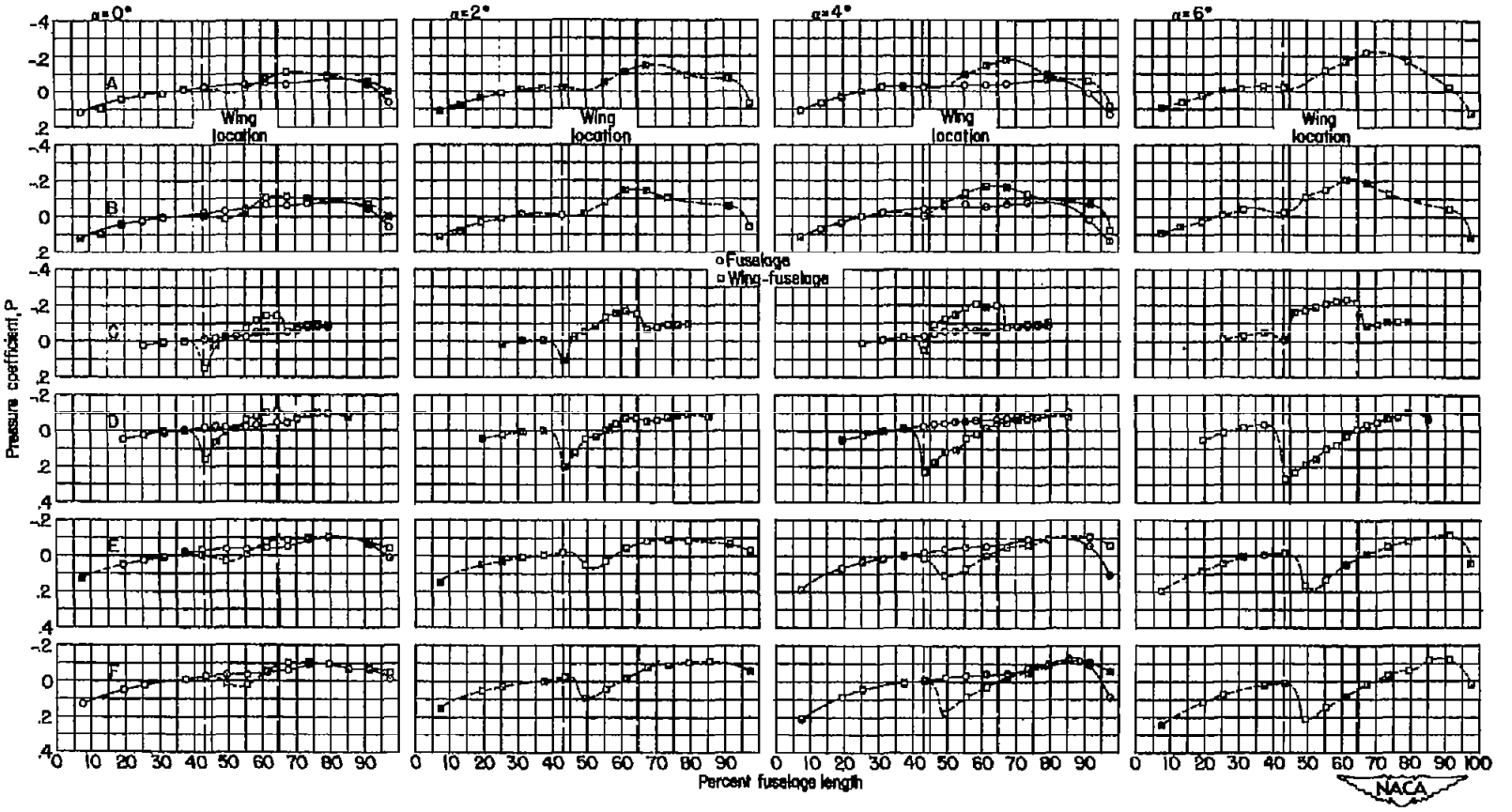

(a) M = 1.2; $\alpha = 0^\circ$, 2°, 4°, and 6°.

Figure 26.- The longitudinal pressure distributions at six radial locations for the fuselage and wing-fuselage configuration at several angles of attack.

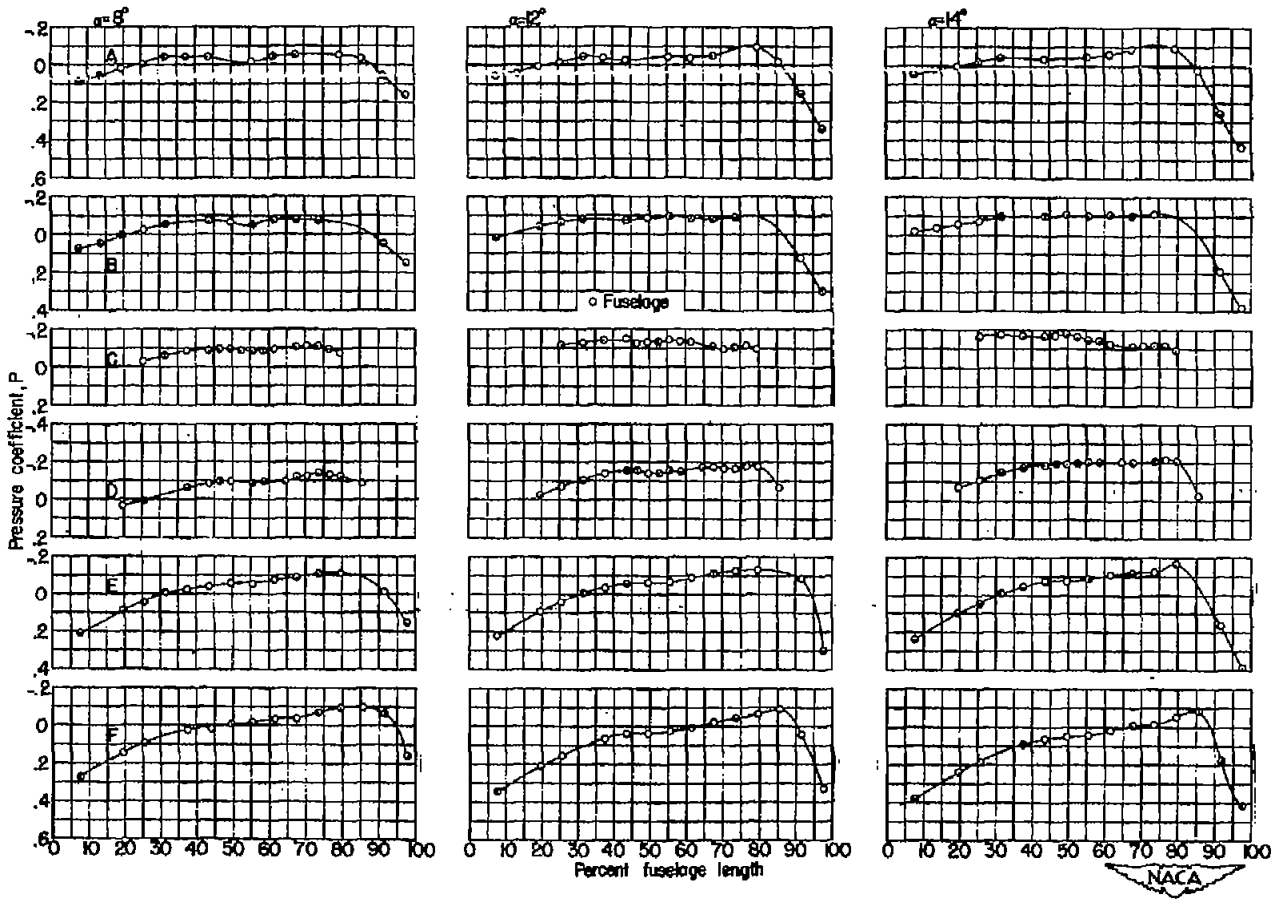

(b) M = 1.2; $\alpha = 8^{\circ}$, 12°, and 14°.

Figure 26.- Concluded.

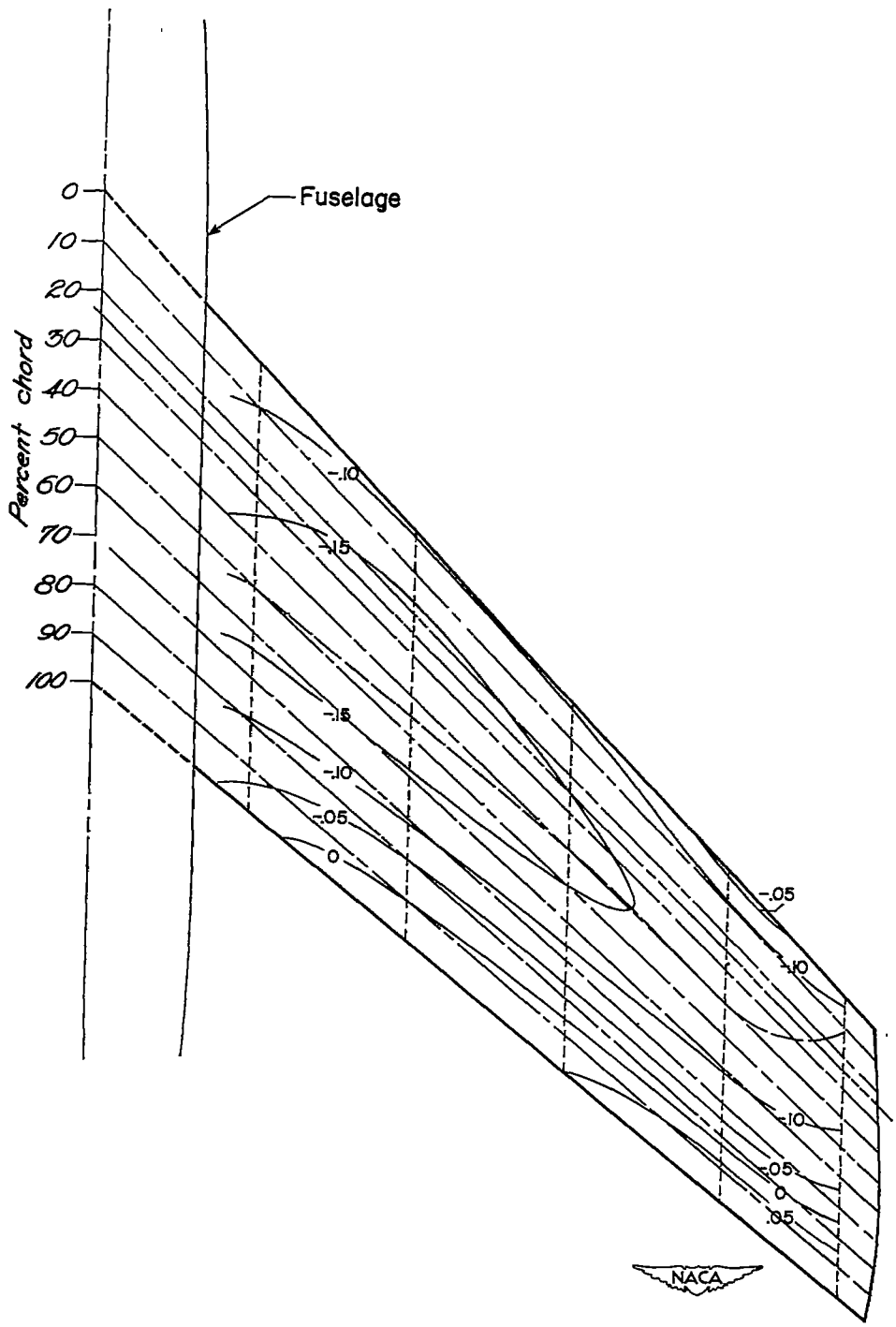

(a) Upper surface; M = 0.60; $\alpha = 0^{\circ}$.

Figure 27.- Contours of constant pressure coefficient.

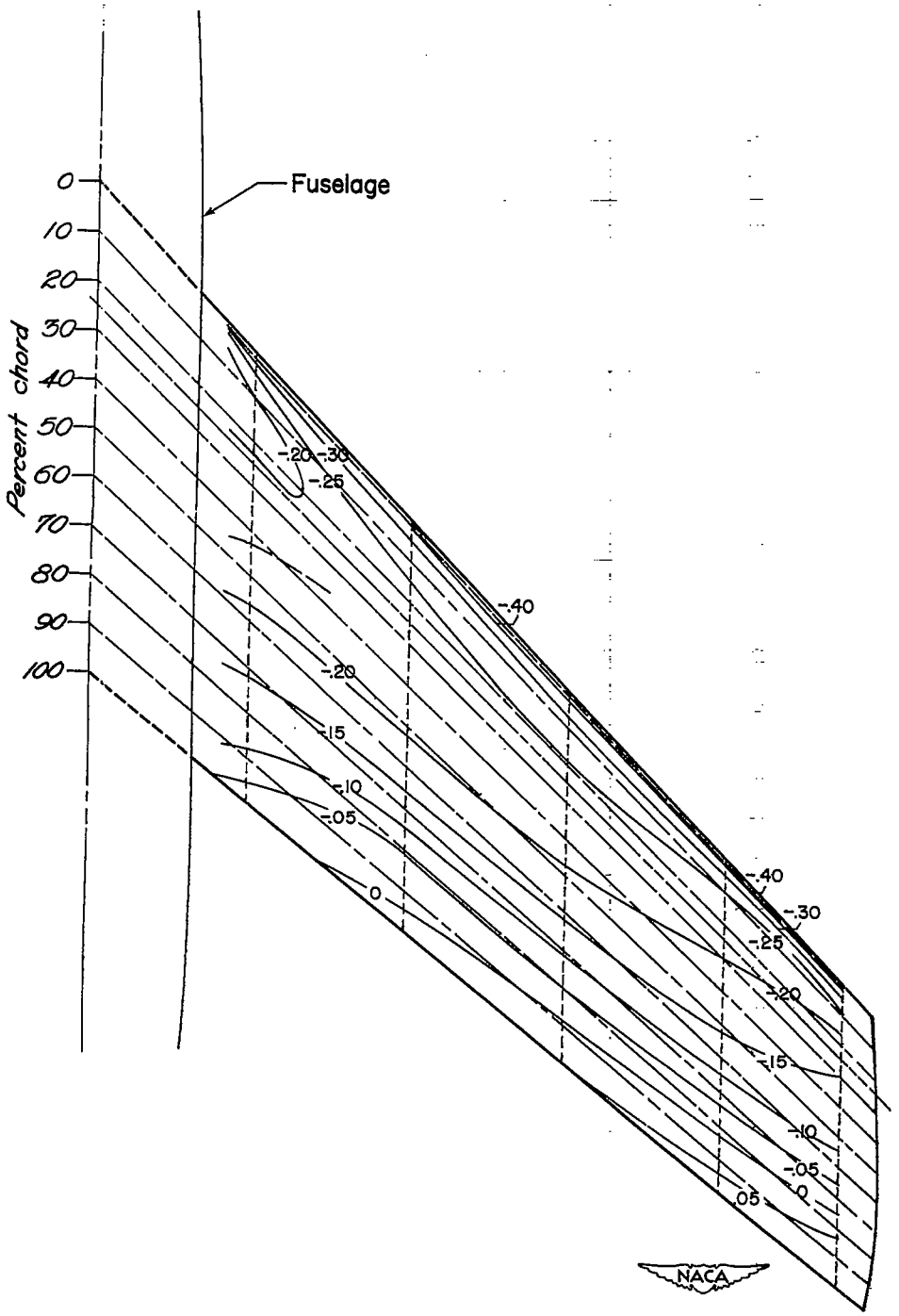

(b) Upper surface; M = 0.60; $\alpha = 2^{\circ}$.

Figure 27.- Continued.

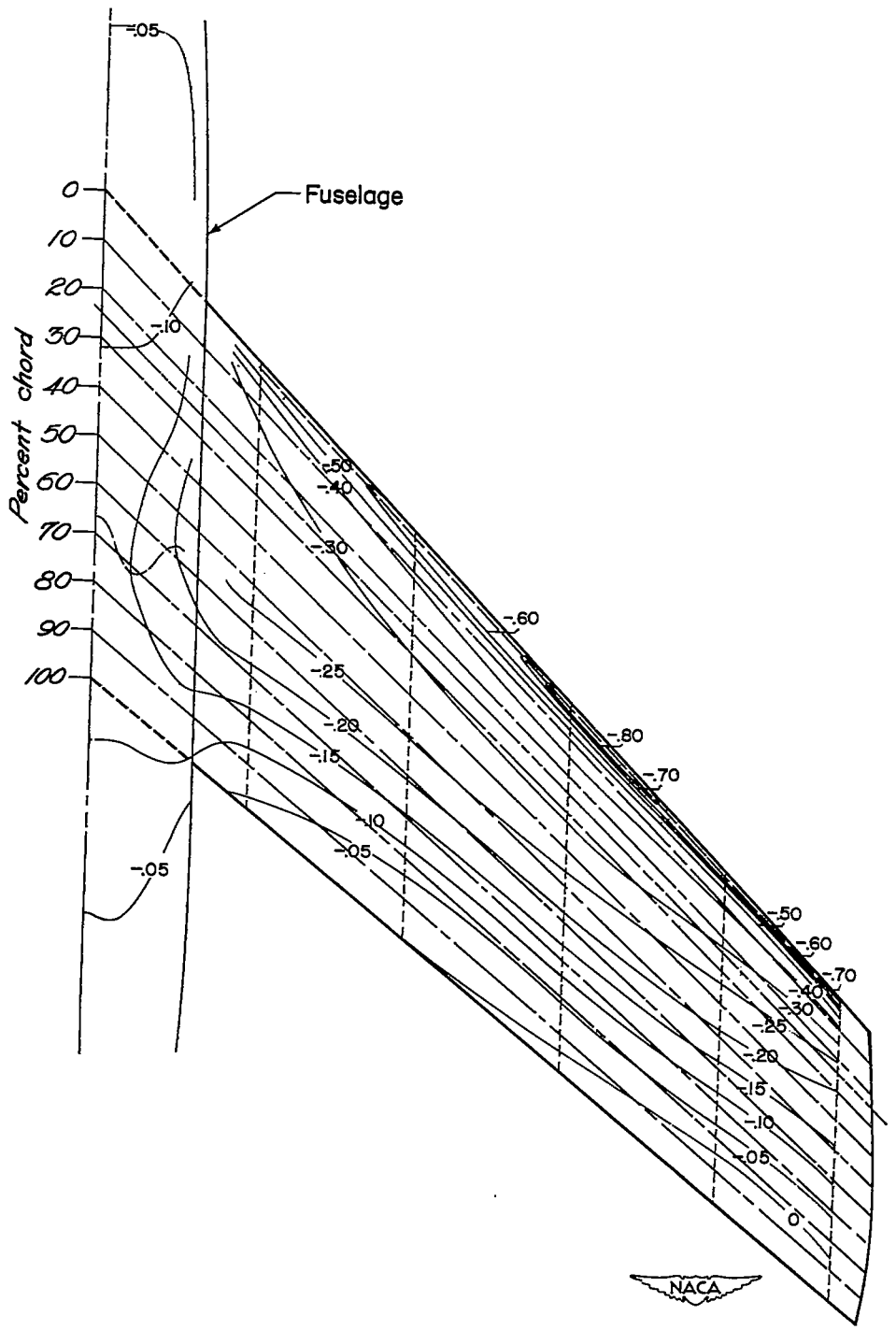

(c) Upper surface; M = 0.60; $\alpha = 4^{\circ}$.

Figure 27.- Continued.

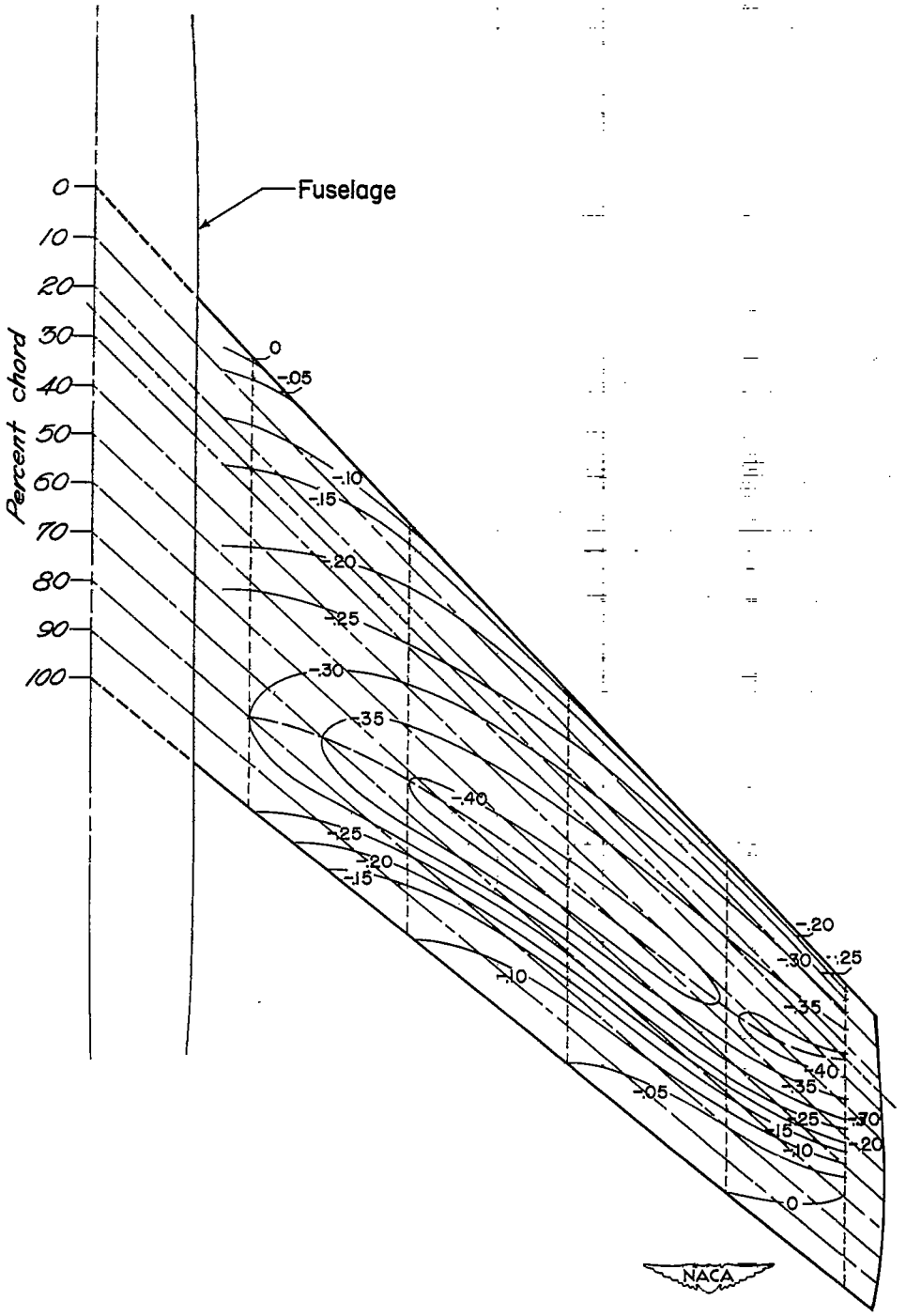

(d) Upper surface; M = 0.96; $\alpha = 0^{\circ}$.

Figure 27.- Continued.

[redacted]

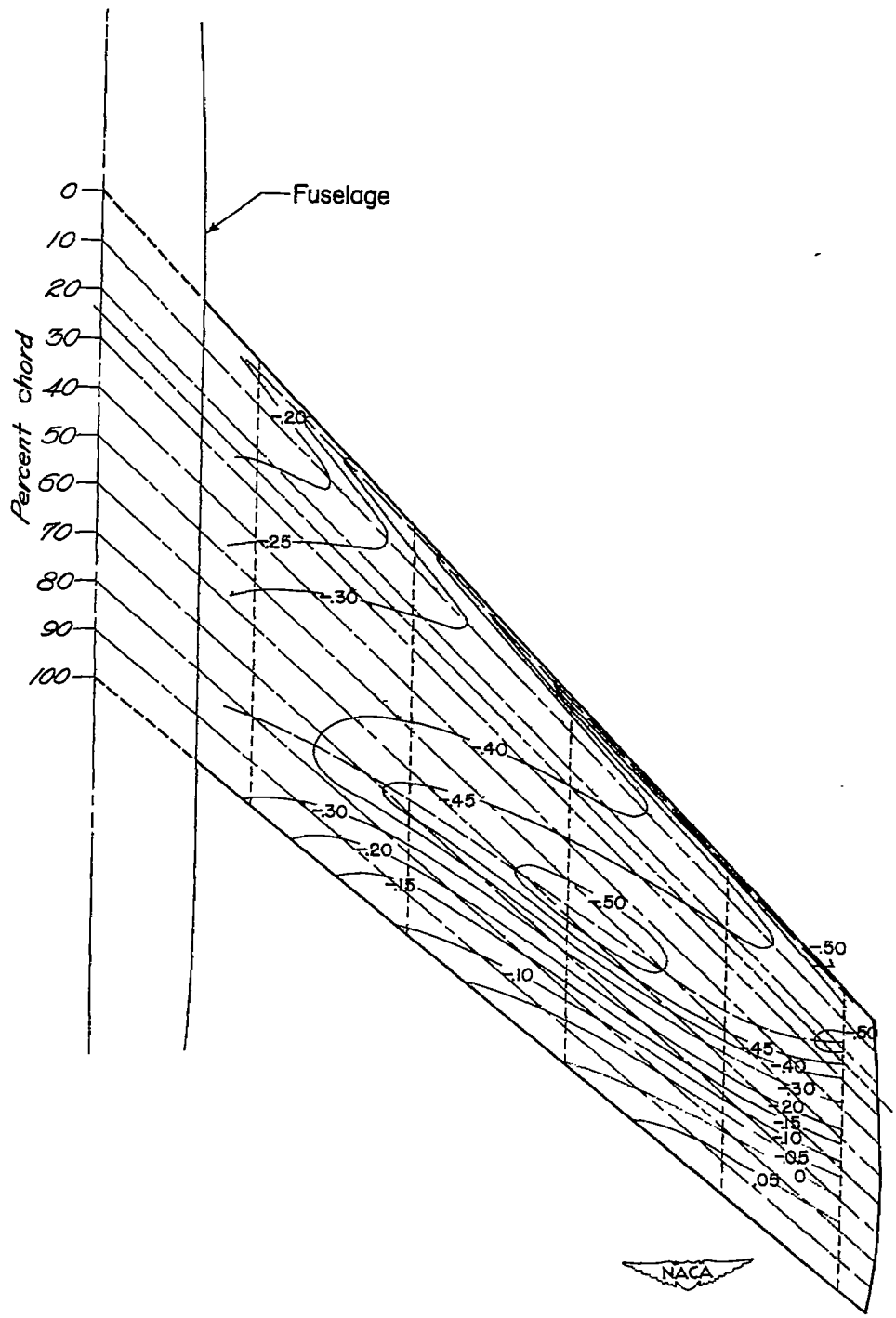

(e) Upper surface; M = 0.96; $\alpha = 2^{\circ}$.

Figure 27.- Continued.

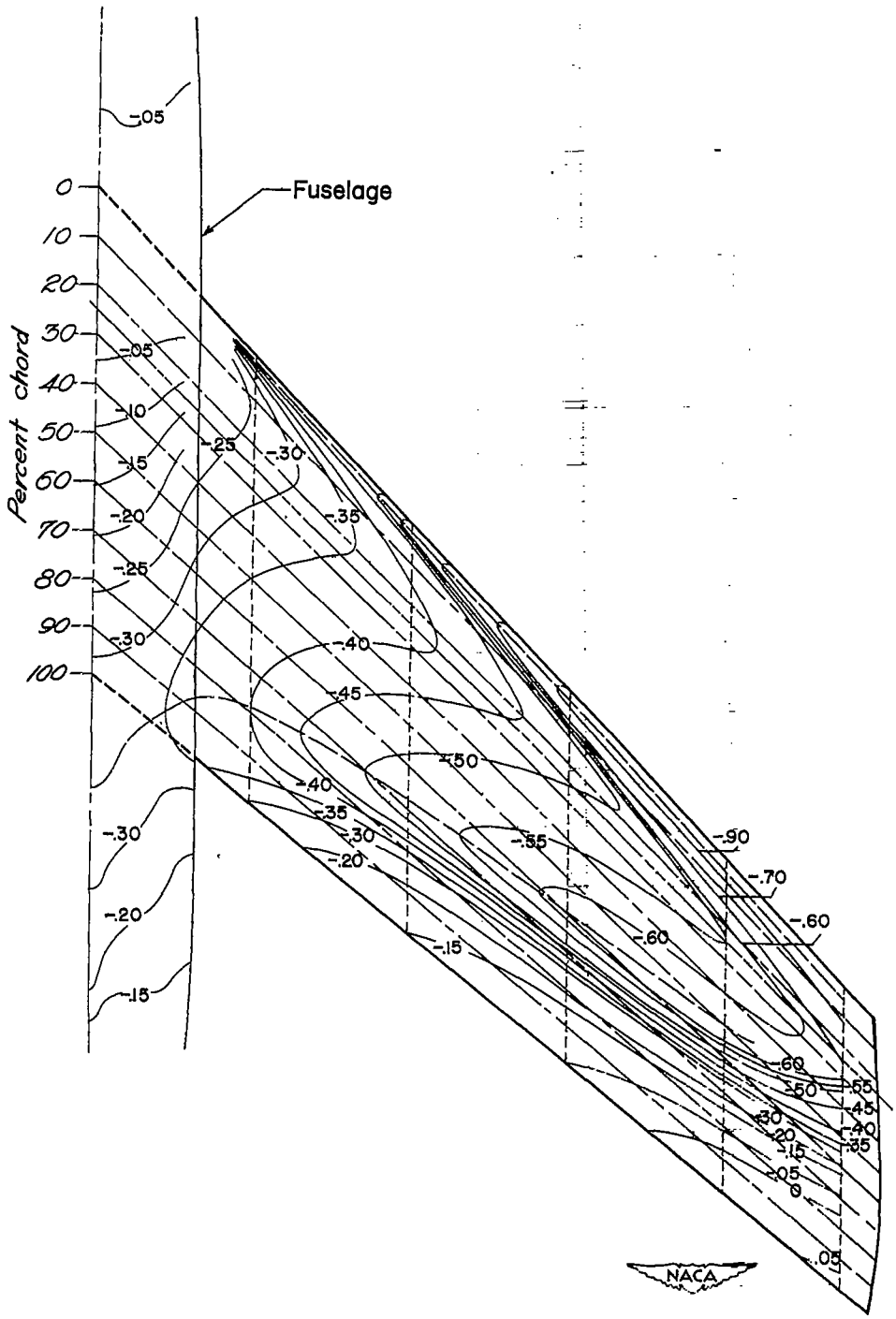

(f) Upper surface; M = 0.96; $\alpha = 4^{\circ}$.

Figure 27.- Continued.

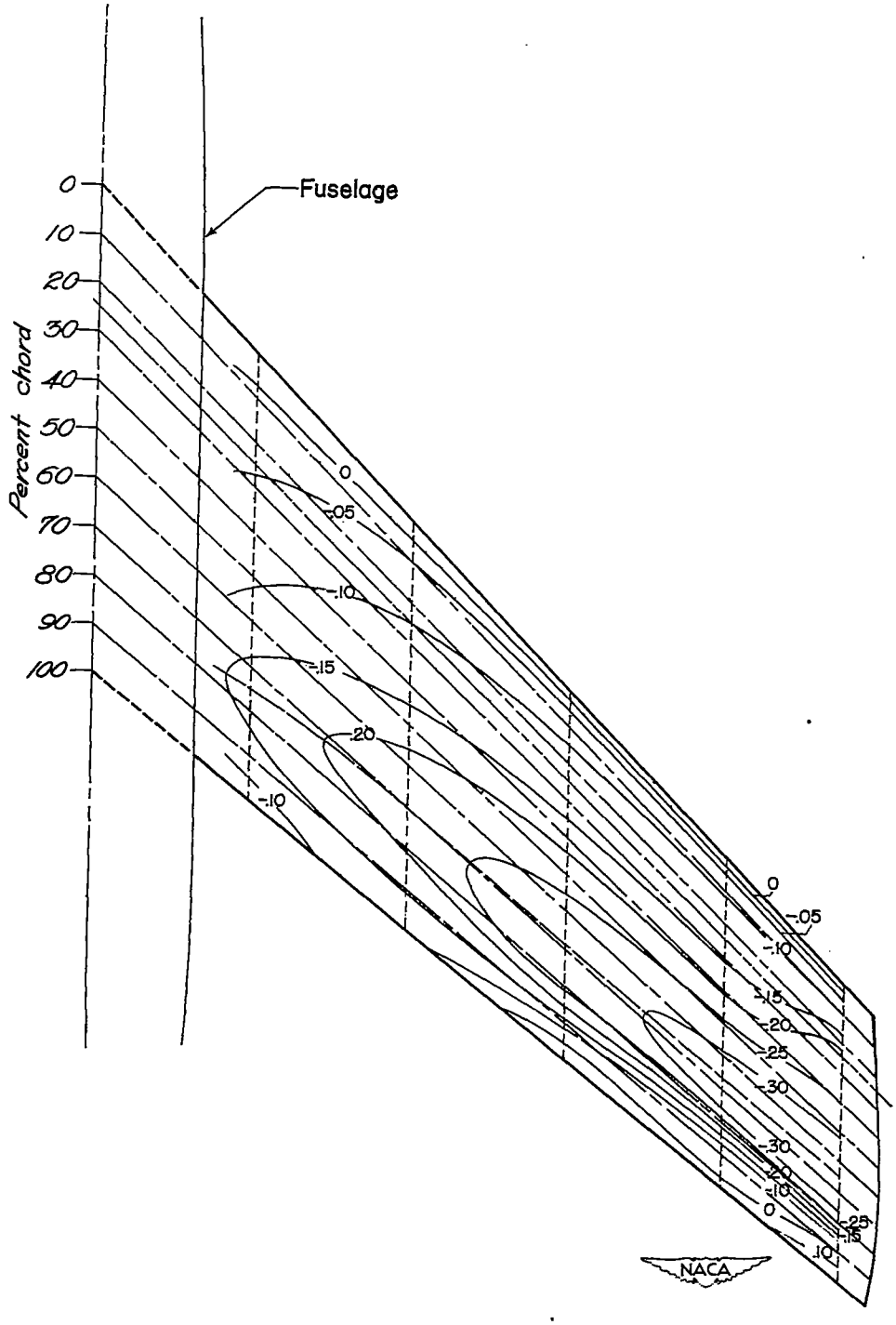

(g) Upper surface; M = 1.2; $\alpha = 0^{\circ}$.

Figure 27.- Continued.

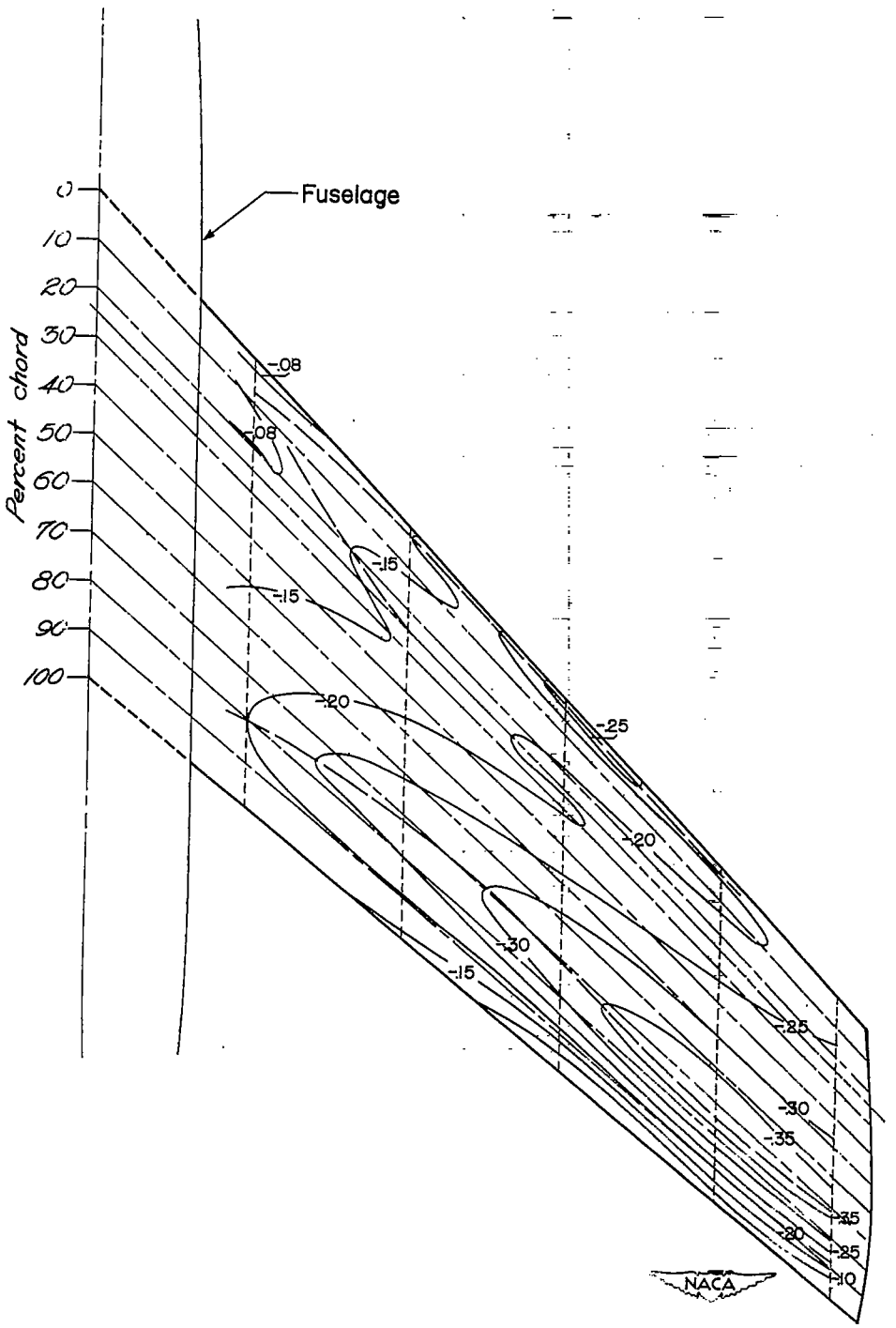

(h) Upper surface; M = 1.2; $\alpha = 2^{\circ}$.

Figure 27.- Continued.

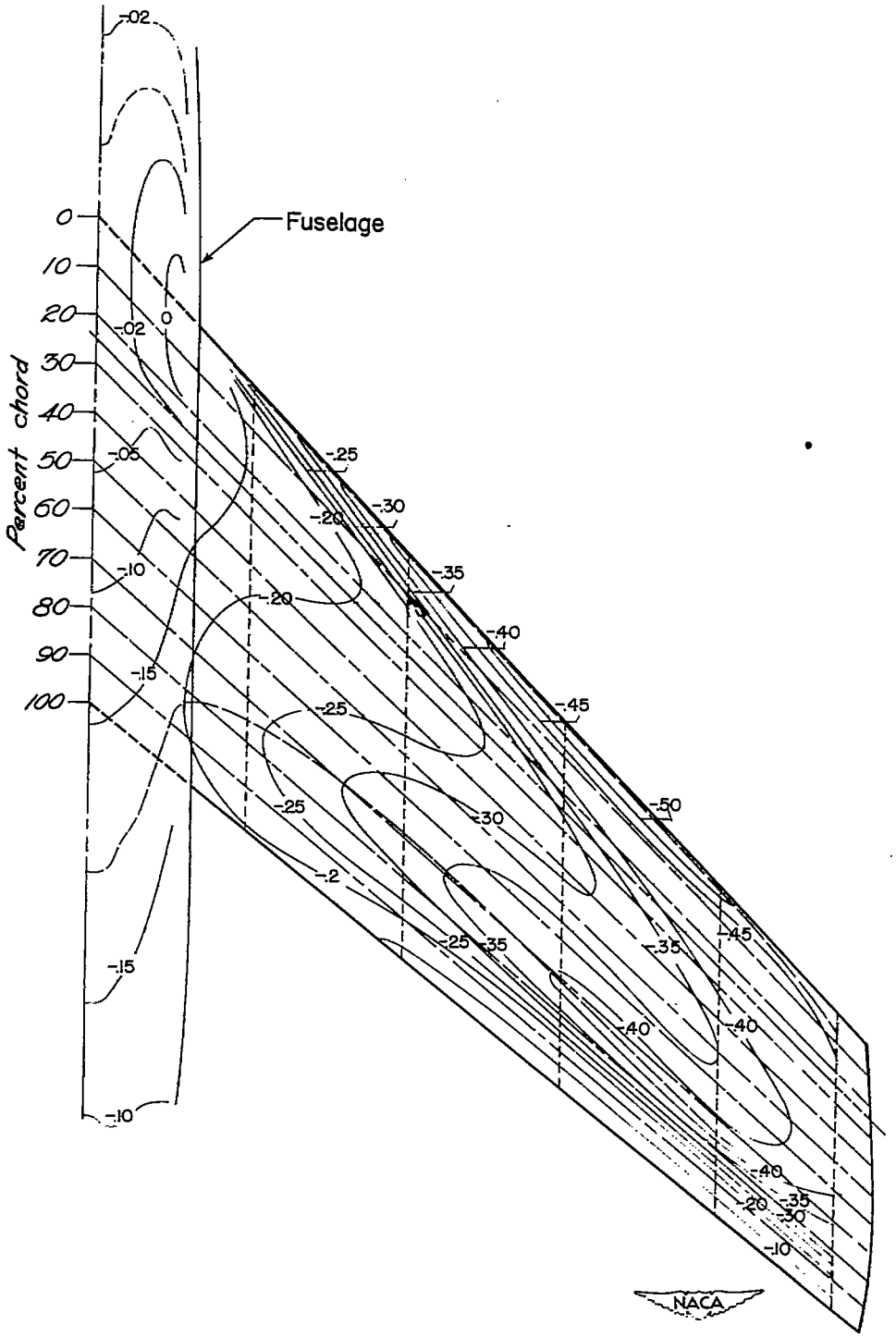

(i) Upper surface; M = 1.2; $\alpha = 4^{\circ}$.

Figure 27.- Concluded.

[redacted]

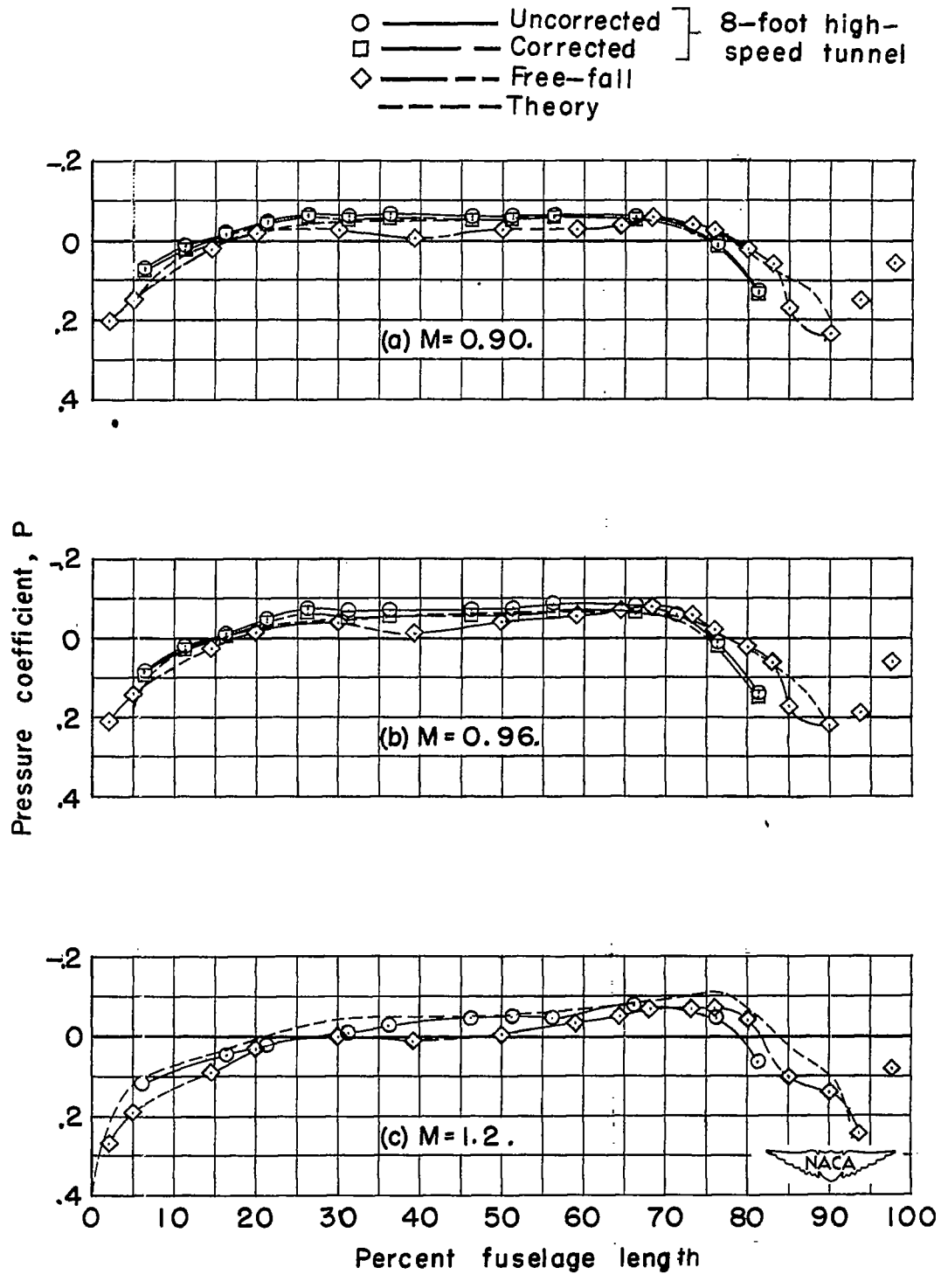

Figure 28.- Comparison of the pressure distributions at zero lift over the upper surface of the fuselage and a similar free-fall model for several Mach numbers.

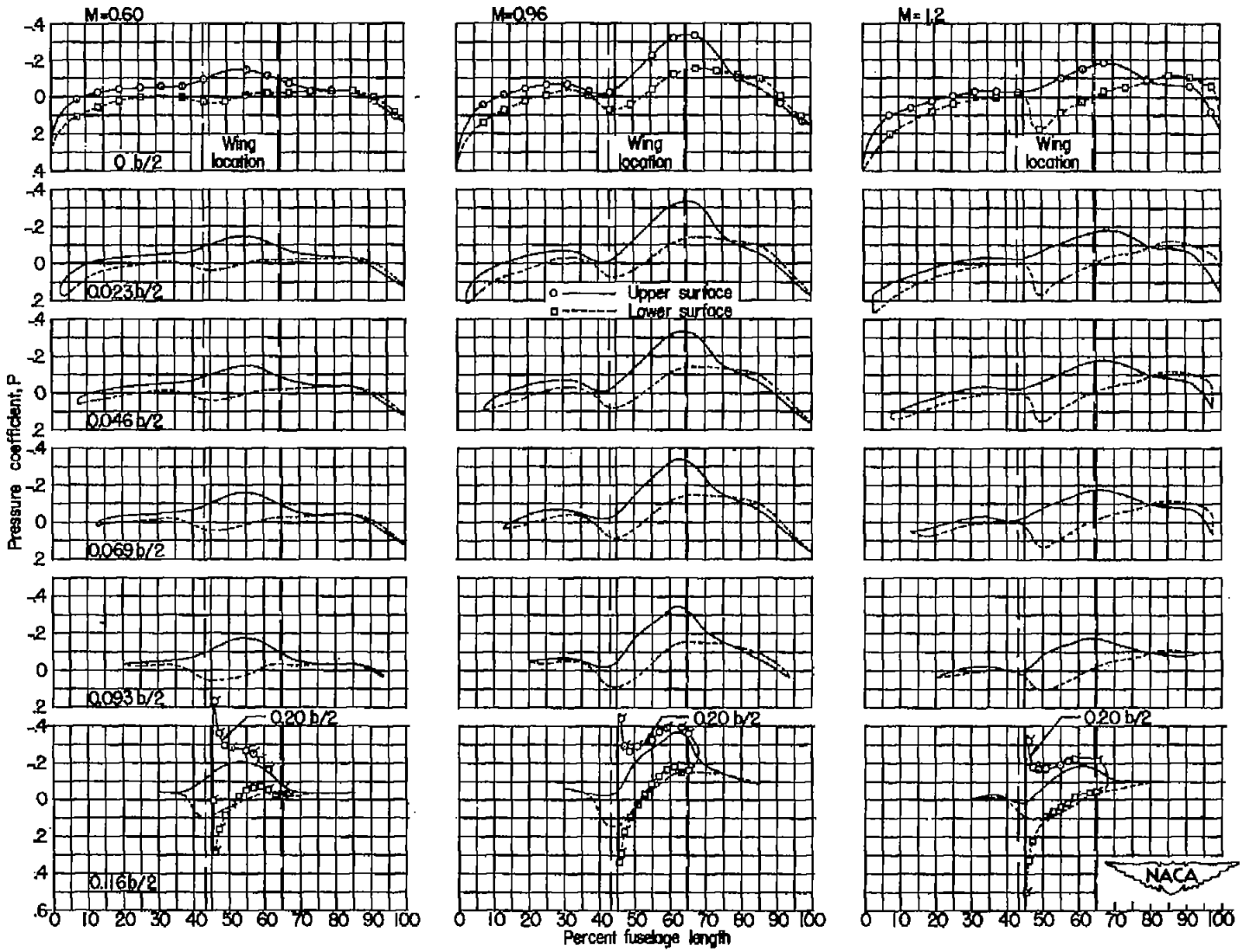

Figure 29.- Pressure distributions along six longitudinal fuselage stations in the presence of the wing at several Mach numbers. $\alpha = 4^{\circ}$.

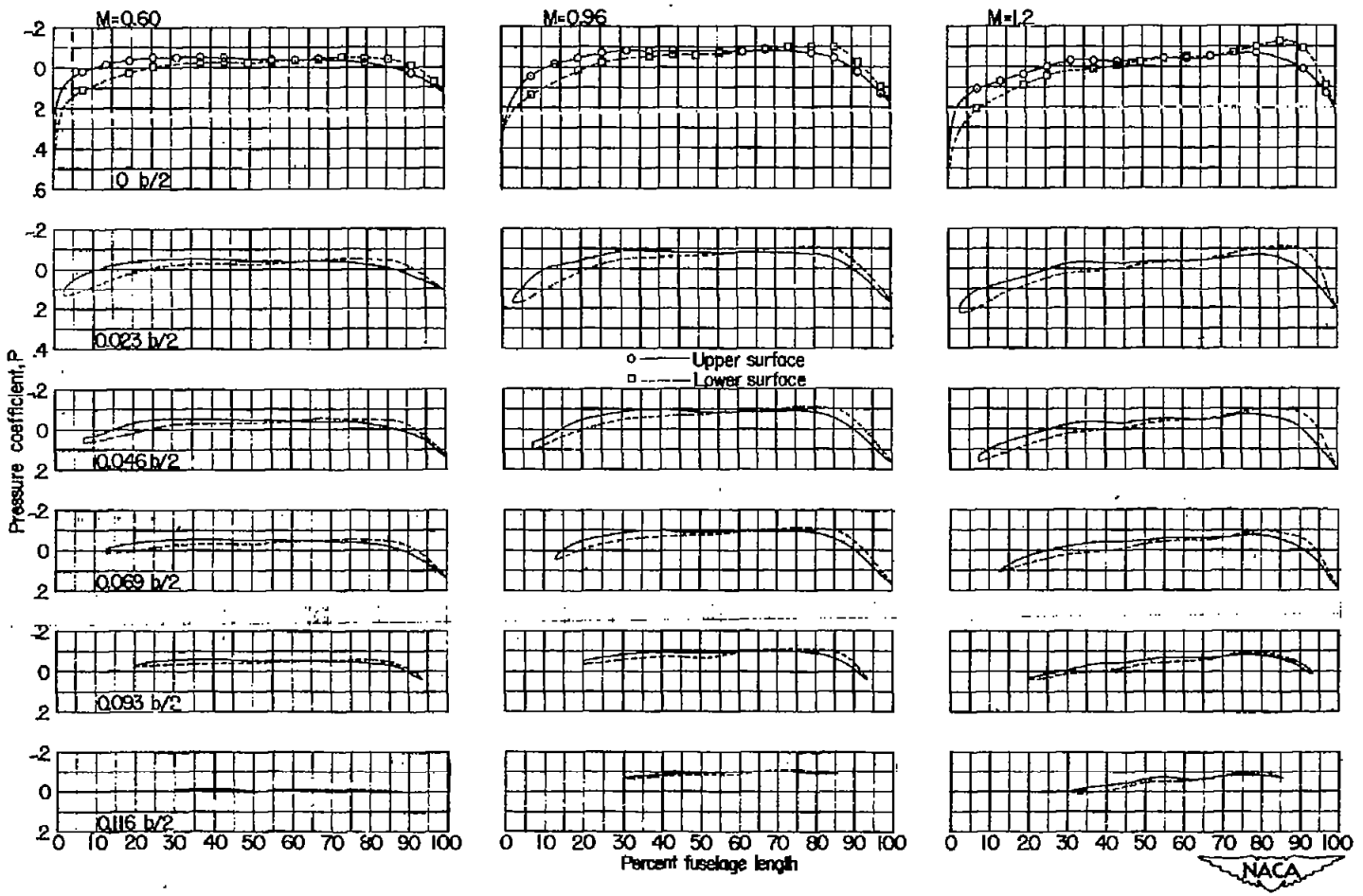

Figure 30.- Pressure distributions along six longitudinal fuselage stations at several Mach numbers for the fuselage. $\alpha = 4^{\circ}$.

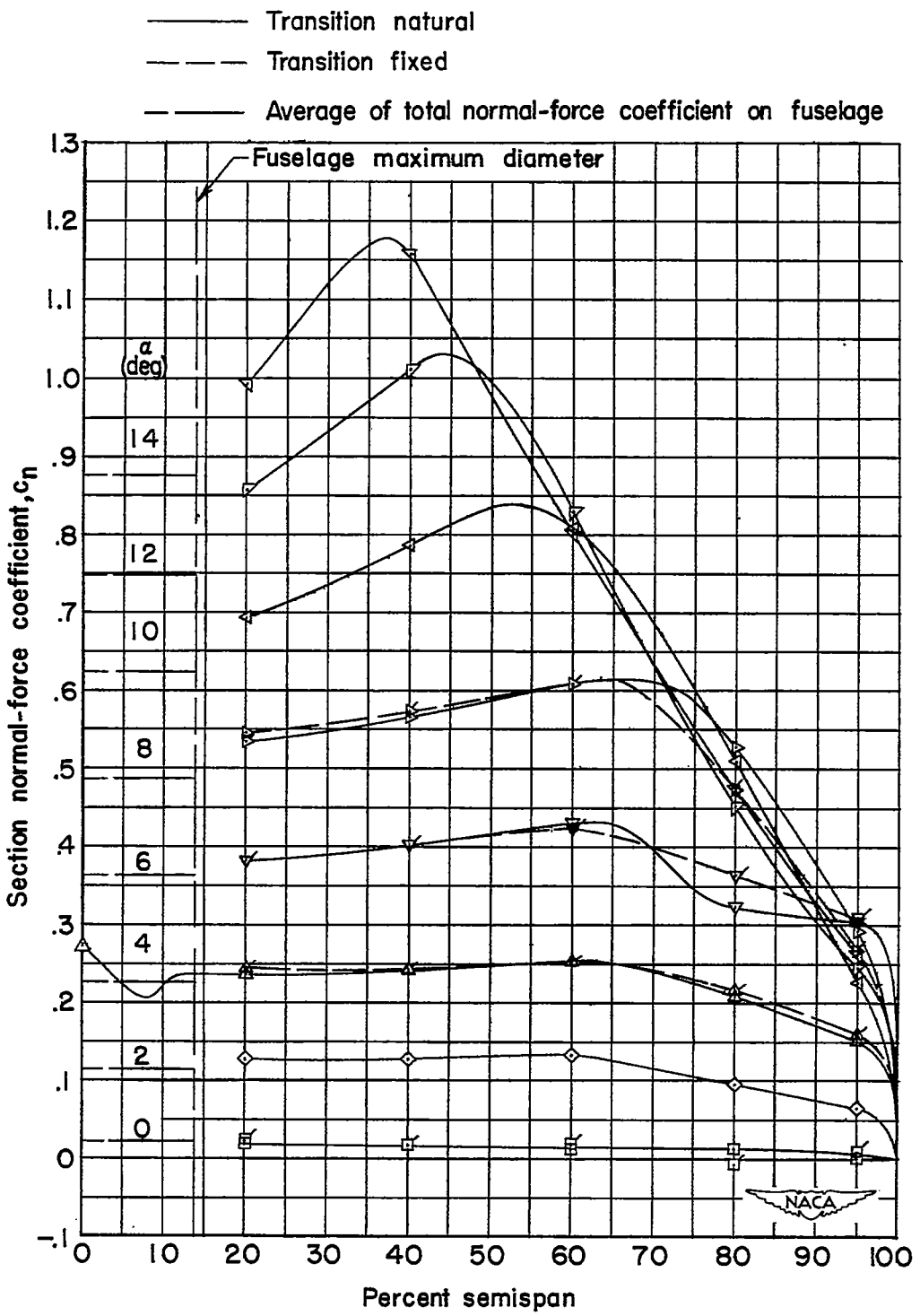

Figure 31.- The spanwise distributions of section normal-force coefficient at several angles of attack. M = 0.60. (Plain symbols indicate transition natural.)

[redacted]

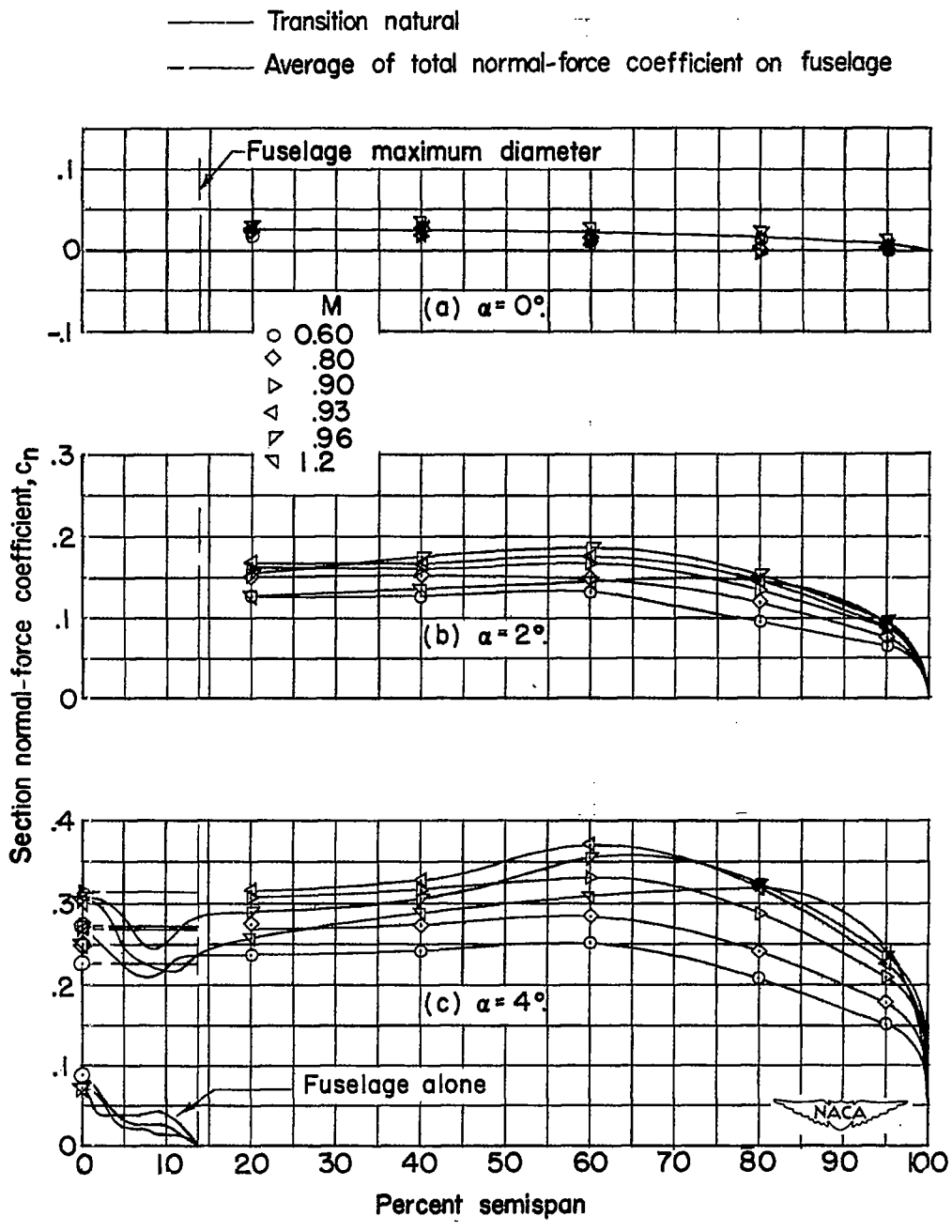

Figure 32.- The spanwise distributions of section normal-force coefficient at several Mach numbers. (Plain symbols indicate transition natural.)

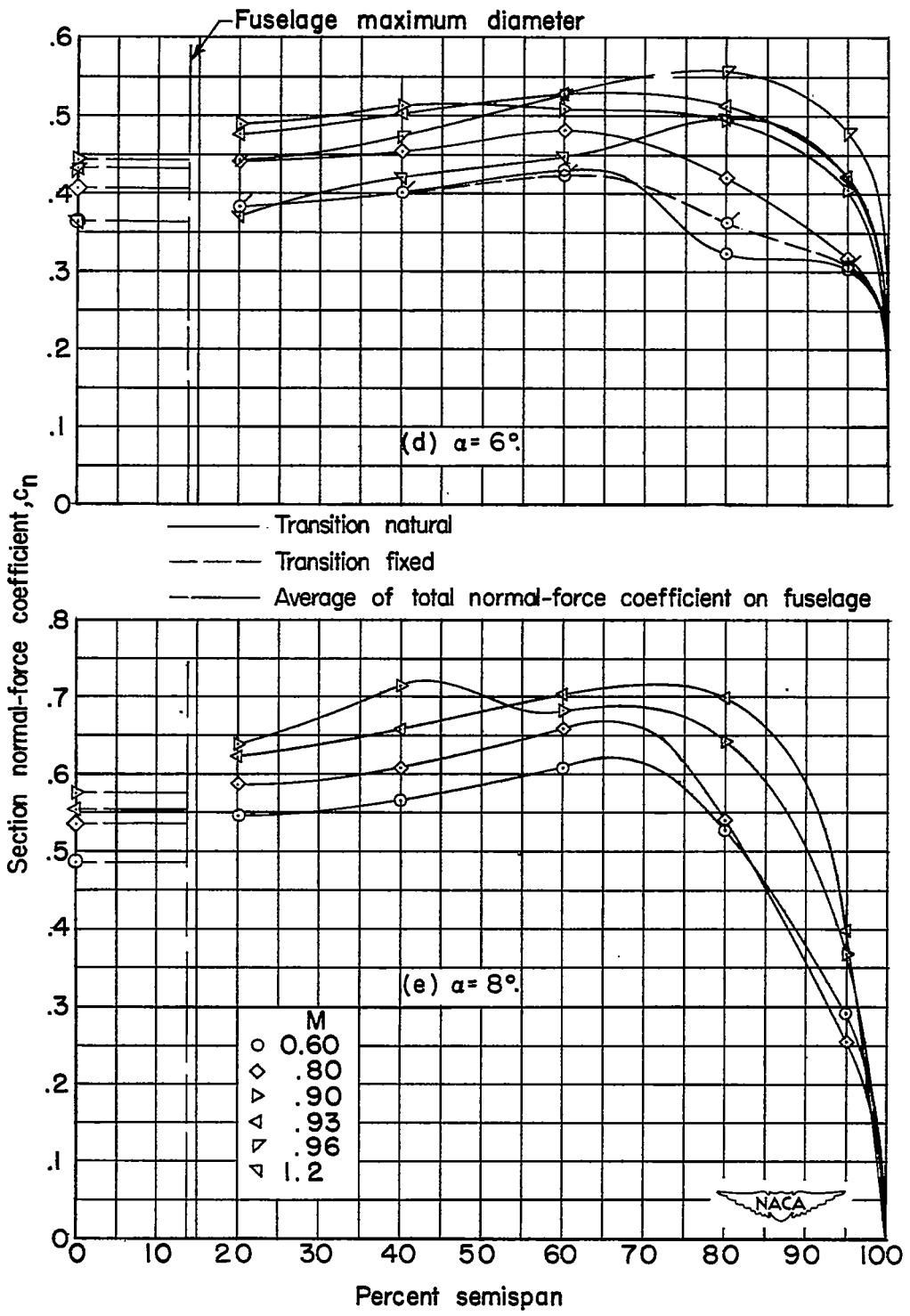

Figure 32.- Continued.

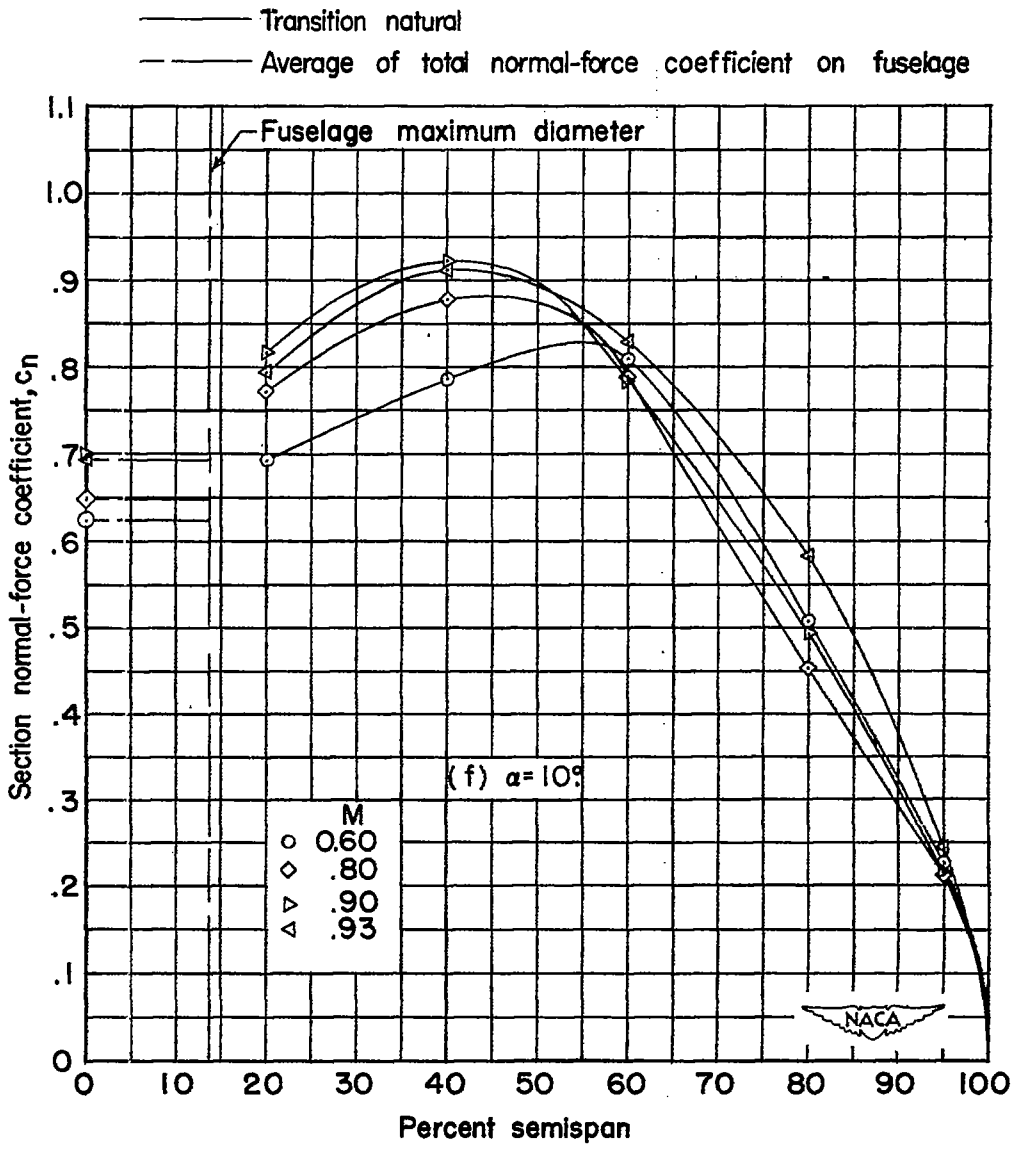

Figure 32.- Continued.

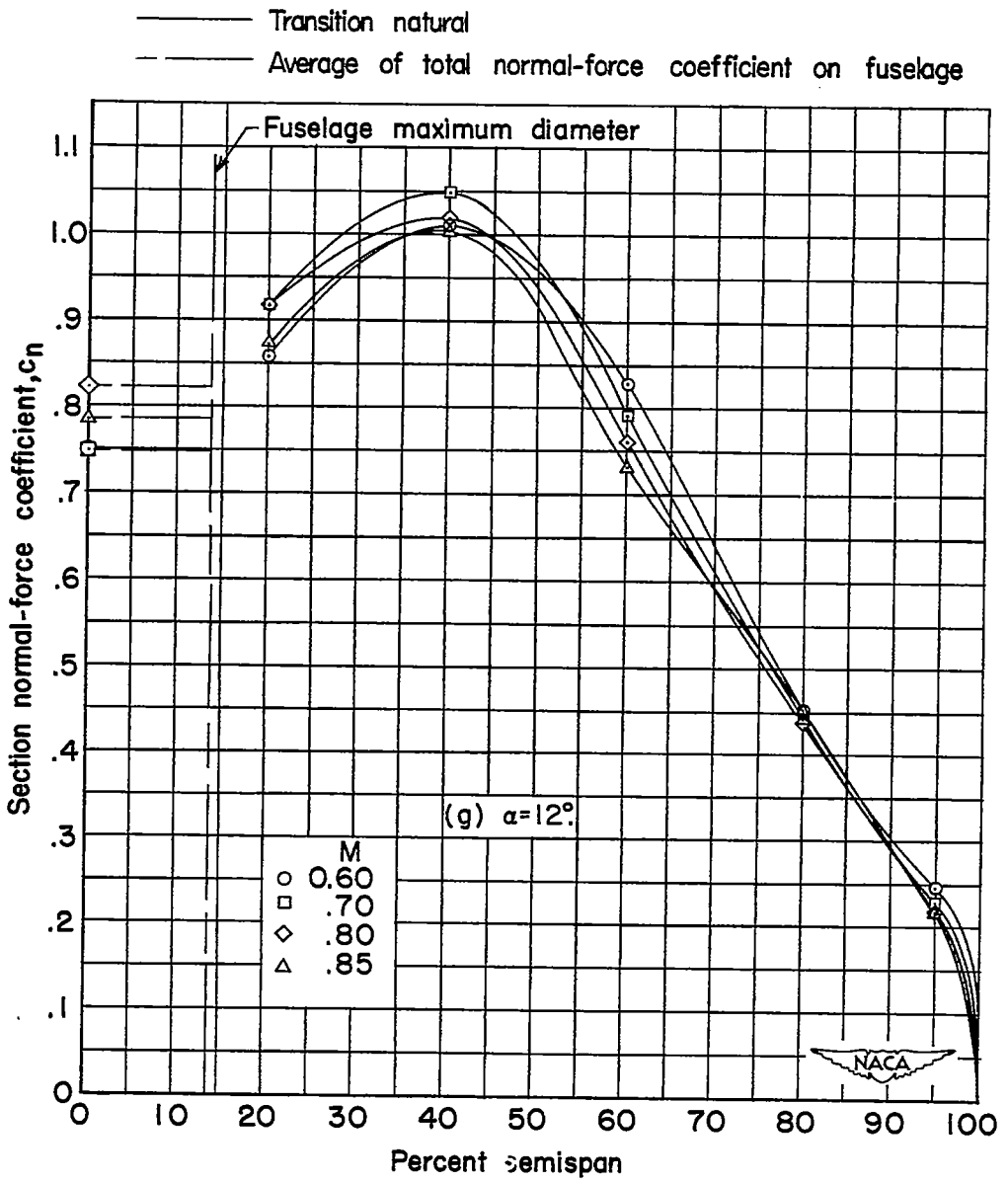

Figure 32.- Continued.

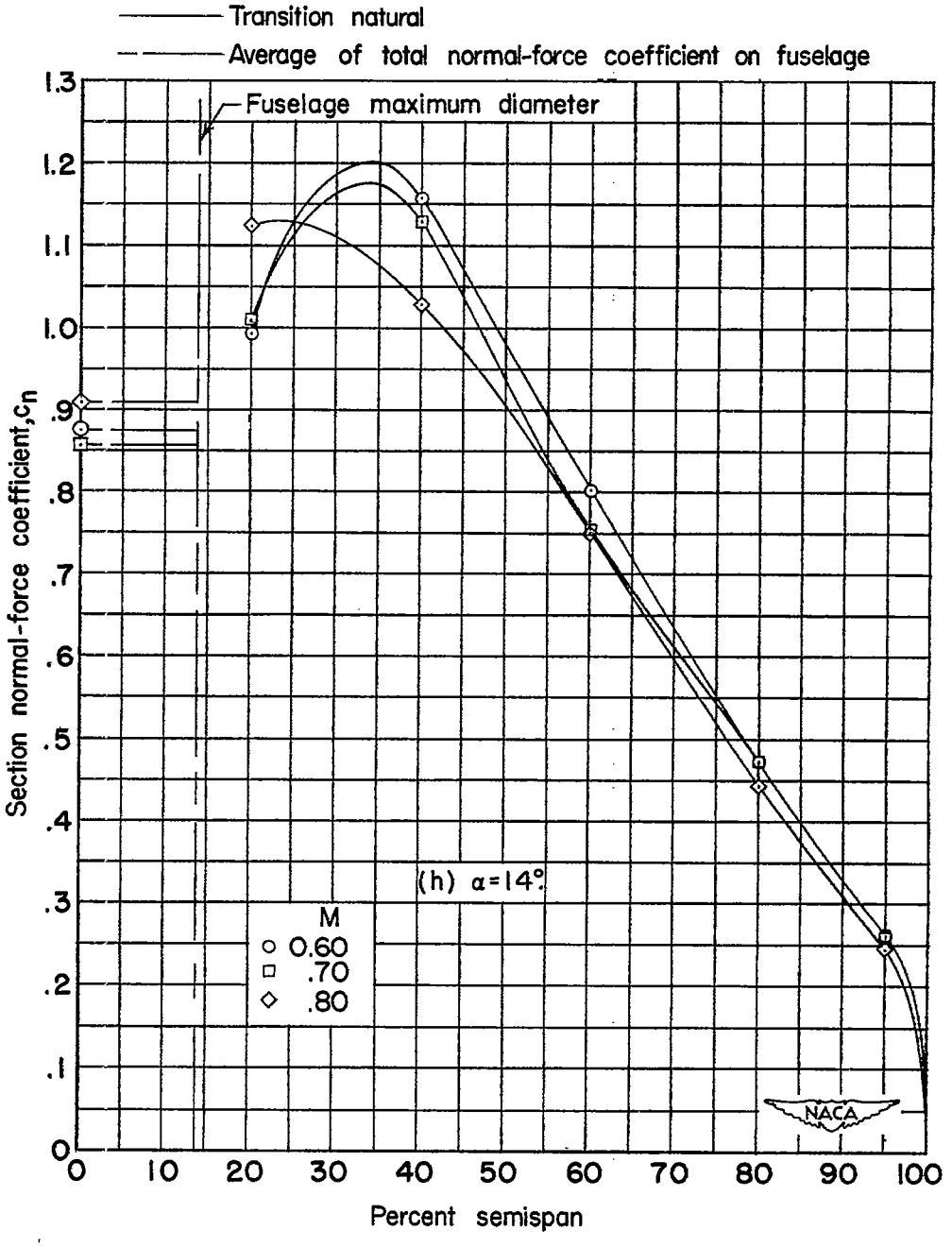

Figure 32.- Concluded.

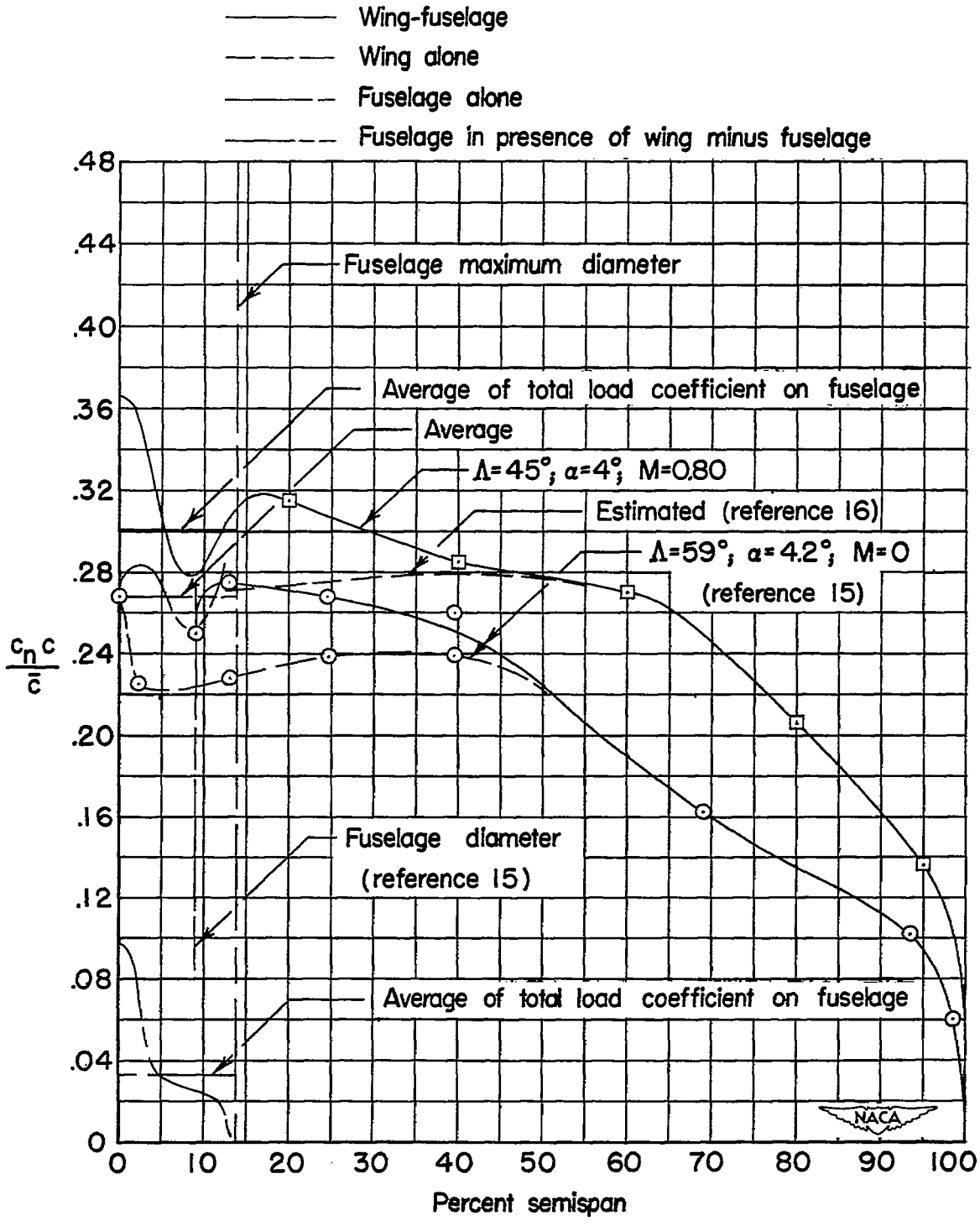

Figure 33.- Analysis of wing-fuselage interference on spanwise variation of normal-force parameter.

[redacted]

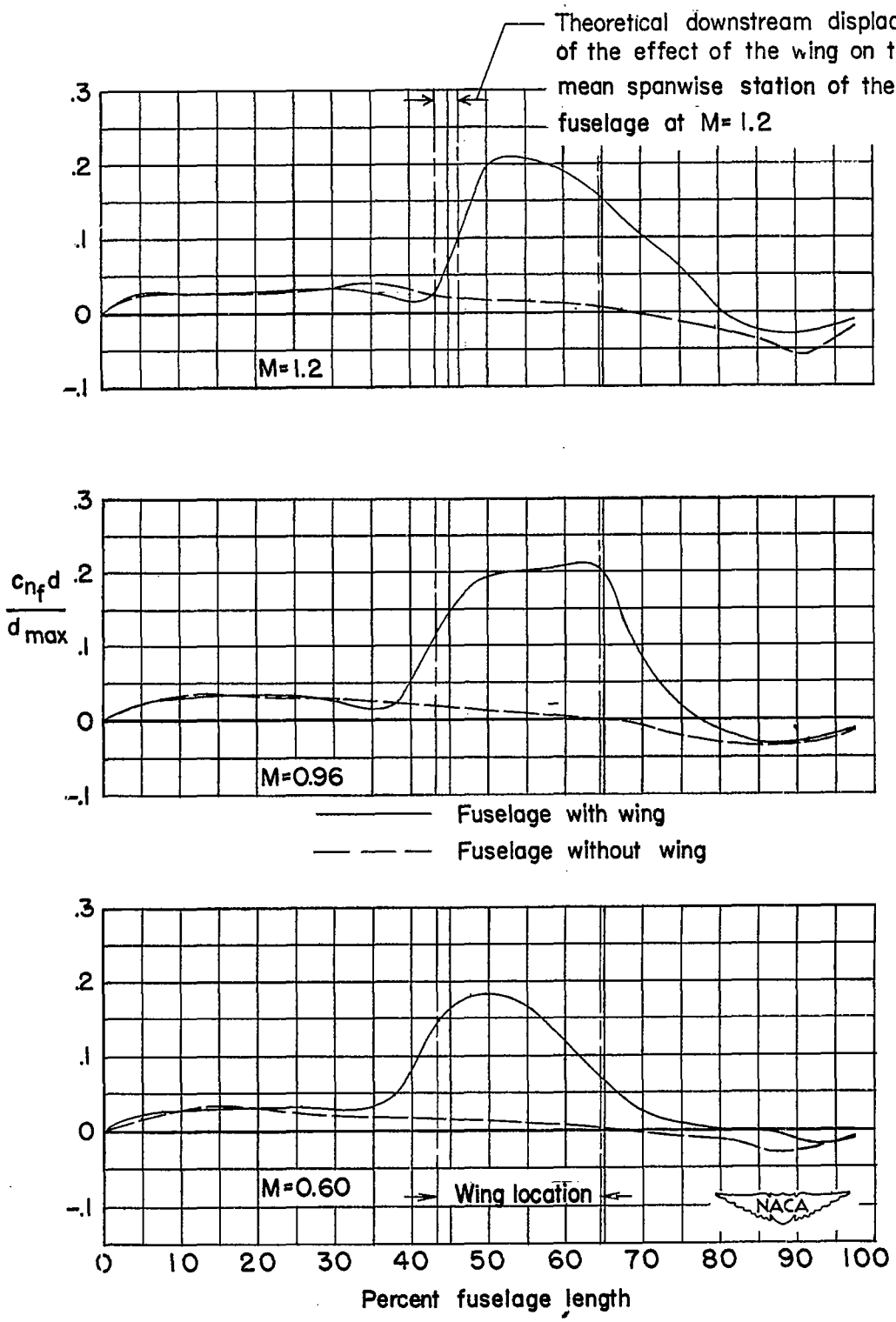

Figure 34.- Longitudinal loading over fuselage with and without wing at several Mach numbers. $\alpha = 4^{\circ}$.

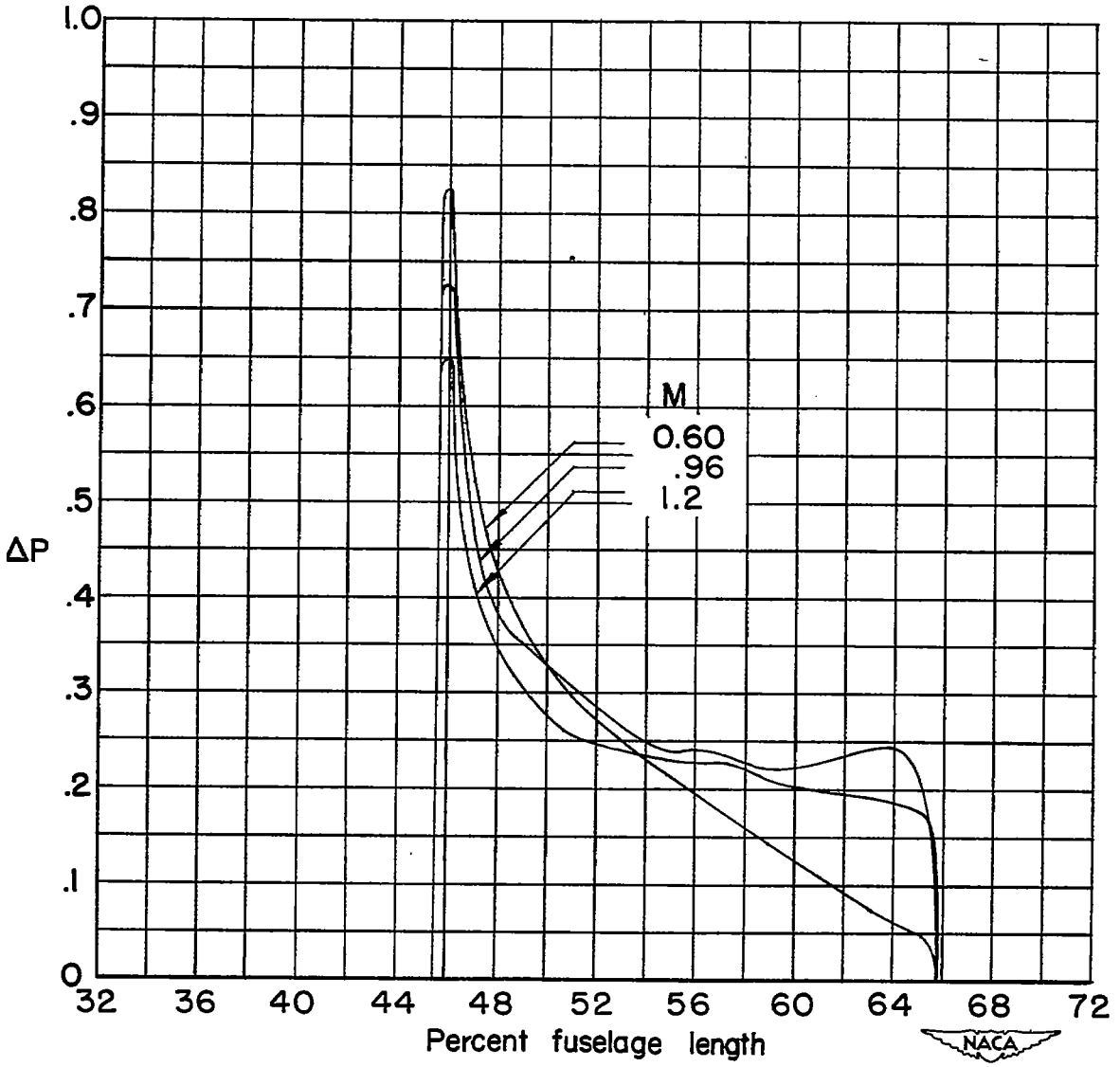

Figure 35.- Chordwise normal loading over 20-percent-semispan station. $\alpha = 4^{\circ}$.

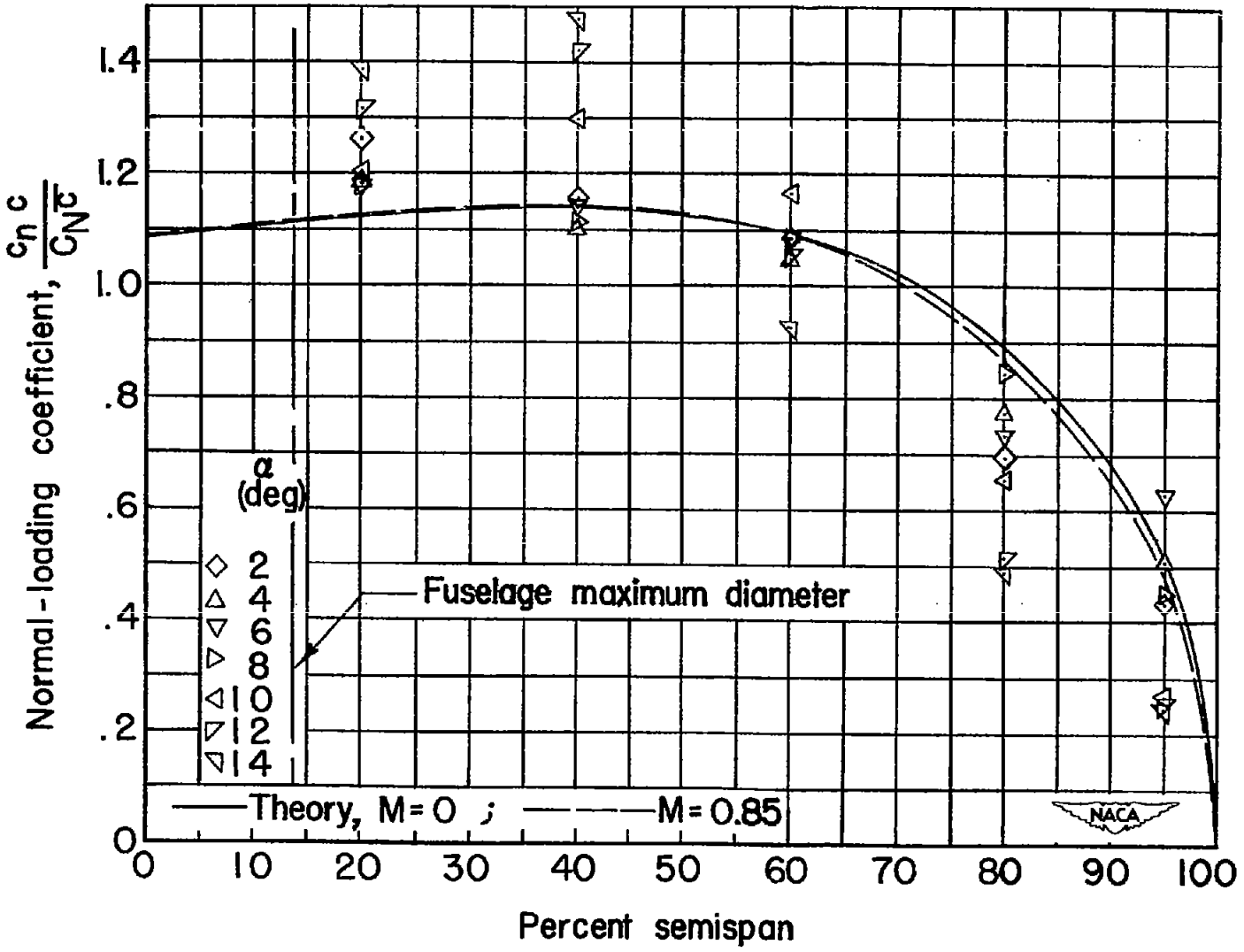

Figure 36.- The spanwise distributions of normal-loading coefficient at several angles of attack. M = 0.60.

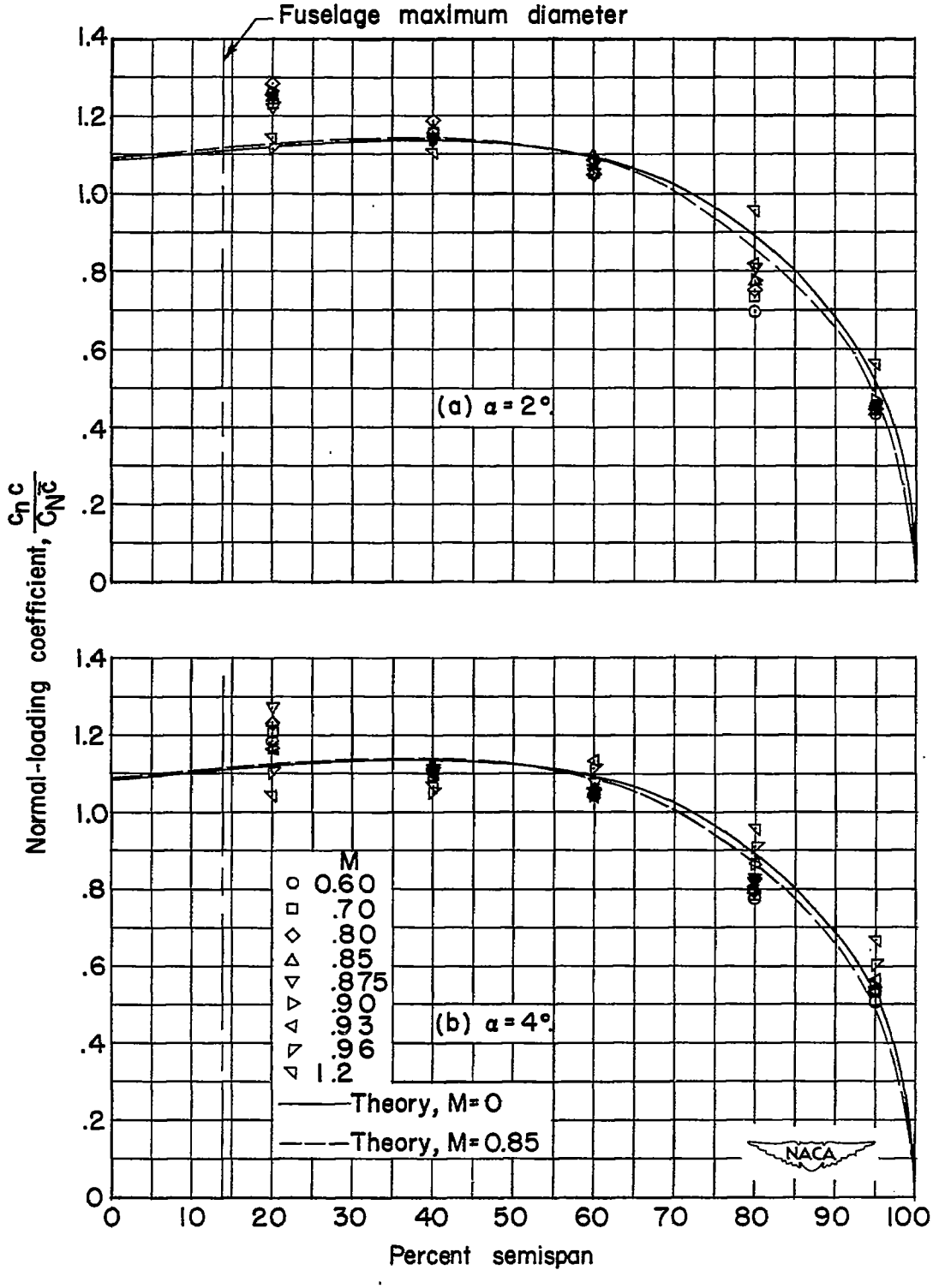

Figure 37.- The spanwise distributions of normal-loading coefficient at several Mach numbers.

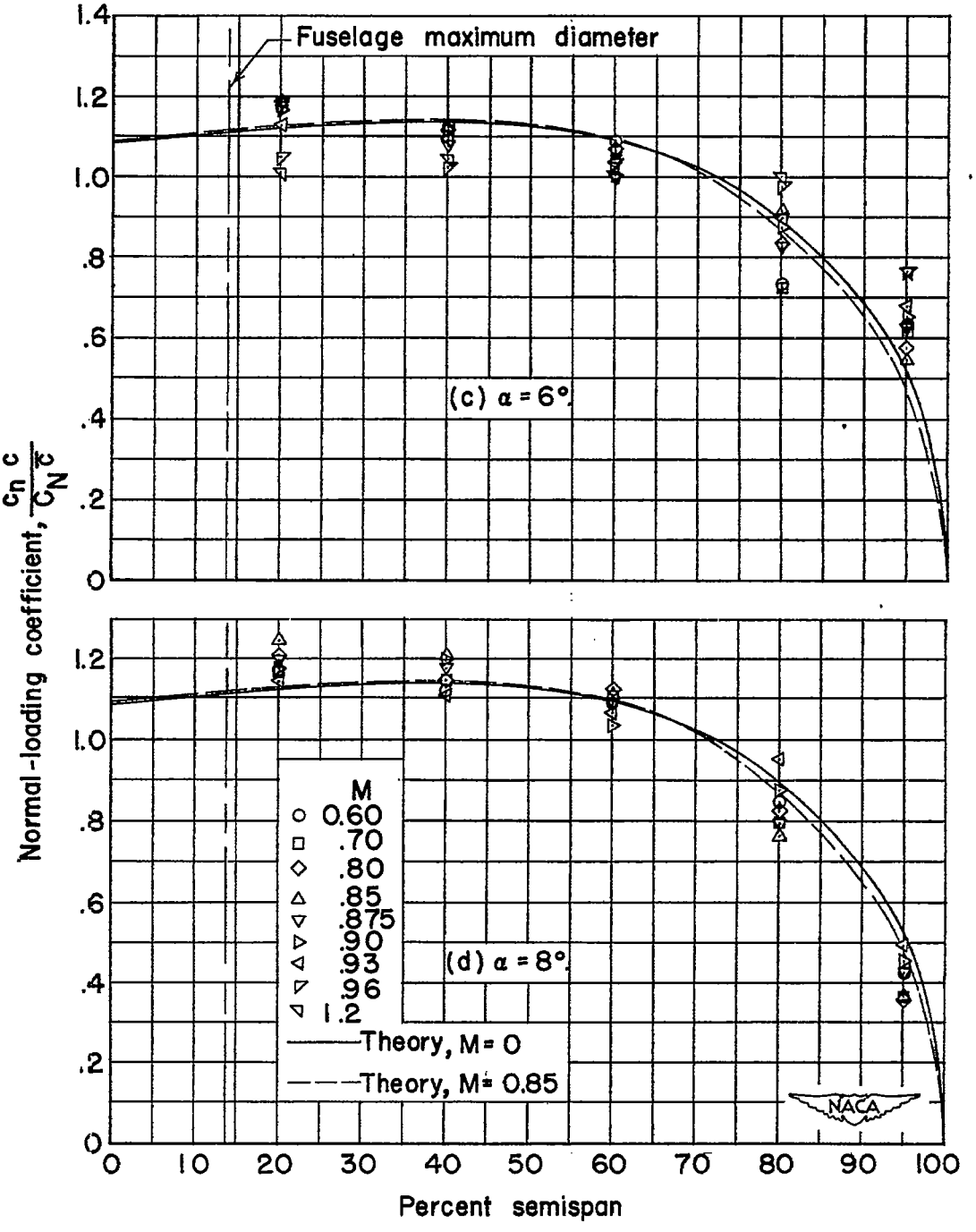

Figure 37.- Continued.

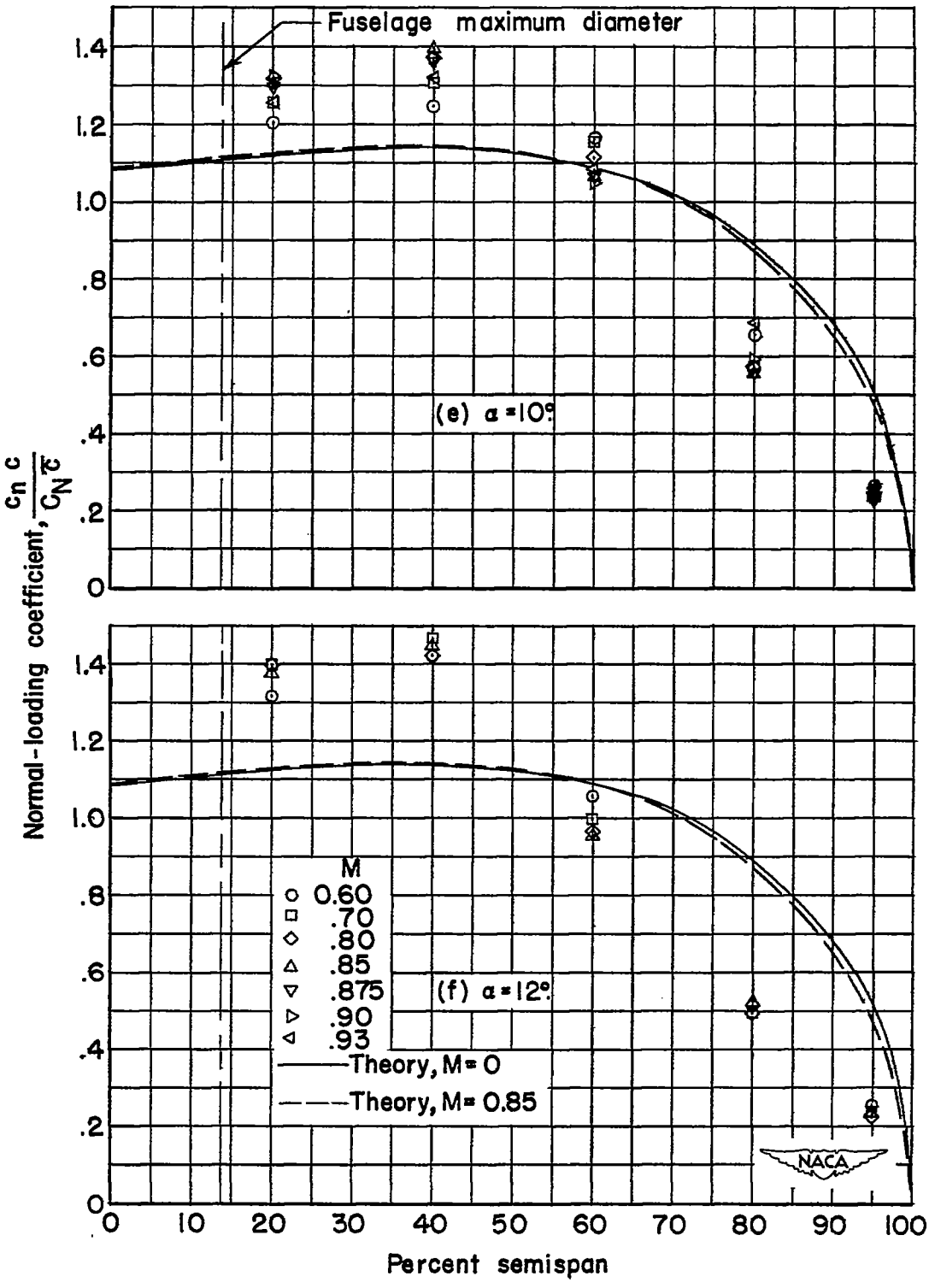

Figure 37.- Continued.

[redacted]

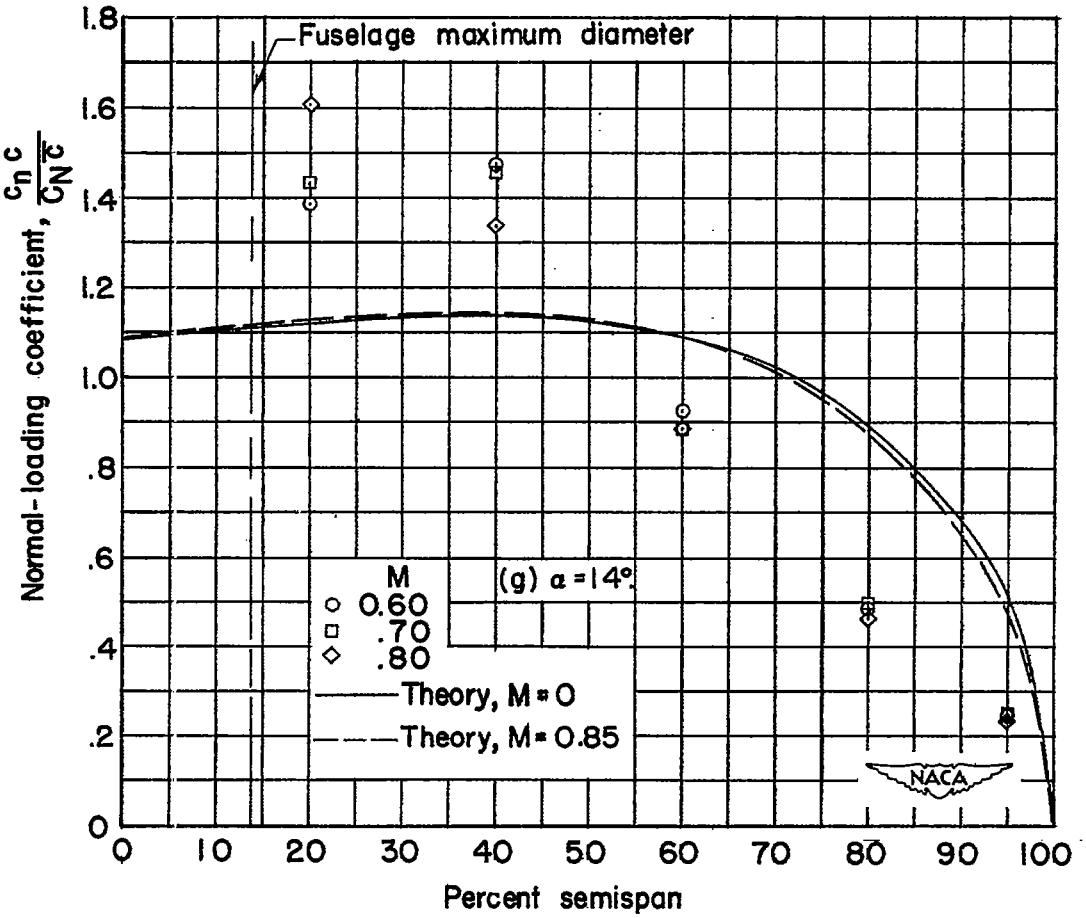

Figure 37.- Concluded.

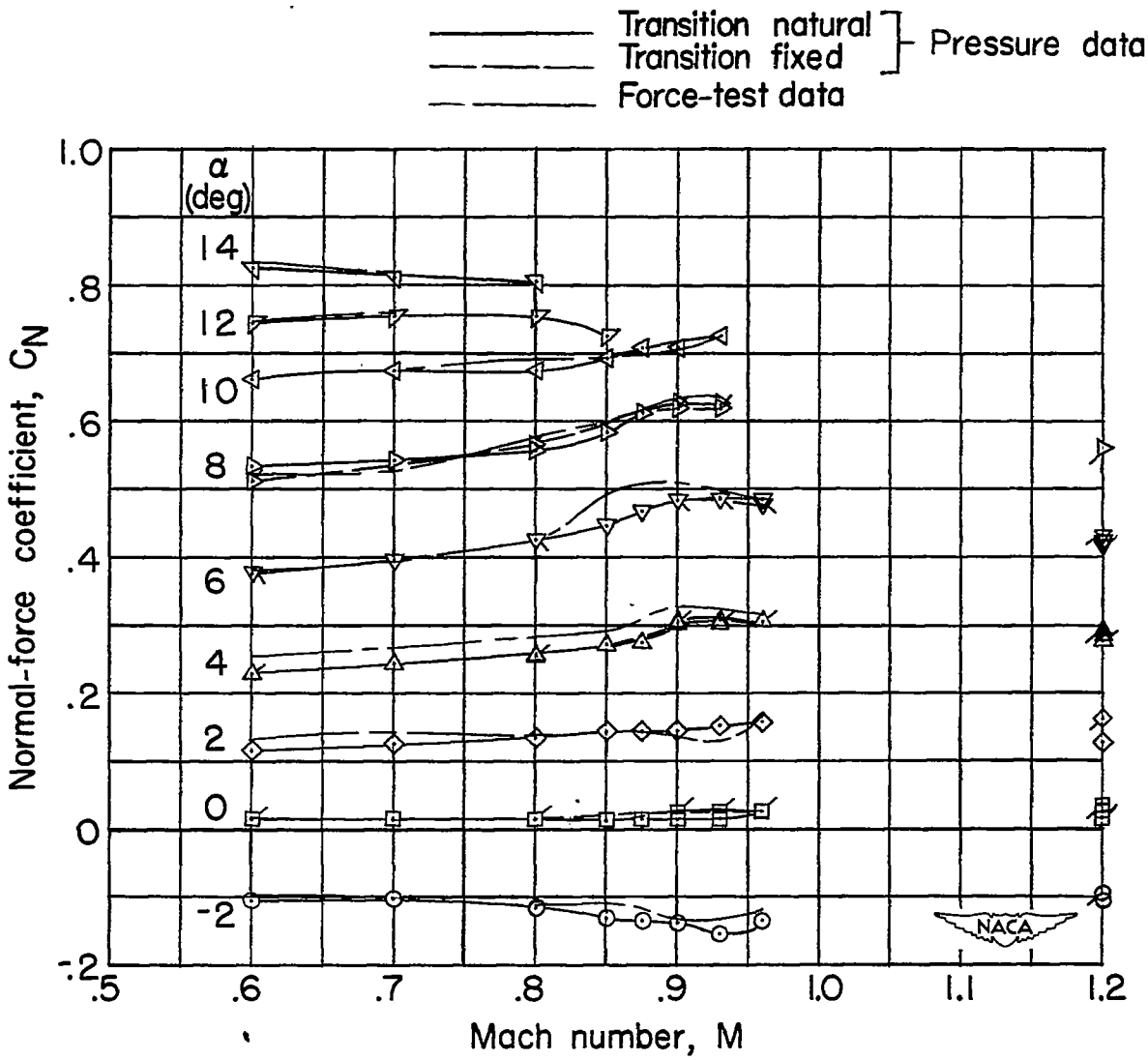

Figure 38.- Variation with Mach number of normal-force coefficient for wing-fuselage configuration with transition natural and fixed. (Flagged symbols to the right indicate transition fixed; tailed symbols to the left, at M = 1.2, indicate force-test data.)

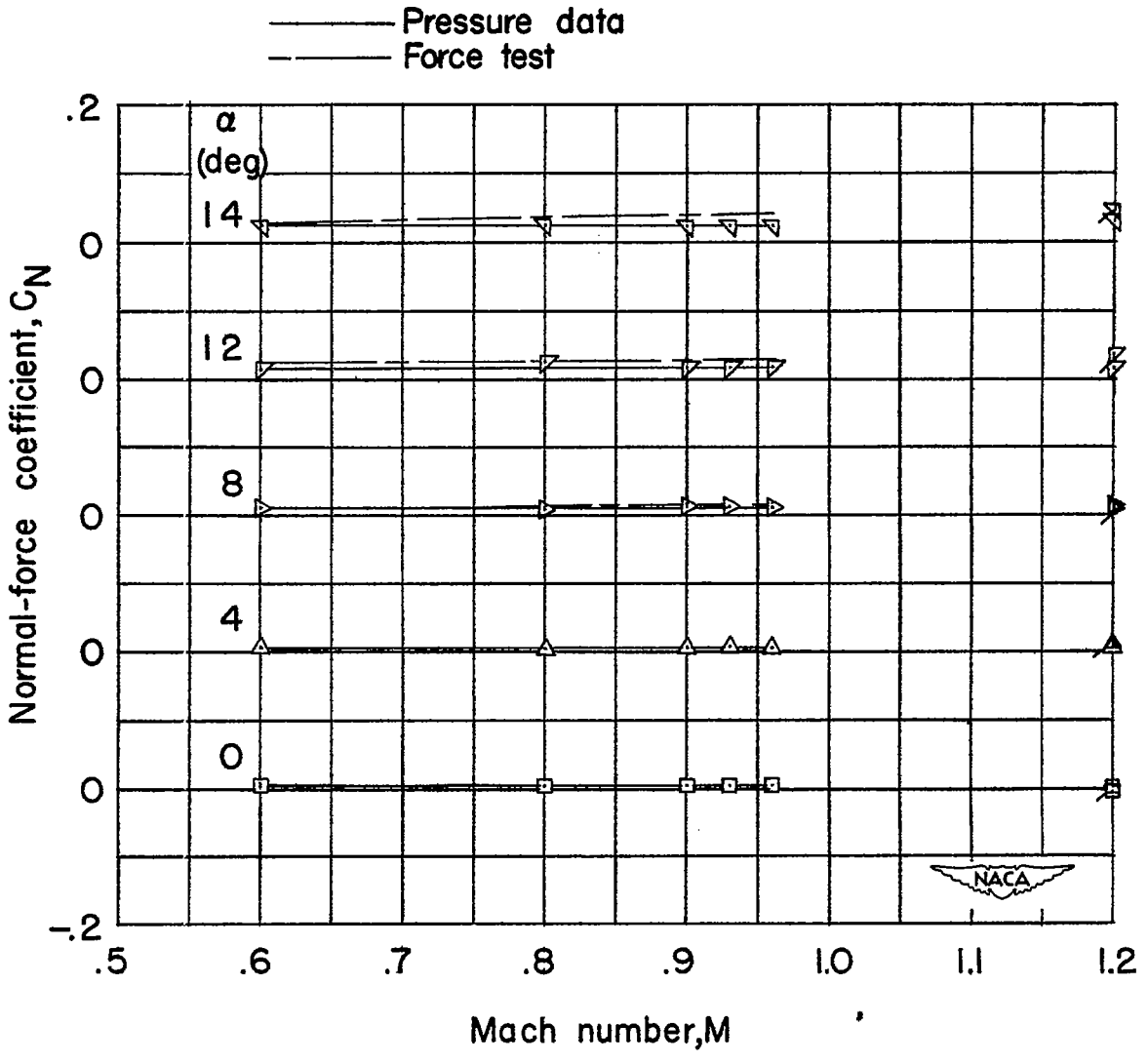

Figure 39.- Variation with Mach number of normal-force coefficient for fuselage. (Plain symbols indicate pressure data.)

[redacted]

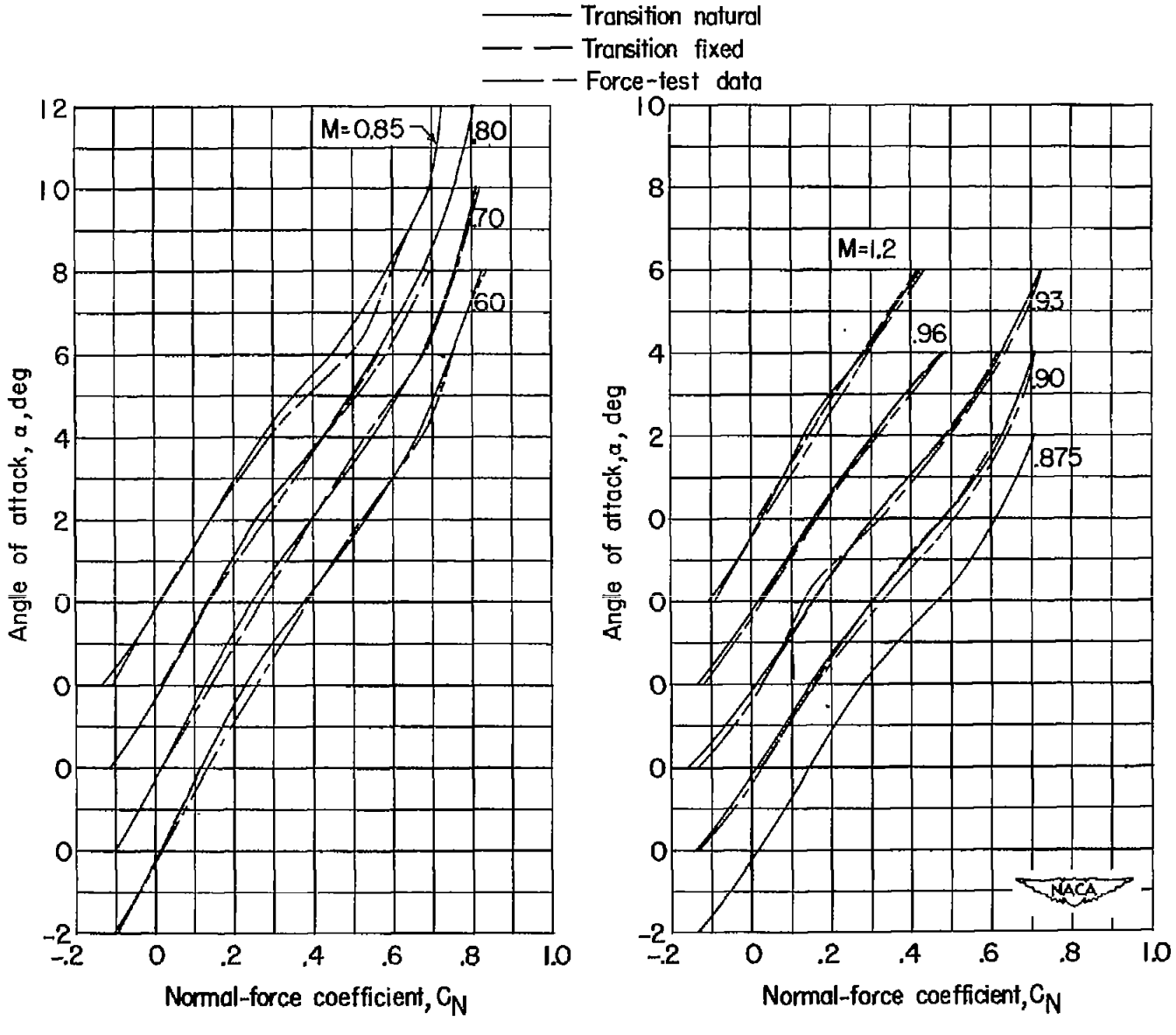

Figure 40.- Variation with normal-force coefficient of the aerodynamic characteristics of the wing-fuselage configuration.

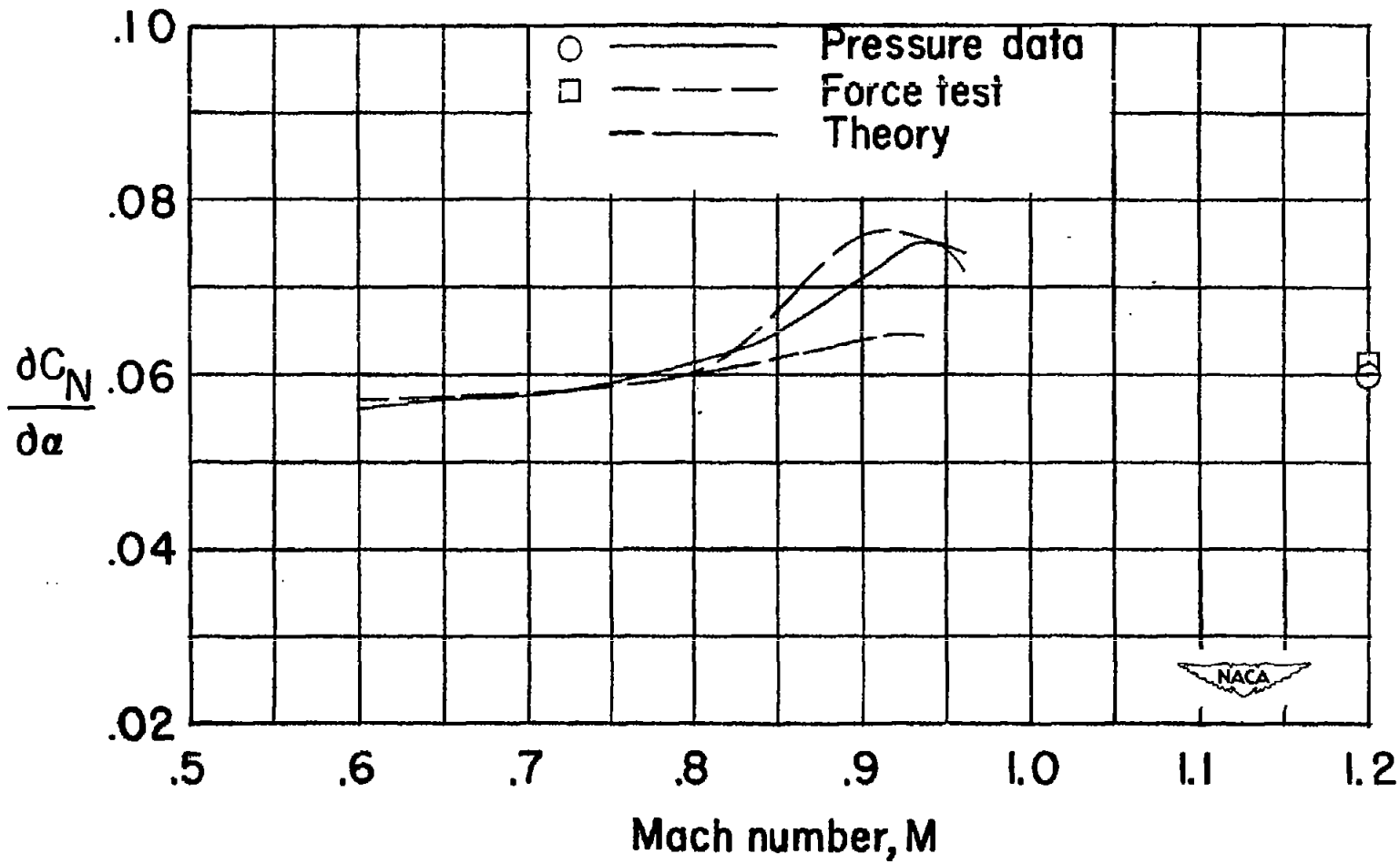

Figure 41.- Variation with Mach number of normal-force-curve slope for the wing-fuselage configuration. $C_N = 0$.

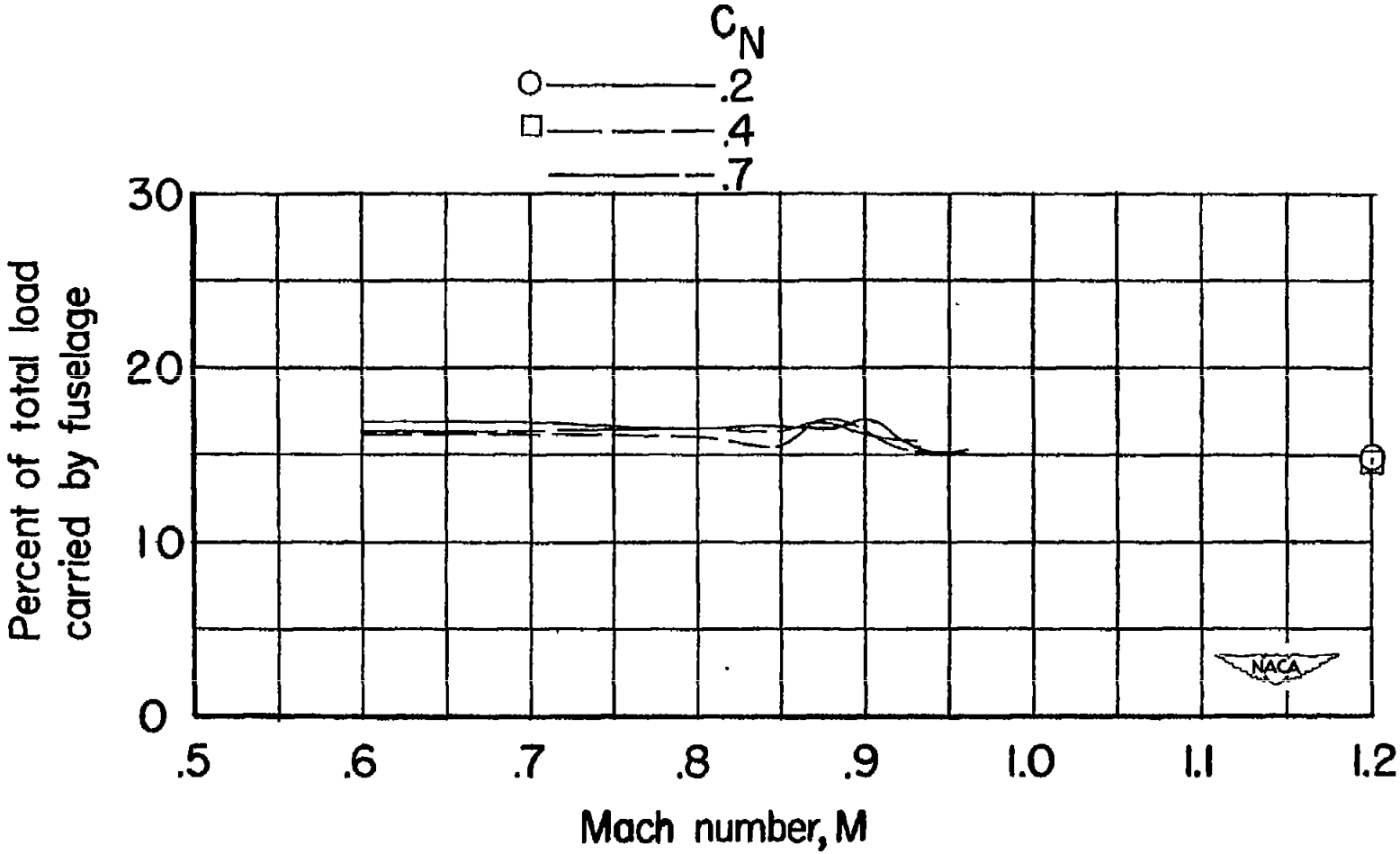

Figure 42.- Load carried by the fuselage with wing present relative to the total load on wing-fuselage combination.

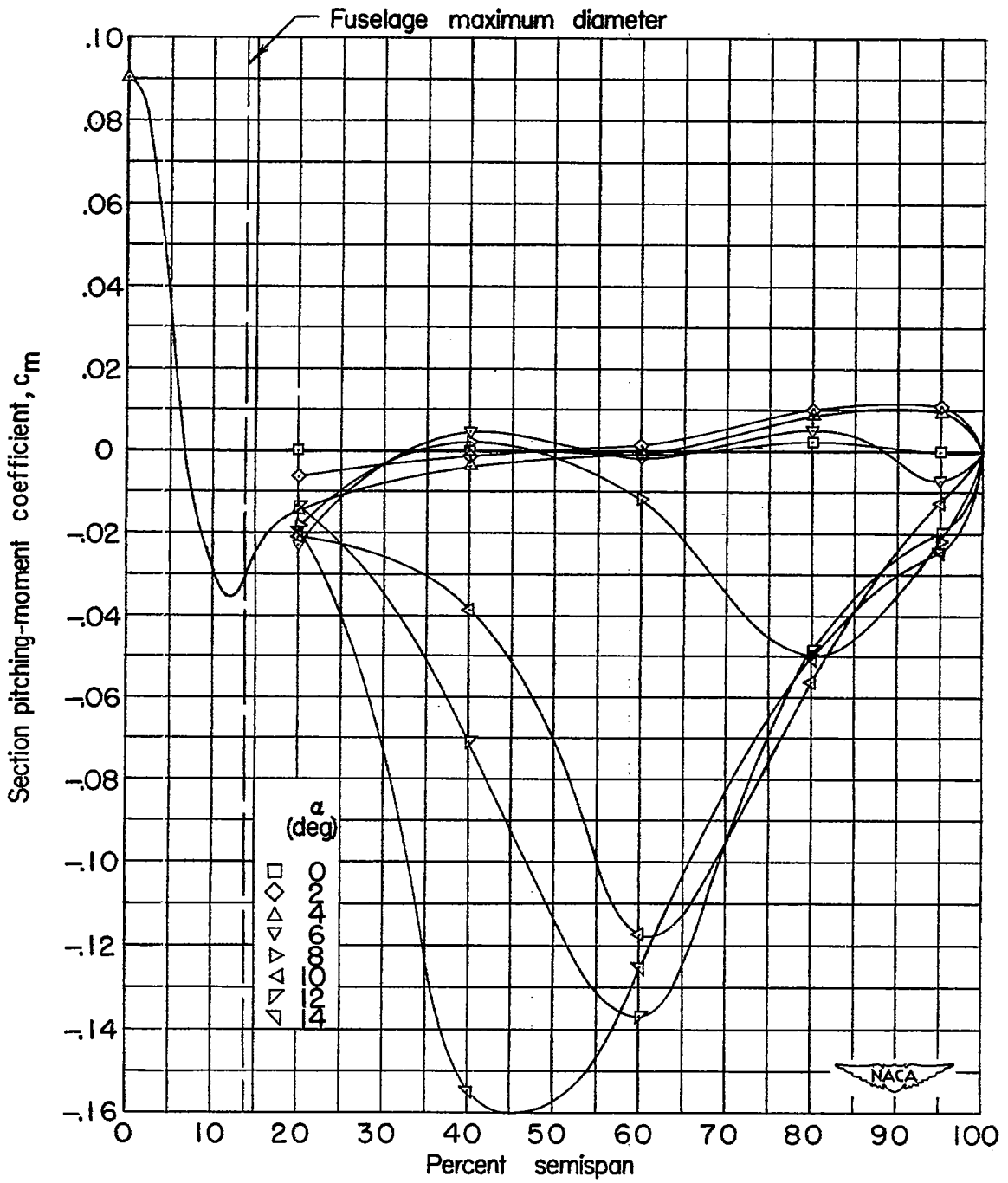

Figure 43.- The spanwise distributions of section pitching-moment ccefficient at several angles of attack. M = 0.60.

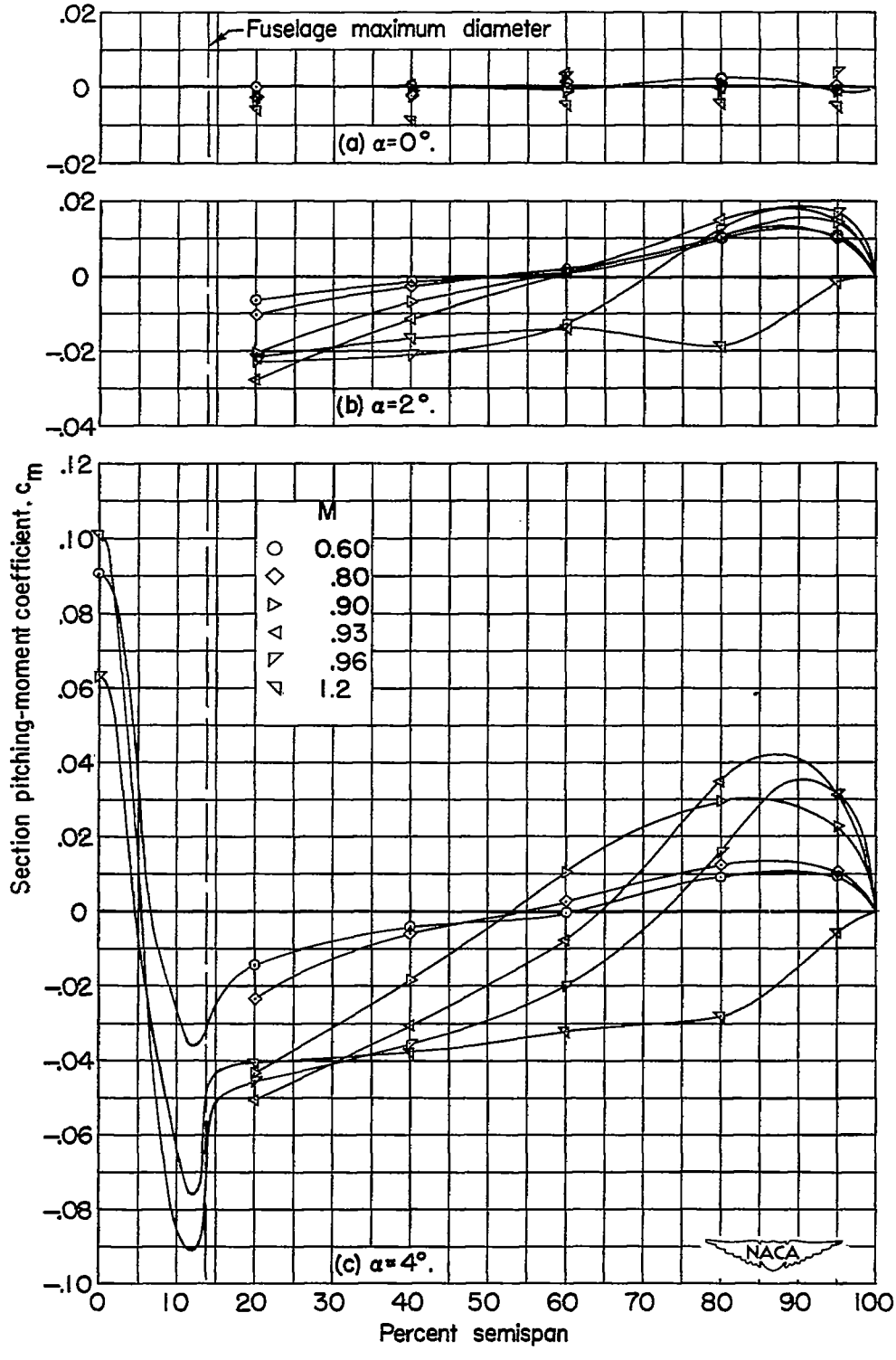

Figure 44.- The spanwise distributions of section pitching-moment coefficient at several Mach numbers.

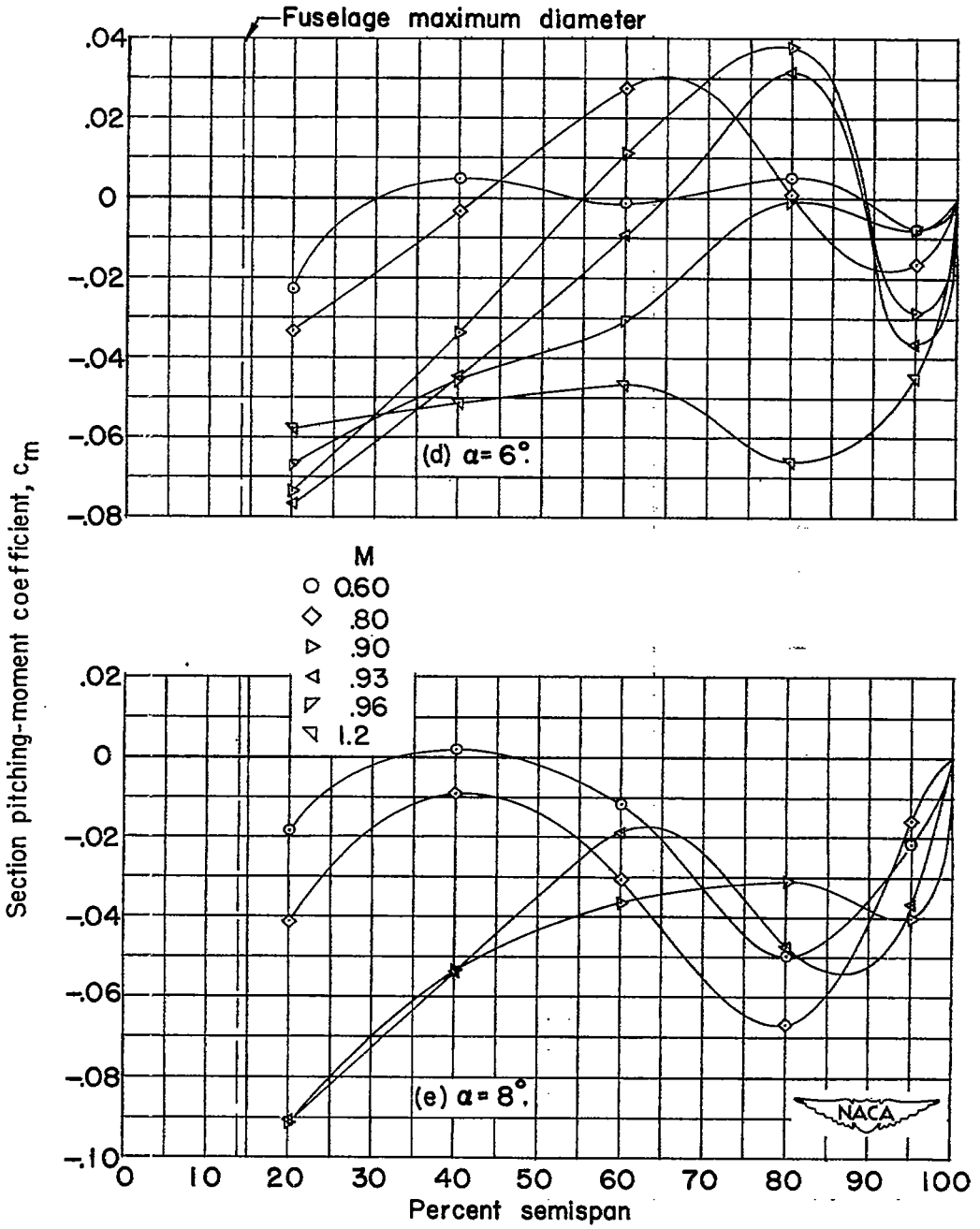

Figure 44.- Continued.

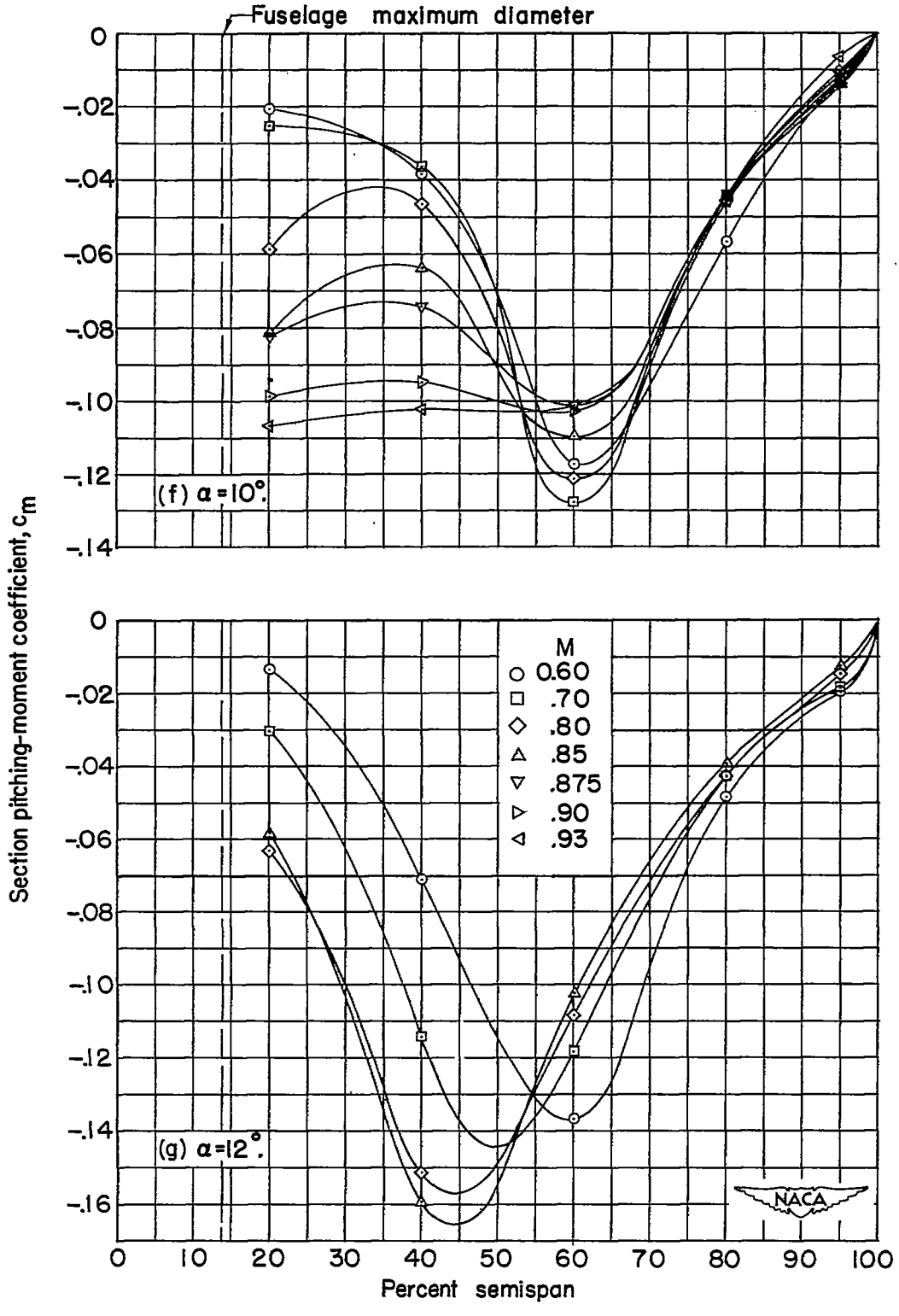

Figure 44.- Continued.

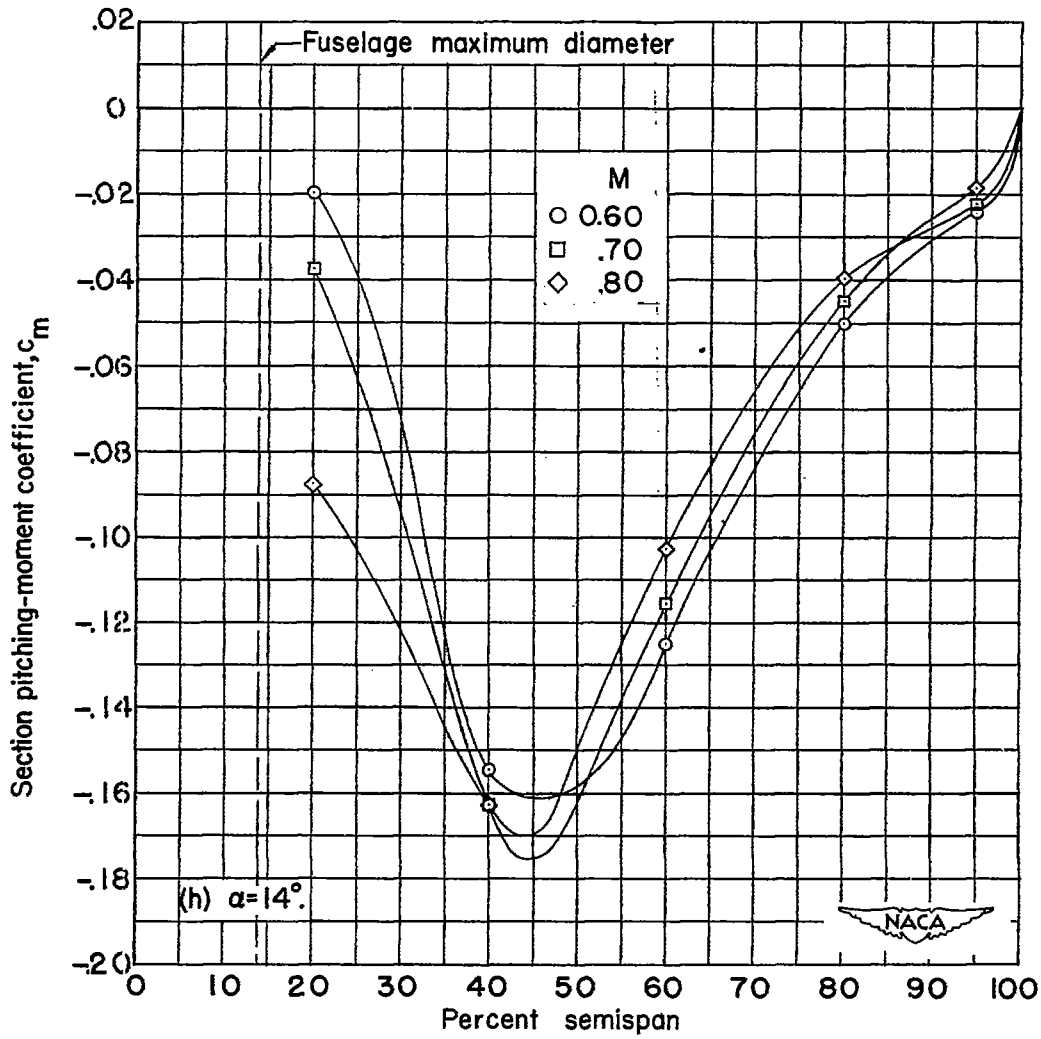

Figure 44.- Concluded.

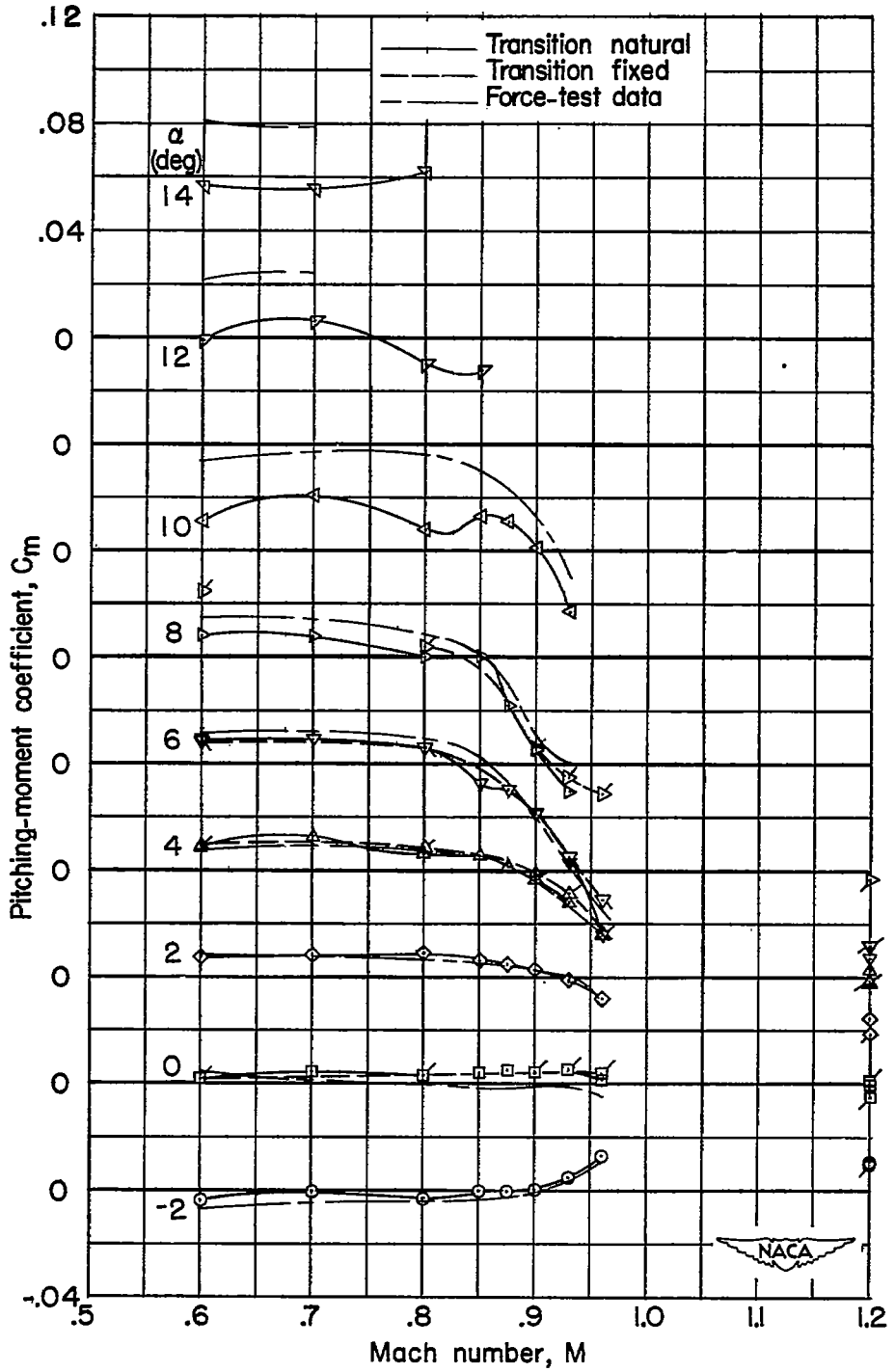

Figure 45.- Variation with Mach number of pitching-moment coefficient for the wing-fuselage configuration with transition natural and fixed. (Flagged symbols to the right indicate transition fixed; tailed symbols to the left, at M = 1.2, indicate force-test data.)

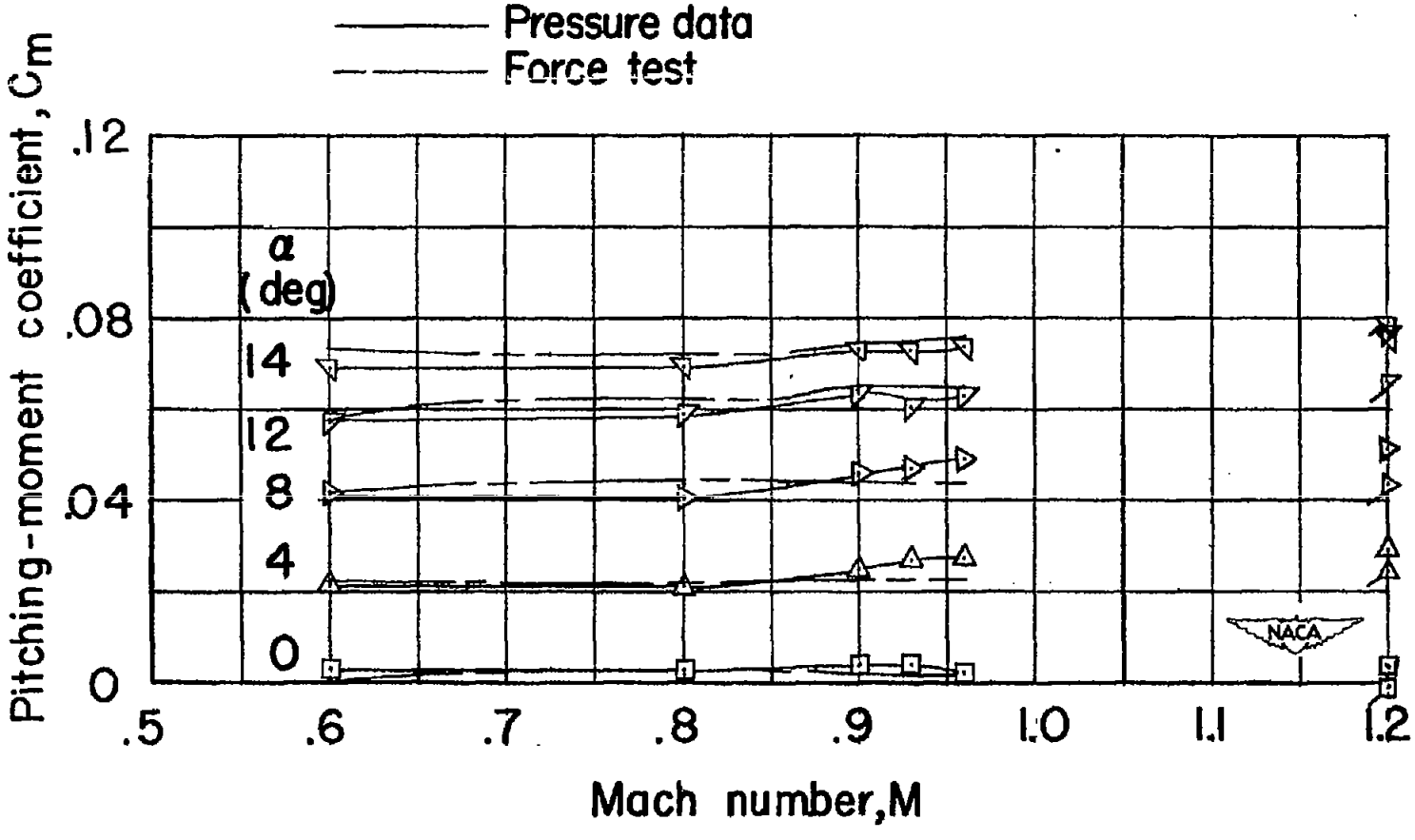

Figure 46.- Variation with Mach number of the pitching-moment coefficient for fuselage. (Symbols with tails indicate force-test data.)

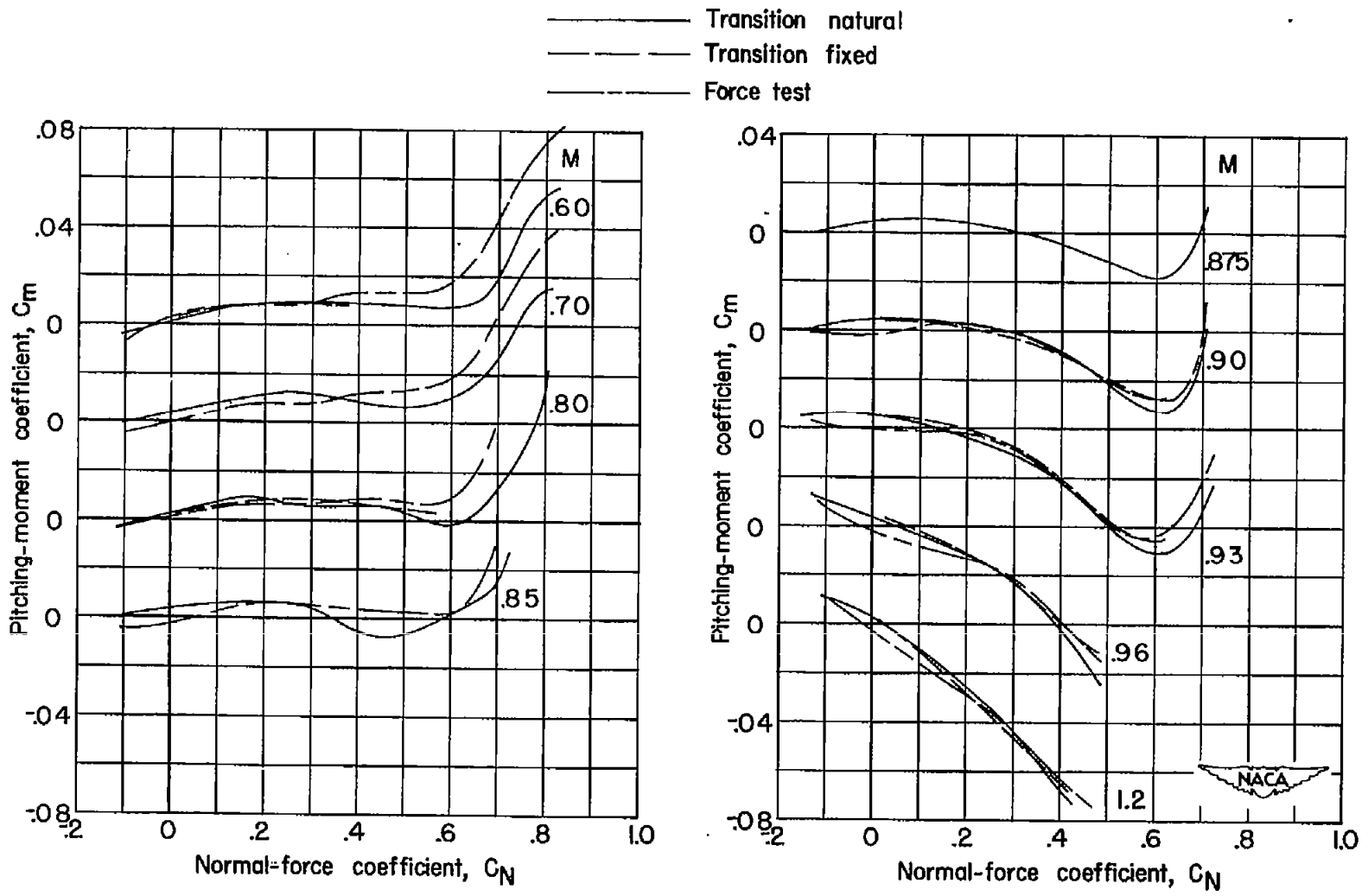

Figure 47.- Variation of pitching-moment coefficient with normal-force coefficient for wing-fuselage configuration with transition natural and fixed.

Figure 48.- Variation with Mach number of the lateral and chordwise position of the center of pressure for the wing with wing-fuselage interference.

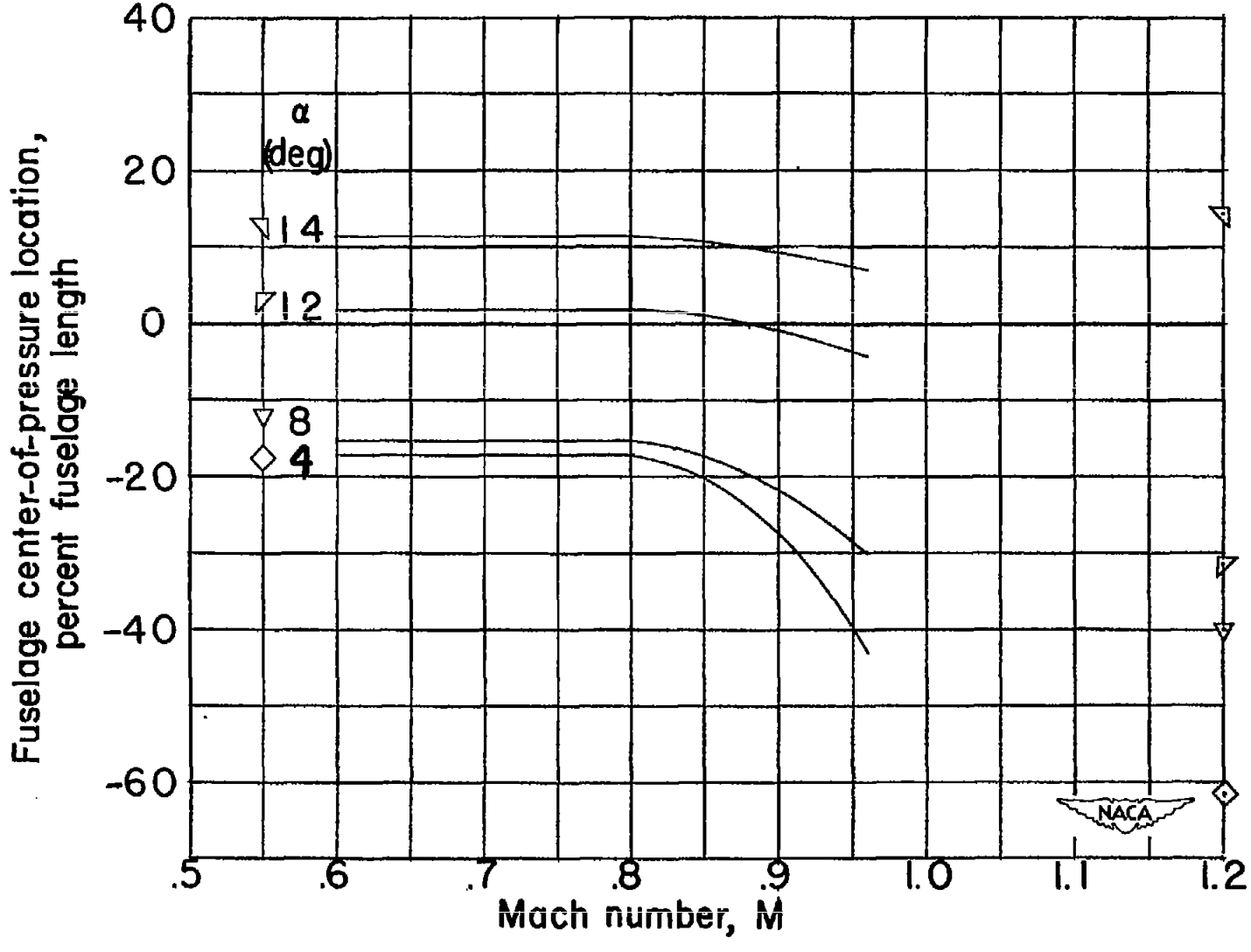

Figure 49.- Longitudinal position of the fuselage center of pressure, relative to the fuselage nose.

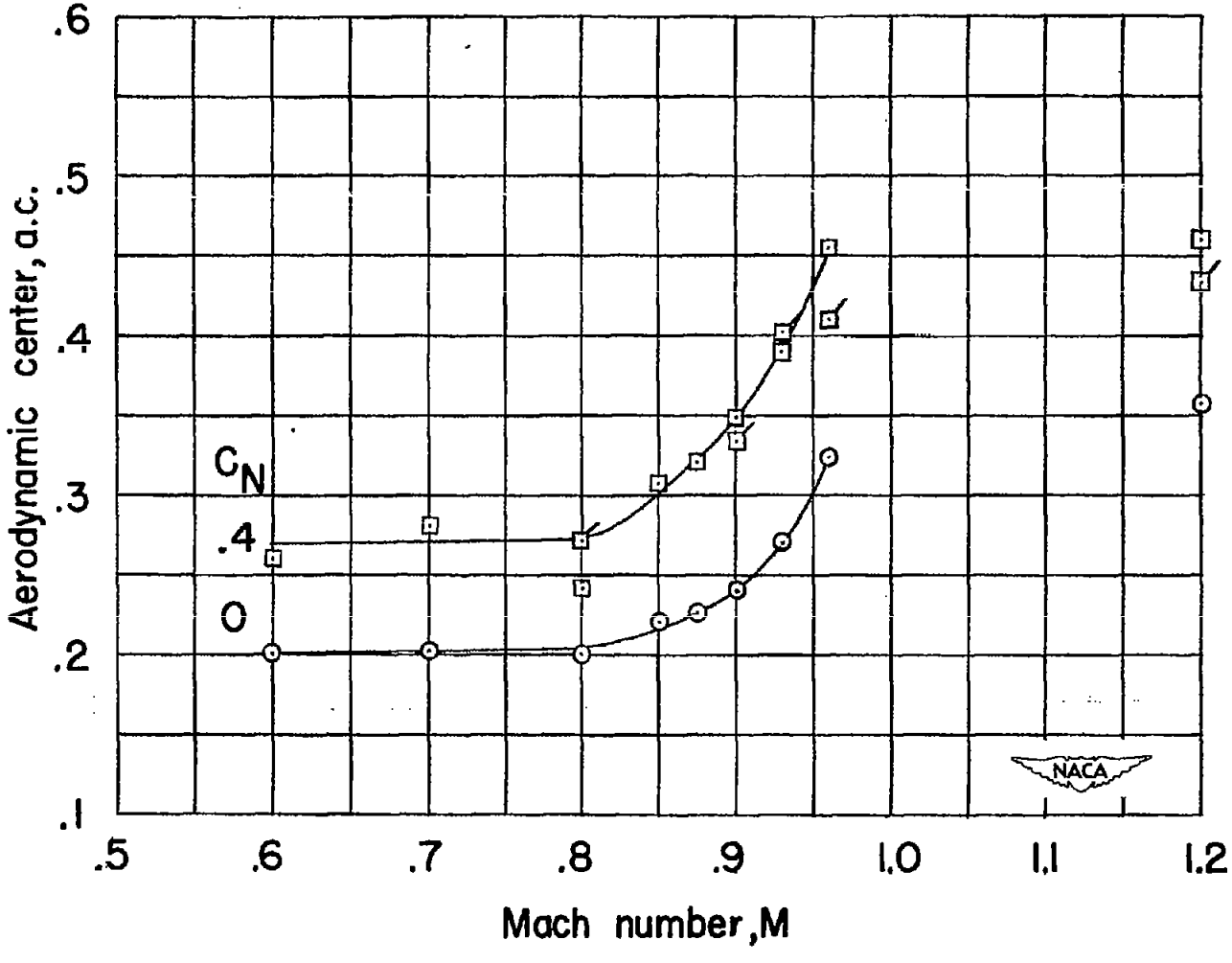

Figure 50.- Variation with Mach number of aerodynamic-center location for the wing-fuselage configuration, relative to the 25-percent position of the mean aerodynamic chord. (Flagged symbols indicate transition fixed.)

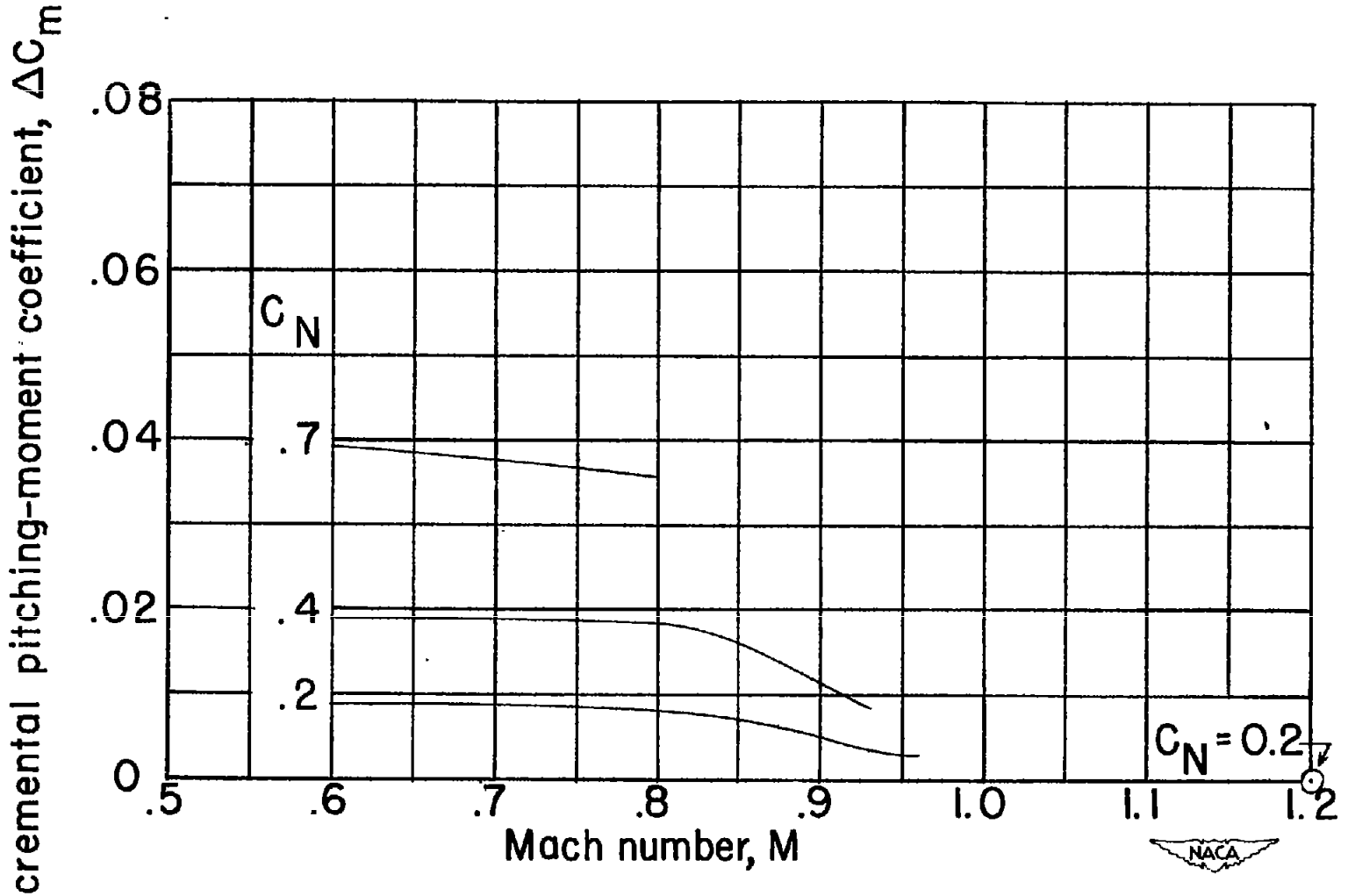

Figure 51.- Incremental pitching-moment coefficient due to addition of wing to fuselage.

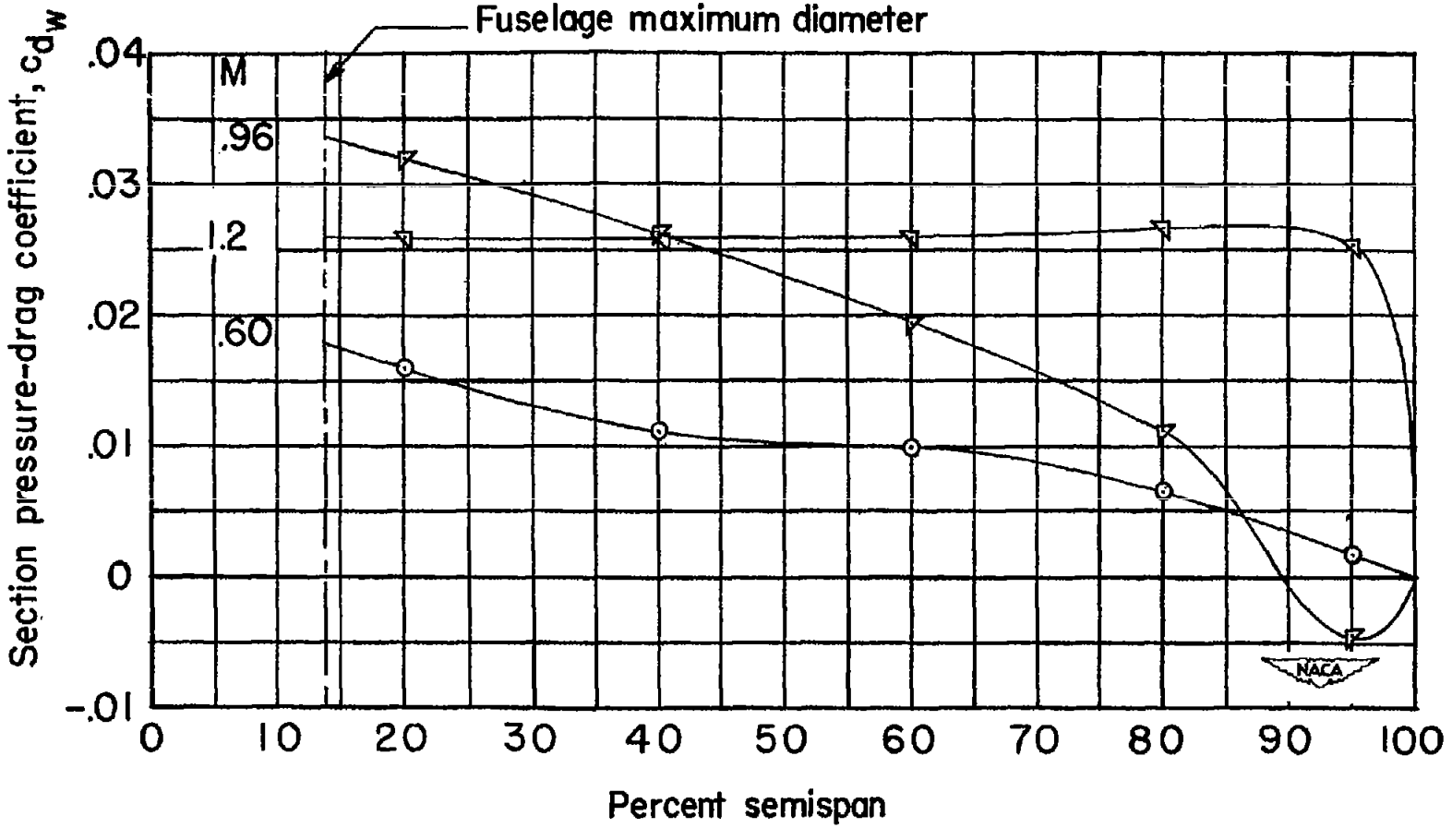

Figure 52.- The spanwise distributions of section pressure-drag coefficient at several Mach numbers. $\alpha = 4^{\circ}$.

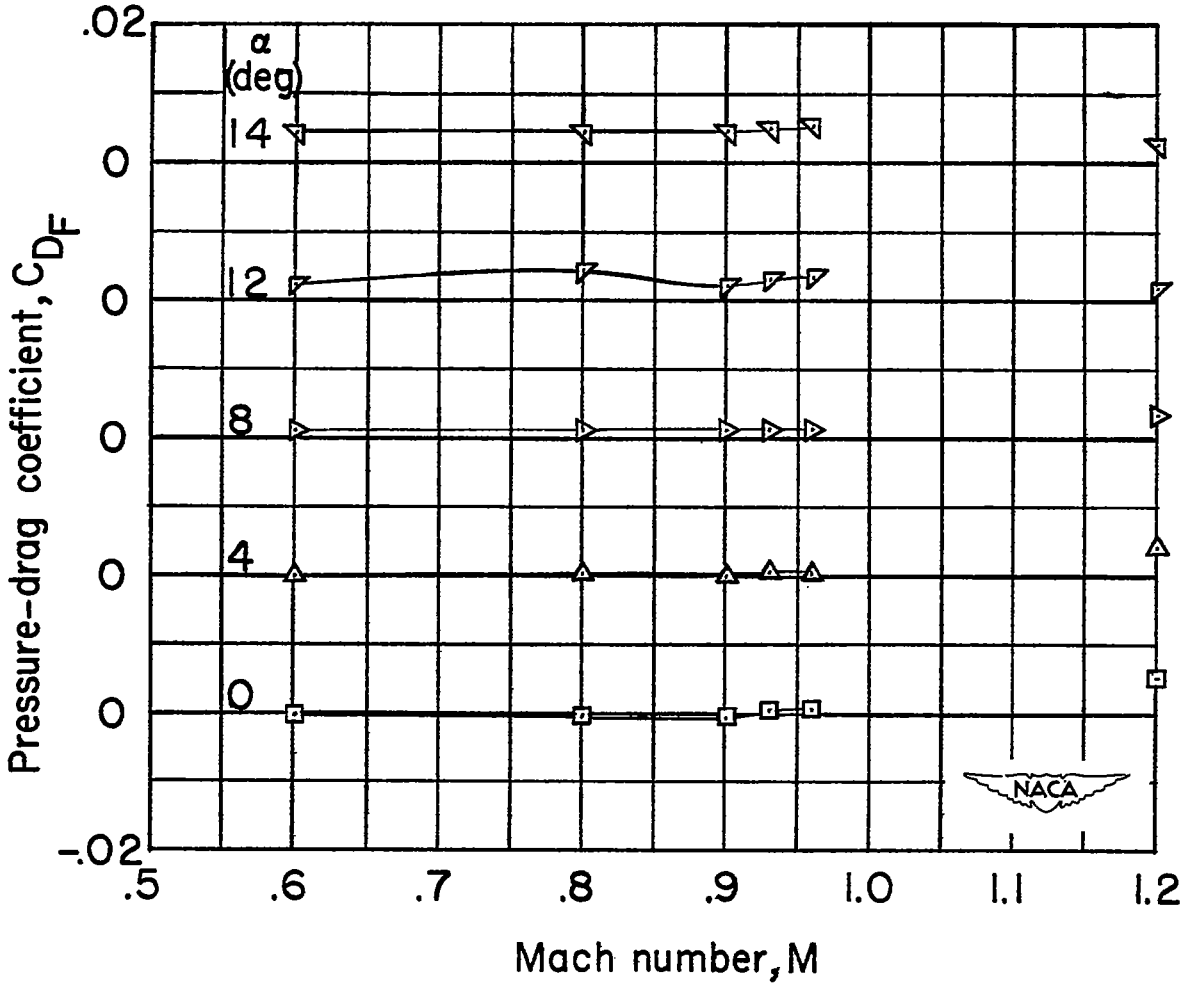

Figure 53.- Variation with Mach number of pressure-drag coefficient for the fuselage.

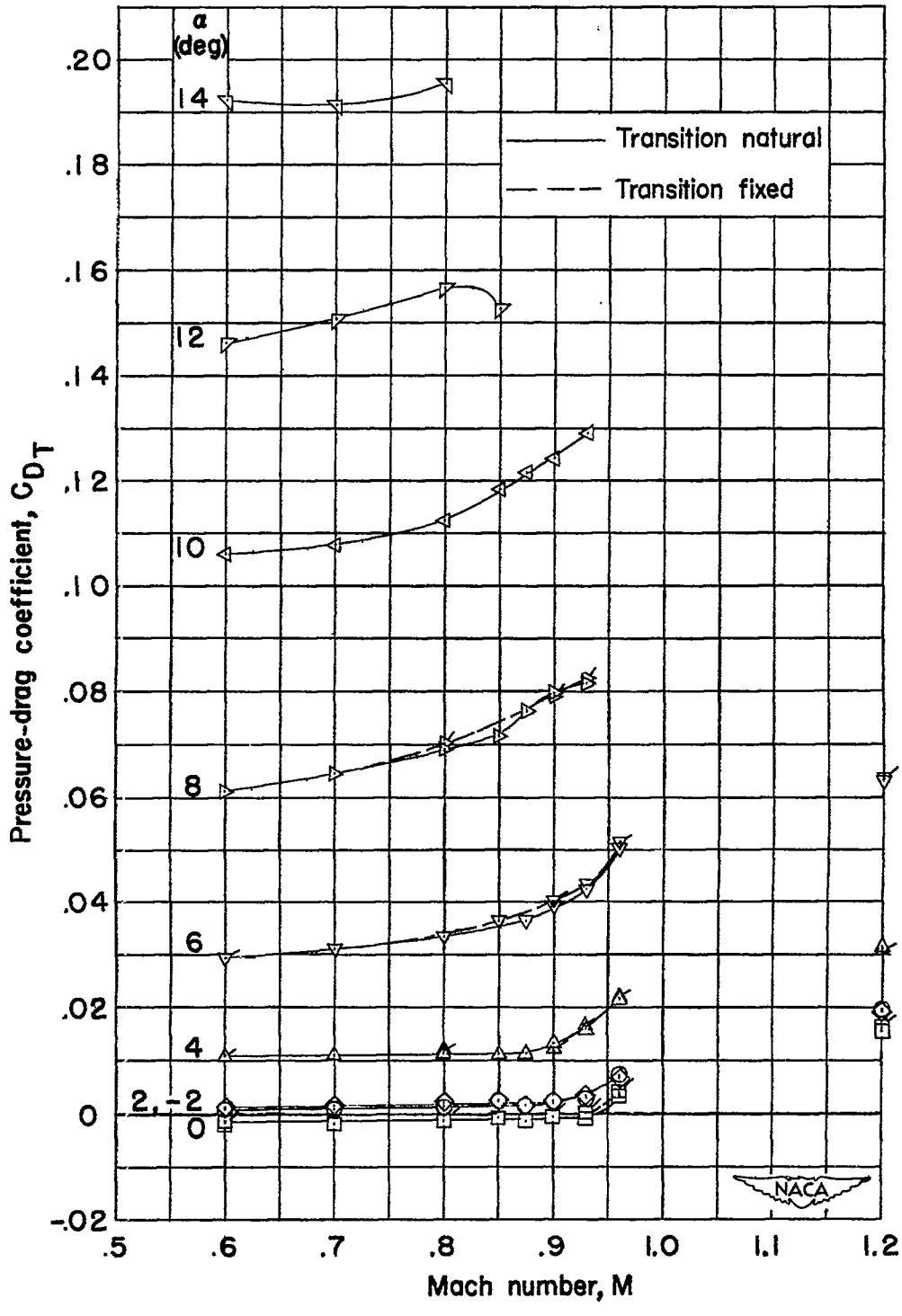

Figure 54.- Variation with Mach number of pressure-drag coefficient for the wing-fuselage configuration with transition natural and fixed. (Plain symbols indicate transition natural.)

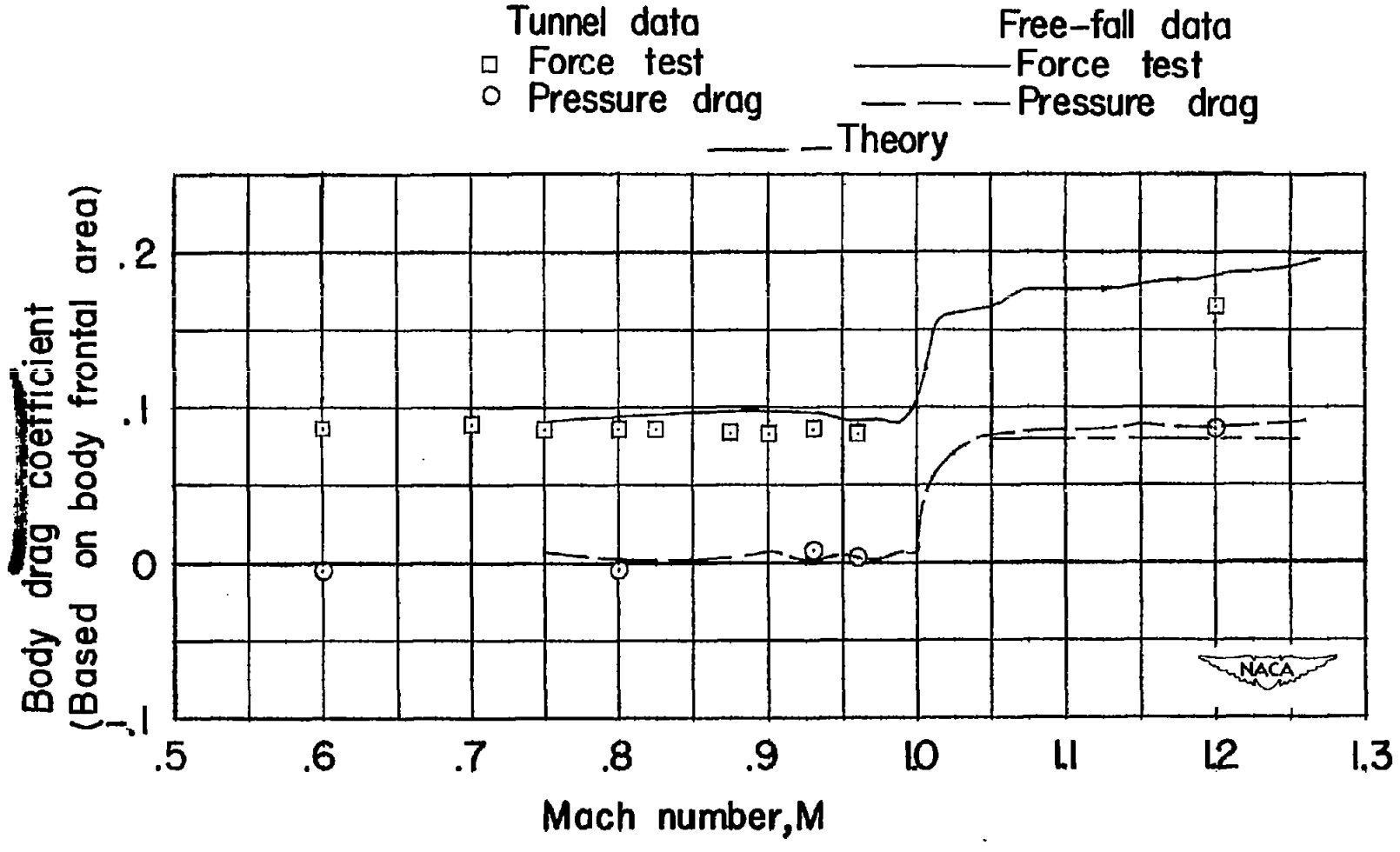

Figure 55.- Comparison of the variation with Mach number of the drag coefficient at zero lift for the fuselage and a free-fall model.

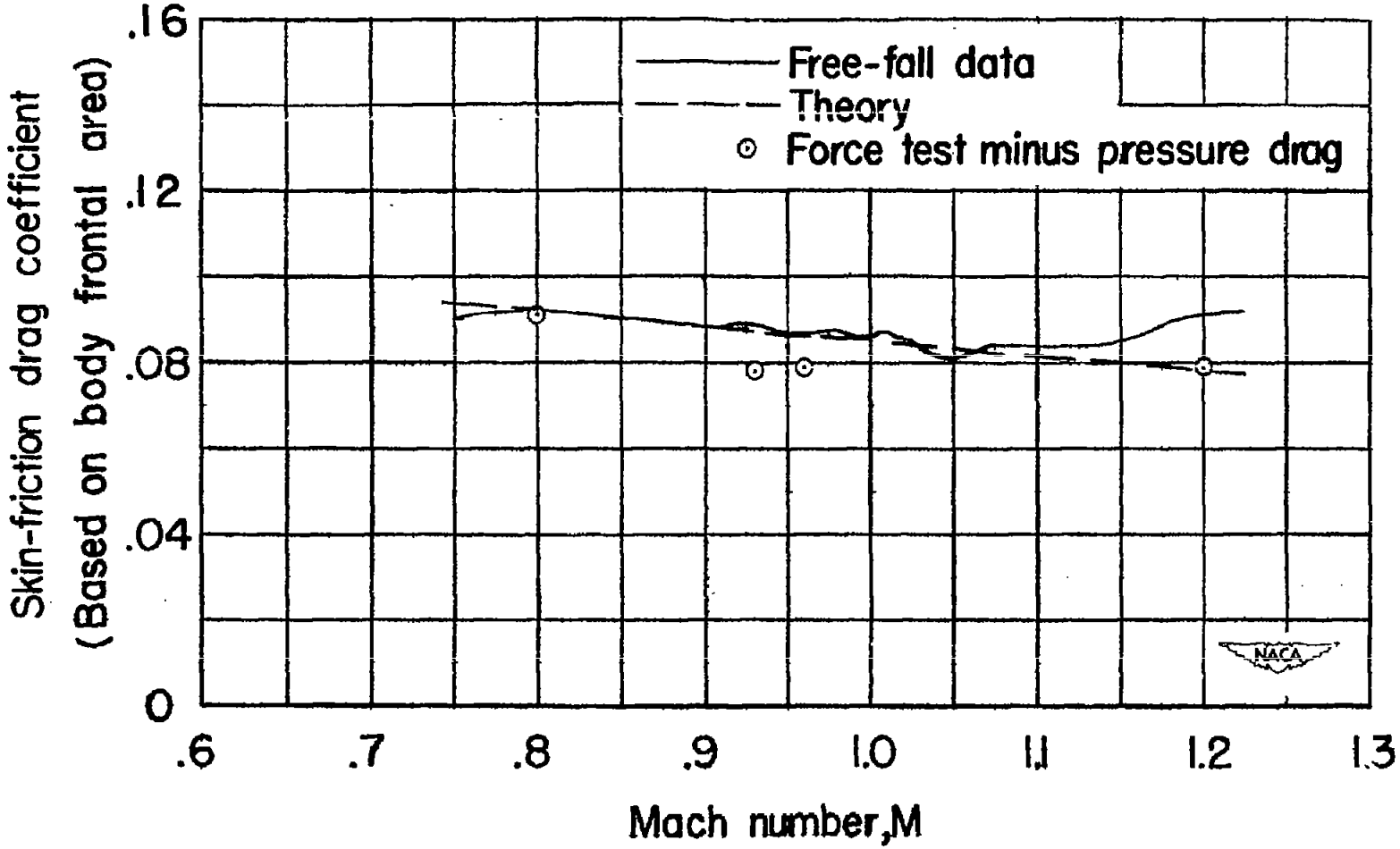

Figure 56.- Comparison of skin-friction drag coefficient, determined from data of figure 55, with free-fall data and theory.